Gene Therapy for Mucopolysaccharidosis Type II

A DISSERTATION
SUBMITTED TO THE FACULTY OF
THE UNIVERSITY OF MINNESOTA
BY

Miles Colby Smith

IN PARTIAL FULFILLMEENT OF THE REQUIREMENTS
FOR THE DEGREE OF
DOCTOR OF PHILOSOPHY

R. Scott McIvor, Ph.D., Advisor

December 2022
MOLECULAR, CELLULAR, DEVELOPMENTAL BIOLOGY &
GENETICS GRADUATE PROGRAM

Acknowledgements

First and foremost, I thank my graduate advisor, Dr. R. Scott McIvor for his mentorship. I could not have achieved this without all the time, advice, and opportunities you provided me. The passion you have for science is infectious and carrying out these projects under your guidance has been a truly enjoyable experience. I know the myriad scientific and professional skills I learned in your lab will be invaluable throughout the rest of my career.

I thank the rest of the current or former McIvor lab members, Dr. Lalitha Belur, Andrea Karlen, Olivia Erlanson, Avery Huber, Kelly Podetz-Pedersen, and Dr. Kanut Laoharawee. I am grateful for their support and guidance scientifically and professionally throughout my journey in MCDB&G. I couldn't ask for more congenial and kind coworkers.

I thank the current or former members of my committee, Dr. Nikunj Somia, Dr. Lihsia Chen, Dr. Paul Orchard, Dr. Elizabeth Braunlin, and Dr. Chester Whitley. Your scientific insights and questions have pushed me to be a better, more thoughtful scientist.

I thank the collaborators who both made this work possible and contributed to my scientific education: Dr. Hsing-Chen Tsia, Dr. Melissa Bonner, Dr. Nicholas Buss, Dr. Kwi Hye Kim, Dr. Troy Lund, Justin Furcich and Brenda Koniar. Additionally, I thank the T32 Stem Cell Biology Training Program, as well as the Center for Genome Engineering for their educational opportunities and financial support.

Lastly, I thank my fellow graduate students in MCDB&G and BMBB, friends outside the program, and my family for their kindness, encouragement, and support.

Dedication

This thesis is dedicated to my parents and sister, Mary Lund, Christopher Smith, and Joy Berthelsen, for their enduring support and love throughout the last 4.5 years. Since the very beginning they have encouraged me to be creative, learn, and explore. Even though my work may seem impenetrable to you at times, you keep asking questions. I love it, and I'll never stop asking questions either.

I also dedicate this thesis to my grandfather, J. Weston Smith. When I was young, I often quit endeavors too early and too often. One day he sat me down and advised me to not give up so easily and always give it my all. I often think of that moment for support when I am struggling.

Thesis Abstract

Mucopolysaccharidosis type II (Hunter syndrome, MPS II) is an inherited X-linked recessive disease caused by deficiency of iduronate-2-sulfatase (IDS). IDS hydrolyzes the C2 sulfate ester bond of terminal α-L-iduronic acid residues on the glycosaminoglycans (GAGs) heparan sulfate and dermatan sulfate. Insufficient IDS results in the accumulation of these GAGs within lysosomes and leads to progressive and multisystemic disease. Disease manifestations include, but are not limited to, cardiopulmonary dysfunction, arthropathy, dysostosis multiplex, and for the neuronopathic form neurological impairment and death by early adolescence. Currently, the only approved treatment for MPS II is enzyme replacement therapy (ERT, Elaprase®); allogeneic hematopoietic stem cell transplantation (HSCT) is conducted on a trial basis. ERT is expensive, time consuming, and administered IDS enzyme does not readily cross the blood brain barrier, leaving the neurological manifestations of MPS II unaddressed. Thus, there is a great need to develop new and better therapies for MPS II that can address these limitations.

Ex vivo lentiviral vector (LVV) based gene therapy is a promising approach to treat MPS II. Chapter II evaluates the efficacy of this strategy by the transplantation of hematopoietic stem and progenitor cells (HSPCs) transduced with a (LVV) carrying a codon optimized human IDS cDNA regulated by a strong, constitutively active MNDU3 promoter into MPS II mice. Treated mice exhibited supraphysiologic levels of IDS enzyme activity in plasma, peripheral blood mononuclear cells (PBMCs), and in peripheral tissues. Additionally, urine GAG excretion, GAG content in peripheral tissues, and zygomatic arch diameter were normalized. Importantly, IDS levels in the brains of

MNDU3-IDS engrafted animals were restored to 10-20% that of wild-type mice, which was sufficient to normalize brain GAG storage and prevent the emergence of neurocognitive deficits. Thus, these results demonstrate the potential effectiveness of *ex vivo* LVV transduced HSPCs as a source of bioavailable IDS for patients with MPS II.

In vivo gene therapy with an adeno-associated virus (AAV) vector is another approach for the treatment of MPS II. Clinical testing of cerebrospinal fluid (CSF)-directed administration of AAV9.CB7.hIDS (RGX-121) is currently underway to treat the neurological manifestations of MPSII. However, it is unknown if IT administration of RGX-121 will also improve systemic manifestations of MPS II or whether supplemental systemic administration will be required. Additionally, a potential minimum effective dose required to alleviate disease manifestations has so far been undetermined. Chapter III compares the delivery of RGX-121 by two routes of administration (ROA), intrathecal (IT) and intravenous (IV), at a range of doses. Doses of $1x10^{7}$gc and $1x10^{8}$gc were ineffective. A dose of $1x10^{9}$gc by either ROA resulted in plasma IDS activity at or above wild type levels but was insufficient to achieve wild type levels of IDS or GAGs in most tissues, including the brain. However, doses of $1x10^{10}$gc and $1x10^{11}$gc by either ROA resulted in supraphysiological plasma IDS activity, and at or above wild type IDS levels and commensurate GAG reduction in nearly all tissues. Notably, these same doses by either ROA showed normalization of zygomatic arch diameter compared to untreated controls, thereby demonstrating that peripheral manifestations are corrected by both IV and IT ROAs. Administration of $1x10^{11}$gc IT resulted in the highest quantifiable levels of IDS activity and greatest reduction in GAG content in the brain, as well as the prevention of neurocognitive deficits. Thus, a $1x10^{10}$gc dose of RGX-121 by either ROA was

sufficient to normalize metabolic and skeletal outcomes in MPS II mice, but neurologic benefit required IT administration of $1x10^{11}$gc, suggesting the prospect of a similar direct benefit in humans.

Current MPS II gene therapy studies use IDS deficient strains, but future preclinical work with human cells require the use of an immunodeficient MPS II mouse model of the disease. Chapter IV details the generation and characterization of an NSG-MPS II mouse strain, where CRISPR/Cas9 was employed to knock out a portion of the murine *IDS* gene on the immunodeficient NSG background. No IDS activity was detected in the plasma, PBMCs, or tissues of these mice. GAG analysis revealed elevated levels of storage material in those same tissues and in the urine. Histopathology showed vacuolized cells in both the periphery and CNS. NSG-MPS II mice also recapitulated skeletal and neurocognitive manifestations associated with MPS II in humans. This immunodeficient model of MPS II will therefore be useful for testing potential treatments for MPS II involving xenotransplantation of human cells. Overall, the data in this work provide preclinical data supporting two different gene therapy approaches for the treatment of MPS II, as well as the development of an immunodeficient of the disease for future studies.

Table of Contents

List of Tables

List of Figures

List of Abbreviations

4-MU	4-methylumbelliferone
4-MU2S	4-methylumbelliferyl α-l-iduronide 2-sulfate disodium salt
6MWT	Six-minute walk test
AAP	Assembly-activating protein
AAV	Adeno-associated virus
AAV-HSC	Hematopoietic stem cell derived AAV vector
AAV9	Adeno-associated virus vector serotype 9
AB	Alcian Blue
ANOVA	Analysis of variance
APC	Allophycocyanin
ATP	Adenosine triphosphate
BBB	Blood-brain barrier
BMP	Bone morphogenetic protein
BMT	Bone marrow transplant
bp	Base pair
BSA	Bovine serum albumin
c/dg	Copy per diploid genome
Ca^{2+}	Calcium
Cas9	CRISPR associated protein 9
CB7	Cytomegalovirus immediate early enhancer with chicken beta actin promotor, exon 1 and
cDNA	Complementary deoxyribonucleic acid
CGN	*Cis* Golgi network
CLEAR	Coordinated lysosomal expression and regulation
CMV	Cytomegalovirus
CNS	Central nervous system
cohIDS	Codon optimized human iduronate-2-sulfatase
COPII	Coated protein complex II
cPPT	Central polypurine tract
CRISPR	Clustered regularly interspaced short palindromic repeats
CSF	Cerebrospinal fluid
DAB	3,3'-diaminobenzidine
DMMB	Dimethylmethylene Blue
DNA	Deoxyribonucleic acid
DNase	Deoxyribonuclease
DS	Dermatan Sulfate

DSB	Double-strand break
ECM	Extracellular matrix
EF1α	Elongation factor 1-alpha
EGT	Electro gene transfer
ER	Endoplasmic reticulum
ERT	Enzyme replacement therapy
FDA	Food and Drug Administration
FFPE	Formalin-fixed, paraffin-embedded
FGF	Fibroblast growth factors
GAG	Glycosaminoglycans
gc	Genome copy
gc/ge	Genome copy per genome equivalent
gDNA	Genomic deoxyribonucleic acid
GFAP	Glial fibrillary acidic protein
GFP	Green fluorescent protein
GNPTAB	N-acetylglucosamine-1-phosphotransferase
GvHD	Graft vs host disease
H&E	Hematoxylin and eosin
hCG	human chorionic gondatropin
h*IDS*	Human *iduronate-2-sulfatase* gene
HIV	Human immunodeficiency virus-1
HPLC	High-performance liquid chromatography
HS	Heparan Sulfate
HSCGT	Hematopoietic stem cell gene therapy
HSCT	Hematopoietic stem cell transplantation
HSPC	Hematopoietic stem and progenitor cell
ICV	Intracerebroventricular
IDS	Iduronate-2-sulfatase
IDUA	α-L-iduronidase
IHC	Immunohistochemistry
iPSC	Induced pluripotent stem cells
ISH	*In situ* hybridization
IT	Intrathecal
ITR	Inverted terminal repeat
IV	Intravenous
kb	Kilobase
kDa	KiloDalton
KO	Knockout
LAMP1	Lysosomal-associated membrane protein-1

LAMP2	Lysosomal-associated membrane protein-2
LD	Lysosomal disease
LDL	Low-density lipoprotein
LIMP2	Lysosomal integral membrane protein-2
LOD	Limit of detection
LOQ	Limit of quantification
LSD	Lysosomal storage disease
LTR	Long-terminal repeat
LVV	Lentiviral vector
LYSET	Lysosomal enzyme trafficking factor
M6P	Mannose-6-phosphate
M6PR	Mannose-6-phosphate receptor
Micro-CT	Micro computed tomography
m*IDS*	Murine *iduronate-2-sulfatase* gene
MNDU3	Myeloproliferative sarcoma virus U3 region with negative control elements deleted and dl
MOI	Multiplicity of infection
MPS	Mucopolysaccharidosis
MPS II	Mucopolysaccharidosis type II, Hunter syndrome
MRI	Magnetic resonance imaging
mRNA	Messenger ribonucleic acid
MS/MS	Tandem mass spectrometry
NHEJ	Non-homologous end joining
NOD	Non-obese diabetic
NSC	Neural stem cell
NSG	NOD scid gamma
PBMC	Peripheral blood mononuclear cell
PBS	Phosphate buffered saline
PCR	Polymerase chain reaction
PCT	Pharmacological chaperone therapy
PE	Phycoerythrin
ProK	Proteinase K
qPCR	Quantitative polymerase chain reaction
R	Repeat region
RBC	Red blood cells
RBG Poly(A)	Rabbit beta globin polyadenylation sequence
RGX-121	AAV9.CB7.hIDS
RNA	Ribonucleic acid
RNase	Ribonuclease

ROA	Route of administration
RRE	Rev response element
RUSP	Recommended Uniform Screening Panel
SCID	Severe combined immunodeficiency
SD	Standard deviation
SEM	Standard error of the mean
sgRNA	Single guide ribonucleic acid
SRT	Substrate reduction therapy
SUMF1	Sulfatase modifying factor-1
TALEN	Transcription activator-like effector nuclease
TFEB	Transcription factor EB
TGB	Thyroxine binding globulin
TGF-β	transforming growth factor-β
TGN	*Trans* Golgi network
TLR	Toll-like receptor
TNF-α	Tumor necrosis factor-α
U3	Unique 3'
U5	Unique 5'
UCE	N-acetylglucosamine-1-phosphodiester a-N-acetyl-glucosaminidase
UTR	Untranslated region
VCN	Vector copy number
VP	Viral capsid protein
VSV-G	Vesicular stomatitis virus G
ZFN	Zinc finger nuclease
Ψ	Packaging signal

Chapter I: Introduction

Lysosomal Diseases

Lysosomes

Albert Claude, in 1946, published a generalized technique for analyzing the distribution of intracellular enzymes using centrifugation[1,2]. This technique was utilized by Charles de Duve et al when they published in 1955 on the discovery of "granules" termed lysosomes[3]. In 1956, electron microscopy revealed the first images of lysosomes in rat liver[4]. Claude and de Duve, along with George Palade, were awarded the Nobel prize in physiology and medicine in 1974, in part for this work.

Lysosomes are intracellular membrane enclosed compartments that house a wide complement of enzymes. Lysosomes are primarily known for their central role in catabolism, where they degrade a range of macromolecules, such as proteins, carbohydrates, and lipids[5-7]. However, it is now appreciated that the organelle also plays a role in several cellular processes, such as membrane repair, autophagy, immune cell signaling, vesicle trafficking, and nutrient sensing[8-10]. Lysosomes are roughly 0.2-1μm in diameter but can maintain a diverse morphology in the cell based on their interior composition and fusion events[7,11,12]. A major regulator of lysosomal morphology are phosphatidylinositols, in particular PI3P and PI(3,5)P_2[10,13-15]. In addition to phosphatidylinositols, the positioning of lysosomes in a cell is coordinated by the BLOC-1-related complex[10,390]. Formation of lysosomes begins with the Golgi apparatus. Transport vesicles carrying lysosomal proteins bud from the *trans* Golgi network (TGN) and form primary lysosomes[7]. Lysosome biogenesis is controlled by transcription factor

EB (TFEB)[16,17]. Upon activation, TFEB transits to the nucleus where it can bind coordinated lysosomal expression and regulation (CLEAR) sequences[18]. Many genes encoding lysosomal proteins have CLEAR sequences ~200bp upstream of the transcription start site that, once bound by TFEB, induce gene transcription[16]. Thus, TFEB coordinates lysosomal function through gene expression and lysosome biogenesis.

How does endocytic cargo reach these nascent lysosomes for degradation? Currently, four main models of lysosome biogenesis have been theorized[7,19]. The maturation model proposes endocytic vesicles progressively develop to early, then late endosomes, and finally lysosomes, that can receive Golgi vesicles[20,21]. The next model, the vesicular transport model, states that endocytic vesicles form multivesicular bodies or late endosomes which mobilize their content via vesicles to deliver cargo to lysosomes[21]. Third, the "kiss-and-run" model which suggests endocytic vesicles form late endosomes that briefly fuse, exchange cargo, and then dissociate from lysosomes[23,24]. The last model is the fusion model, where endocytic vesicles mature to late endosomes and fuse with lysosomes to form a "hybrid" organelle, from which lysosomes can be reformed[25]. Like the endoplasmic reticulum (ER), lysosomes maintain a large store of calcium ions (Ca^{2+}), at a concentration up to 500-600μM[26-28]. This calcium reserve plays vital functions in trafficking of lysosomes and late endosomes, vesicular fusion events involving SNAREs, nutrient sensing, and regulating autophagy[29].

The lumen of lysosomes must maintain a pH level lower than the surrounding environment, within a span of 4.6-5.5[29-31]. This pH range is maintained by vacuolar

ATPases, which use ATP hydrolysis to move H^+ ions from the cytosol into the lumen[32-33]. This acidic environment is essential to lysosomal function, as it plays a central role in the activity of hydrolases and facilitates the degradation of macromolecular substrate structures. Acid hydrolases, among other lysosomal proteins, play a central role in lysosome function and by extension cellular homeostasis. Conversely, deficiencies in hydrolases or their regulation leads to cellular dysfunction, which in turn manifests as disease. Thus, it is crucial to understand the synthesis, processing, and secretion of these enzymes.

Biosynthesis and Processing of Lysosomal Enzymes

Synthesis of lysosomal enzymes takes place at the rough ER. Soluble enzymes, such as the nearly 60 acid hydrolases, are synthesized with a 20-25 N-terminal amino acid sequence directing their translocation into the ER[34]. Newly synthesized proteins can be modified by glycosylations, and proteolytic cleavages involved in quality control, protein folding, activity, and sorting[34,35]. Additionally, sulfatases are further modified here by the formylglycine generating enzyme, sulfatase modifying factor 1 (SUMF1)[36,37]. SUMF1 generates a formylglycine residue from a cysteine residue crucial to sulfatase activity[36]. Vesicular transport by COPII coated vesicles transits these proteins to the *cis* Golgi network (CGN)[39]. Here, an important modification is made on *N*-linked mannose glycosylations of asparagine residues, with the formation of mannose-6-phosphate (M6P). Two key enzymes are required in this process, UDP-N-acetylglucosamine-1-phosphotransferase (GNPTAB) and N-acetylglucosamine-1-phosphodiester α-N-acetyl-glucosaminidase (UCE). GNPTAB transfers a GlcNac-1-phosphate to the sixth carbon of

mannose sugars[40]. Recent work has also highlighted the role of lysosome enzyme trafficking factor (LYSET), which acts as a chaperone for GNPTAB[387,388]. A GNPTAB hydrophobic transmembrane domain is stabilized by LYSET binding, allowing the transfer of GlcNac-1-phosphate to proceed[387]. After this addition in the CGN, the proteins transit to the TGN. Here, UCE then removes GlcNac from the mannose, leaving a phosphate behind to generate a M6P moiety[41]. In the TGN, mannose-6-phosphate receptors (M6PR) recognize this M6P modification and bind to the protein. Once bound, clathrin coated vesicles form around the receptor-ligand cargo[42]. These vesicles then bind to endosomes, which carry substrates for degradation, before ultimately reaching lysosomes. Alternatively, about 40% of lysosomal enzymes are not bound to M6PRs and can be routed for extracellular secretion[43]. Soluble enzymes secreted in this way can bind to M6PRs on the surface of the same or nearby cells and endocytosed for delivery to lysosomes. Metabolic cross correction depends upon this alternative route for delivering lysosomal enzymes to enzymatically deficient cells[44,45]. M6PR independent sorting to lysosomes occurs via transmembrane proteins such as lysosomal integral membrane protein 2 (LIMP2) and sortilin that act as transport receptors for lysosomal proteins[46,47].

Lysosomal Diseases

Lysosomal diseases (LD), also called lysosomal storage diseases, are a set of rare, inherited metabolic disorders characterized by lysosomal dysfunction. Philippe Gaucher described the LD now known as Gaucher disease in 1882[48]. A full 16 years after, in 1898, a second LD called Fabry disease, was simultaneously discovered by Johannes Fabry and William Anderson[49]. More LDs were reported in the intervening years, but it wasn't until

fundamental work by de Duve and others on the lysosome that led to greater molecular understanding of LDs. In 1963 Hers and colleagues classified the first LD, by detailing the cause of Pompe disease as a deficiency in α-glucosidase[50]. Today, over 70 different diseases are grouped to comprise LDs, each with their own molecular basis described.

Although individual disease incidence for any single LD ranges from 1:50,000-250,000, they collectively occur in ~1:5000-5,500 live births[51,52]. Most diseases are autosomal in nature, but a few, such as Hunter syndrome and Fabry disease are X-linked. LDs are multisystemic in nature, and as such disease manifestations impact several organs. Manifestations can include cardiopulmonary dysfunctions, organ enlargement, joint issues, blindness, deafness, skeletal dysplasias, neurocognitive (developmental) delay, and premature death[51,53]. Symptoms can first begin to emerge as early as a few months to years after birth. Disease manifestations can vary greatly between diseases[54]. Even within a single disease, patients can present with a variety of symptoms based on the molecular characteristics and severity of the disease. As such, disease severity is often considered on a spectrum from mild/attenuated to severe.

All LDs are caused by deficiency in a protein related to lysosomal function. Mainly, these consist of diseases related to a deficiency in an acid hydrolase. For instance, deficiency in the HEXA protein leads to the accumulation of GM2 gangliosides, leading to Tay-Sachs disease (GM2 gangliosidosis). However, some LDs result from an insufficiency in a membrane transport protein, chaperone, activating protein, or enzyme that modifies lysosomal proteins. One example of this is I-cell disease (mucolipidosis II),

where GNPTAB deficiency causes lysosomal proteins to lack the M6P modification required for lysosomal targeting. Generally, for any LD, the deficient protein leads to the accumulation of undegraded substrate(s). These substrates are generally lipids and polysaccharides, as well as cystine accumulation[51]. The traditional subset classification of LDs relies on groupings related to the accumulated substrate, such as glycoproteinoses, sphingolipidoses, lipidoses, and mucopolysaccharidoses.

Mucopolysaccharidoses

Mucopolysaccharidoses (MPS) are a group of recessively inherited metabolic disorders. Nearly 30% of patients with LDs have MPS and collective incidence is ~1 per 25,000 births[55,56]. All MPS are caused by deficiency in a lysosomal hydrolase that degrades glycosaminoglycans (GAGs, formerly mucopolysaccharides)[57]. MPS, as a group, are comprised of 7 different named diseases (I, II, III, IV, VI, VII, and IX). However, the group encompasses 11 different enzyme deficiencies and has two subsets to reflect this (MPS IIIA-D and MPS IVA-B). These 11 enzymes act on at least one of five GAG substrates: dermatan sulfate, heparan sulfate, keratan sulfate, chondroitin sulfate, and hyaluronan. GAGs are long chain sugar carbohydrates mainly located in the extracellular matrix attached to proteins, such as decorin and betaglycan, to form proteoglycans. Insufficiency in any of these hydrolases leads to cellular GAG accumulation in the lysosome.

As a result, MPS emerge as a group of multisystemic and progressive diseases. As with LDs in general, patients exhibit a spectrum of disease severity for any given MPS.

Symptoms generally manifest within the first 2 years of life[57]. Disease manifestations for the MPS include cardiopulmonary dysfunction, organomegaly, skeletal dysplasias, hearing loss, reduced vision, and joint stiffness[58]. Neurocognitive decline is also manifests in the severe forms of MPS I, II, III, and VII. While attenuated patients can live for decades, those with severe forms of disease often die from disease complications within the first decade of life. Clinical diagnosis is complicated, given the rare and heterogenous nature of MPS[58]. MPS screening is carried out by enzyme activity assay, generally with a blood sample. Screening for elevated urine gag excretion and molecular analysis of the suspect gene can also be done[58]. Another possible screening modality is tandem mass spectrometry (MS/MS) that allows for both protein and substrate analysis from dried blood spots[59-60]. For those diseases with approved therapies, early screens are pivotal, as early time to treatment results in better outcomes and a vastly improved quality of life for MPS patients.

While no cures exist for any MPS, there are approved treatments in the form of enzyme replacement therapy (ERT) and allogeneic hematopoietic stem cell transplantation (HSCT). ERT is available for MPS I (Aldurazyme®), II (Elaprase®), IVA (Vimizim®), and VII (Naglazyme®)[61]. ERT infuses recombinant enzyme into patients that deficient cells can endocytose via the M6P pathway. Although HSCT is available for some MPS disease, such as MPS I, its efficacy remains uncertain for others, such as MPS II and MPS III[62]. Several other treatment approaches are under investigation for MPS, including substrate reduction therapy and a variety of gene therapies, which are discussed below specifically for MPS II.

Mucopolysaccharidosis Type II (MPS II, Hunter syndrome)

History of MPS II

Mucopolysaccharidosis Type II (MPS II, Hunter syndrome) is an X-linked recessive metabolic disorder caused by deficiency in the lysosomal hydrolase, iduronate-2-sulfatase (IDS). Insufficient IDS impairs the catabolism of two GAGs, dermatan sulfate (DS) and heparan sulfate (HS). Accumulation of these undegraded GAGs is pathological, leading to a progressive, multisystemic disorder[57,58].

In 1917, the physician Charles Hunter reported a "Rare Disease in Two Brothers", where he described a disorder with coarse facial features, distended abdomen, broad chest, short stature, skeletal alterations, hernias, throat issues, hearing loss, and an enlarged liver[63]. However, it wasn't until 35 years later that a hypothesis on the molecular basis of the disease was posited[64]. It was observed that substances called mucopolysaccharides accumulated in MPS patient samples[64,65]. The disease was known as Hunter-Hurler syndrome, mistaking MPS II and MPS I as a single disease due to common disease characteristics and a lack of molecular understanding. The first notions that Hunter syndrome and Hurler syndrome were separate diseases was published in 1968. The authors proposed Hunter syndrome as a related, but less severe X-linked disease caused by faulty degradation of mucopolysaccharides (rather than an overproduction)[66]. That year, seminal work from Elizabeth Neufeld's lab described *in vitro* experiments that co-cultured MPS I and MPS II fibroblasts[67,68]. They observed mutual correction of disease pathology in the fibroblasts by co-culturing, suggesting a

compensation mechanism between the two. Additionally, they found simply culturing one fibroblast line with conditioned medium from the other was enough for metabolic correction, suggesting the compensating factor was secreted. This secreted factor would become known as the "Hunter corrective factor"[69]. This was the first report of metabolic cross correction, which is now known to occur via the M6P pathway. This was a foundational discovery on which the first approved therapy for MPS II, ERT, is based on and that potential MPS II gene therapies utilize. The Neufeld group also discovered that the Hunter corrective factor was a protein[70]. Around the same time, it was proposed that deficits in lysosomal acid hydrolase activities were responsible for MPS diseases. Experiments measuring hydrolase activities from patient samples gave the first concrete evidence for this hypothesis[71]. A few years later, it was reported that the protein had sulfatase activity[72]. The isolation and sequencing of the first human *IDS* gene was carried out in 1990s[73-75]. In 2006, ERT with Elaprase® (idursulfase, recombinant IDS) was approved for Hunter syndrome[76,77].

Disease Inheritance and Incidence

MPS II is inherited in a recessive X-linked fashion, meaning nearly all patients are male. Nevertheless, female cases of MPS II have been reported[78,79]. These female cases are the result of disruptions to the *IDS* gene by chromosomal rearrangements or defects in X inactivation[80].

MPS II has a low incidence rate, but cases occur globally. Disease incidence of MPS II is highly variable, with prevalence of the disease changing greatly between

geographic regions[56]. Cases range from 0.13 per 100,000 in Norway to 1.09 and 2.16 per 100,000 in Portugal and Estonia, respectively[81-83]. For Europe and North America, MPS II occurs ~1:160,000[84]. MPS II is more prevalent in Asia, reaching upwards of ~1:62,000[84]. In fact, MPS II constitutes 50% of MPS cases in Asia[56].

Clinical Features of MPS II

There is significant heterogeneity in the clinical features presented by MPS II patients. Because *IDS* plays a role in cellular homeostasis, pathological accumulation of GAGs affects nearly all tissues and organs[85]. While disease severity is considered to be a spectrum, patients have commonly grouped into two main forms: mild/attenuated and severe. However, these terms are no longer accurate, as a patient without neurocognitive manifestations can still exhibit severe somatic manifestations. Today, MPS II is generally referred to as non-neuronopathic and neuronopathic, while recognizing patients exist on a continuum of disease phenotypes[86]. Non-neuronopathic symptoms are related to dysfunction in somatic tissues and organs. There are little to no central nervous system (CNS) manifestations, and patients can live for several decades[87]. The neuronopathic form, which occurs in about 2/3rds of cases, develops CNS manifestations[87-89]. These include neurological impairment, developmental delay, and behavioral problems[57,86,87].

Disease Presentation

MPS II patients present disease symptoms at variable ages. Generally, somatic disease manifestations start before the second year of life and neurologic manifestations within 2-4 years[87,90]. Patients with MPS II often appear normal at birth, although those

with neuronopathic MPS II may be heavy, develop hernias, and/or display Mongolian blue spots[87,91]. Those with neuronopathic MPS II reach early cognitive milestones until 36-42 months of age, when development begins to stall[92]. A variety of somatic manifestations can manifest depending on the patient. Most common is the coarsening of facial features. Inguinal and umbilical hernias are quite common and require surgical intervention[86,93]. Large amounts of GAG storage material leads to hepatosplenomegaly, and thus a distended abdomen, in most patients[94]. Enlargement of the tonsils, adenoids, and tongue can occur, leading to difficulties swallowing and eating[94,95]. Food intake becomes restrictive until finally gastric feeding tubes are required[95]. Epidermal symptoms, such as thickened skin with pebble formation and Mongolian spots occur in a small number of patients[91,96]. Although corneal clouding is not part of MPS II symptomatology, mild vision loss can happen because of changes in field of vision[97]. Conductive and sensorineural deficits lead to hearing loss, which arise in most cases of MPS II[57,94,95]. Otitis media is also common[87]. GAG accumulation impacts connective tissue and in combination with skeletal abnormalities leads to arthropathy. This manifests as joint stiffness, pain, and range of motion restriction[87]. Most MPS II patients exhibit poor growth and short stature[57,98]. Periodic episodes of watery diarrhea occur in MPS II[87]. The suggested cause of these episodes is GAG storage interfering with neural cells of the gastrointestinal system. Other manifestations, which are discussed below, include respiratory complications, cardiovascular problems, skeletal abnormalities, and neurological impairments.

Morphology

While infants with MPS II are born without much disease morphology, coarse facial features (sometimes called facial dysmorphia) can manifest within 3 years[87,94]. Thickening of the alae nasi, lips, ear lobes, and tongue becomes apparent. These are associated with trouble communicating and eating[95]. Other facial aspects include large jowls, flared nostrils, and a broadening of the calvaria[87]. This can lead to macrocephaly features that are present throughout life. A ruddy or rosy colored complexion can develop. Shortness of stature begins around 4 to 5 years of age in MPS II cases[94]. Distension of the abdomen, caused by organomegaly, can appear. Hypertrichosis on the face and body can emerge, with the hair often becoming coarse and straight[87]. Mongolian spots on the skin of MPS II patients, especially those of Asian, Hispanic, and African descent[91,86]. Additionally, ivory white papular skin eruptions of 2-10 mm in diameter are a distinctive trait of MPS II[96].

Skeletal Manifestations

There are wide variety of skeletal dysplasias, often grouped together and termed dysostosis multiplex, in MPS II[94]. These manifest in 80% of cases with a median onset of four to seven years of age[100]. Radiographical analysis reveals that nearly all bones show thickening[63,94]. Joint and skeletal complications have been attributed to dysfunction in chondrocytes and osteoblasts[87]. Additionally, GAG storage accumulates in connective tissue, cartilage, and bone which impacts joint and skeletal function[100]. Inflammation likely plays a role in the emergence of joint and skeletal manifestations[101]. Abnormal ossification and arthropathy occur in joints of the hand, shoulder, elbow, and hip[87,94]. Carpal tunnel syndrome is common and can result in loss of function in the affected

hand[57]. Ribs and clavicles are thickened and take on irregular shapes[94]. Hips joints are particularly sensitive, and severe hip dysplasia restricts ambulation. Patients with hip dysplasias and a deformed pelvis are often wheelchair bound[87]. About 30% of MPS II cases have kyphosis[86]. Poor bone growth in the lumbar vertebrae results in wedging and displacement of the vertebral column. The nature of the skeletal manifestations means surgical interventions are not routinely undertaken in MPS II cases. While the most common surgery is carpal tunnel decompression, hip replacements and spinal decompressions are almost never conducted[100]. Arthropathy intensifies with age and impacts most joints, leading to stiffness and pain. The arthropathy can lead to a restriction in range of motion as well[94].

Cardiopulmonary Manifestations

Cardiac manifestations are prevalent in MPS II, affecting nearly all patients[93]. These cardiac manifestations emerge as early as 5 years of age and can be detected by echocardiography[87,94]. Cardiac valve disease in particular occurs in approximately 50% of MPS II cases[86]. Commonly, valvular hypertrophy will lead to mitral and aortic regurgitation and stenosis[87]. Valve replacement surgery is a potential surgical intervention for valvular disease. Other less common heart conditions include heart murmurs and cardiomyopathy, coronary artery occlusion, and hypertension[87,98,102]. Evidence suggests DS rather than HS accumulation may cause valve dysfunction[102]. MPS III, in which only HS accumulates, there is a remarkable absence of a cardiac phenotype. Conversely, MPS I, II, and VI accumulate DS and have a cardiac phenotype.

Additionally, MPS I and VI patients have both a higher ratio of DS to HS and a higher prevalence of cardiac manifestations compared to MPS II[86].

Nearly 100% of MPS II patients develop progressive respiratory disease and/or airway obstruction[86,94]. Upper airway infections such as pneumonia occur frequently and cause rhinitis and nasal discharge[87]. Contributing factors to airway obstruction are the weakening and narrowing of the trachea, vocal cord thickening, increased mucosal secretions, and enlargement of tonsil, adenoids, epiglottis, and the tongue[87,94]. Surgical removal of the tonsils and adenoids is commonly carried out to ease airway obstruction[87]. Other clinical features, such as distended abdomen and joint stiffness contribute to breathing difficulties[94]. Because of respiratory manifestations, patient breathing is loud. These breathing issues become prominent at night and evolve into obstructive sleep apnea[103]. This leads to hypoxic episodes, but treatment with positive airflow from a CPAP machine can alleviate these problems[104].

CNS Manifestations

CNS manifestations occur in approximately 2/3rd of MPS II cases[87-89,95]. A fall off from developmental milestones begins between the ages of 2 and 4[94,105]. Complete arrest of development occurs between the ages of 5 and 8[92,94]. Behavioral issues, such as hyperactivity and aggression are common[93,94]. As the disease progresses, CNS manifestations severely handicap the patient to the point where they require a full-time care giver[87]. Once handicapped, behavior becomes hypoactive in patients[95]. Variable ability to sit, walk, and speak impacts self-sufficiency and communication skills[93].

Magnetic resonance imaging (MRI) scans reveal a variety of structural changes to the brain. Extensive decrease to brain white matter volume and development occurs, including signs of brain atrophy[106-108]. Impaired CSF maintenance leads to hydrocephalus, large perivascular spaces, and ventriculomegaly[108,109]. Seizures are reported in greater than 50% of cases[86,94]. Spinal cord compression, from the narrowing of the spinal canal, results in cervical myopathy and transverse ligament hyperplasia[110]. If left unaddressed, permanent spinal cord damage can occur. Although sleep apnea from airway obstructions is the main cause of sleep disturbances, neurologic manifestations can impact sleep with seizure like activity[111].

Hearing loss is nearly ubiquitous in MPS II[86,95]. The loss is both conductive and sensorineural in nature[112]. Causes of the loss include middle ear dysostosis, tympanic membrane scarring, Eustachian tube dysfunction, and nerve damage[87].

Elevated intracranial pressure from hydrocephalus can contribute vision problems[86,94]. This includes optic disc swelling, atrophy of the optic nerve, and retinopathy[113]. Retinopathy can lead to decreased peripheral vision and poor dark vision[87]. Exophthalmos and hypertelorism can result in some corneal problems, such as abrasions, but clouding is almost never seen[114]. Pigment changes and glaucoma rarely occur[114].

Non-neuropathic cases of MPS II exhibit essentially no CNS manifestations. In terms of development, they reach normal milestones and levels of intelligence[94,115]. Nonetheless, MRI scans show white matter abnormalities in the brain[106]. Seizures have

also been reported in these cases[115]. Difficulties in motor skills, executive function, and behavior have been noted as well[107]. Overall, this suggests that while there are no development issues in non-neuronopathic MPS II, the brain is nevertheless impacted by the disease.

Death

MPS II patients that develop extensive and severe CNS manifestations often die early in life. Most neuronopathic MPS II patients will die in their teenage years, aged 10-15 years[57]. While neurological degeneration plays a role, the cause of death is generally attributed to airway obstruction or cardiac failure[87,94]. Specific common causes are valvular disease, myocardial thickening, hypertension, coronary artery narrowing, and myocardial disease[57]. Those with non-neuronopathic forms of MPS II can expect to survive into adulthood. Survival depends upon the severity of the somatic symptoms, particularly the cardiac and respiratory manifestations. Patients with extensive complications usually live two to three decades, while those with milder symptoms can live up to five or six decades[57,87].

Diagnosis

Diagnosis of MPS II is difficult, as many clinical features manifest in related MPS, LDs, and non-lysosomal diseases. As such, differential diagnosis is required to accurately identify the disease. Further issues arise with the fact that MPS II cases can show variable phenotypes, even those with the same underlying genetic mutation. Generally, the first sign of the disease begins with recognition of coarse facial features.

Lack of family history related to MPS II makes diagnosis difficult[94]. These issues with accurate diagnosis work against the need to provide treatment as early as possible[58]. For those with a known family history, prenatal diagnosis is possible. IDS activity assays can be carried out with samples of amniotic fluid or in chronic villus tissue[116,117]. Fetal sex determination in combination with enzyme activity can also assist in prenatal diagnosis[118]. Non-neuronopathic MPS II is diagnosed within 3-4 years of age but can go undiagnosed until age 8[87,119,120]. Neuronopathic MPS II is diagnosed much earlier, due to the severity of the disease, at 18 to 36 months of age[87].

Newborn screening has been proposed as a method to improve the time to diagnosis, and thus hopefully time to treatment for MPS II patients[121]. The screening takes the form of an enzyme activity assay or GAG quantification. Fluorometric based assays or mass spectrometry have been used to screen for IDS[122,123]. Tandem mass spectrometry (MS/MS) has also been used for GAG detection and quantification[124-126]. MPS II was recently added to the recommended uniform screening panel (RUSP)[127].

Biochemical Testing

Diagnosis of MPS II through biochemical means is carried out by two main approaches, IDS enzyme activity and GAG analysis[58,94]. The enzyme activity assay uses patient samples, such as fibroblasts, leukocytes, plasma, or serum[58]. Dried blood spots have also been used for determining enzyme activity[123,128]. The activity of one or more sulfatases is also confirmed to rule out related disorders such as multiple sulfatase deficiency[87,94]. While most patients will show no activity, some non-neuronopathic and

female carriers will show low levels of activity[94,129]. Enzyme measurements are either made using a fluorometric substrate (4-methylumbelliferyl-α-L-iduronate-2-sulfate) or more recently by HPLC mass spectrometry[130,131].

Quantification of GAG levels is carried out by dye-based assay, or more precisely with mass spectrometry[132-136]. Elevated levels of GAGs are excreted in the urine and are thus a common sample for GAG analysis. The dye-based assay consists of dimethylmethylene blue (DMMB) that can bind to GAGs in a given sample. A colorimetric readout via spectrophotometry is then used to quantify GAG levels[132-134]. This is often followed up by electrophoresis of GAGs for a readout of which specific GAGs have accumulated[137]. More recently, tandem mass spectrometry (MS/MS) has been used for rapid and precise GAG quantification in patient samples[135,136]. These are generally urine or blood samples, but CSF has been used to quantify elevated GAGs[86,138]. Readouts from either method determine GAG composition and an excess DS and HS may indicate MPS II. Elevated GAGs indicate MPS I, II, or VII. Thus, additionally testing must be done by enzyme activity assay and/or gene analysis[57]. The lack of elevated urine GAGs does not necessarily rule out a Hunter syndrome diagnosis[94].

Genetic Testing

Genetic testing is undertaken after biochemical tests have indicated Hunter syndrome as a possible diagnosis. Sequencing of the *IDS* gene gives a direct mutational readout and is a reliable way to confirm an MPS II diagnosis[57,94]. Rapid molecular diagnosis of MPS II was first carried out in the 1990s using PCR amplicon sequencing[139]. PCR based methods rely on amplification of the *IDS* gene at the 3’ and 5’ exon

boundaries, followed by Sanger sequencing. Newer methods of genetic testing have been implemented for the identification of MPS II mutations that are more complex, such as splice variants or structural mutations. These analyses include mRNA analysis, next generation sequencing, and whole exome sequencing[140-142]. The presence of a pseudogene, *IDSP1*, should be taken into account for genetic testing[143]. By identifying mutations at the *IDS* locus in a Hunter syndrome patient relatives can be offered carrier testing and genetic counseling[58].

IDS Gene Characteristics

In Hunter syndrome, insufficient IDS is caused by mutations at the *IDS* locus. The human *IDS* gene spans approximately 24 kb and includes 9 exons[87,94]. The gene is located on the X chromosome and mapped to the long arm, at Xq28[144]. The 5' promoter sequence of the gene includes multiple CpG islands and binding sites for at least five transcription factors[144,145]. As a housekeeping gene, the promoter lacks a TATA box, but has GC box consensus sequences[75,146]. The 3' untranslated region is recognized by five known miRNAs[147]. These regulatory features possibly contribute to the differential gene expression across tissue types, the highest of which is found in the brain[144,145]. *IDS* cDNA is 1653 bp in length. Four mRNA species have been identified. The gene encodes a polypeptide of 550 amino acid in length.

Over 660 mutations in the human *IDS* gene have been detailed[144]. Missense and nonsense mutations comprise nearly half of all recorded variants. Mutations in splice sites, insertions, and deletions account for nearly 40% of variants. The remaining

mutations consist of large structural changes, such as large insertions, large deletions, and rearrangements[144]. Rearrangements are often due to recombination with a pseudogene, *IDSP1*[94]. *IDSP1* is located about 20 kb from *IDS* with homology to exons 2, 4 and introns 2,3, and 7[87,144,148].

Genotype-phenotype correlation is challenging due to the high rate of private mutations, poor numbers for cohort analysis, and phenotypic variability in MPS II cases with identical mutations[94,109,144]. Nonetheless, several studies have investigated the possibility of such correlations[149-153]. Overall, no definite correlations have been made. One exception to this are large structural mutations which are associated with neuronopathic MPS II[154].

IDS Enzyme Structure and Function

IDS gene expression can lead to 3 different isoforms (A, B, and C) that vary at their C terminus. Enzyme synthesized from the A isoform produces the canonical form of IDS, and deficiency in this form causes MPS II[144]. The IDS enzyme is 550 amino acids in length with a mass of 76 kDa. Post-translational modifications in the Golgi convert this to a 90 kDa form[144]. Maturation of the enzyme consists of two proteolytic cleavages that occur at the N terminus. The first cleavage removes a signal peptide (amino acids 1-25)[144]. The second cleavage event removes an eight amino acid (26-33) propeptide[144]. This mature enzyme has two domains, SD1 and SD2. SD1 is the larger of the two at 55 kDa (42 kDa deglycosylated)[144,155]. SD1 is termed the heavy chain that is formed from amino acids 34-443. The light chain domain, SD2, is 18 kDa (14 kDa deglycosylated)

and is comprised of amino acids 455-550[144,155]. Amino acids 444-454 form a disordered loop connecting the two domains[155].

As a lysosomal hydrolase, glycosylations and phosphorylations are crucial post-translational modifications to IDS. *N*-linked M6P glycosylations are attached at 8 asparagine residues[156]. The most important of these is at Asn280, where the M6P modification is essential for trafficking IDS to the lysosome[157]. Vital to IDS activity is the alteration of a cysteine in its active site, Cys84. In the ER, SUMF1 converts the cysteine residue to a formylglycine residue, a modification that is conserved across human sulfatases[144]. Other structural features include 2 disulfide bonds at Cys171-184 and Cys422-Cys432[155].

IDS functions as the first step in the catabolism of DS and HS. The enzyme catalyzes the hydrolysis of a C2 sulfate ester bond. Specifically, it hydrolyzes the sulfate ester in the 2-*O*-sulfo-α-L-iduronic acid of both GAGs[144].

Heparan and Dermatan Sulfate Structure, Synthesis, and Function

HS and DS are the two GAGs which accumulate in MPS II patients. GAGs are a group of linear, heterogenous, and polar sulfated glycans that are composed of repeating disaccharide units[158]. Each disaccharide unit consists of alternating hexosamine and uronic acid[158]. The uronic acid is either β-d-glucuronic, α-l-iduronic acid, or galactose which can be incorporated instead. The hexosamine can be either glucose based (α- or β-d-glucosamine) or galactose based (N-acetyl-β-d-galactosamine). Generally, there are six types of GAGs: chondroitin sulfate, keratan sulfate, heparin, heparan sulfate, dermatan

sulfate, and hyaluronan[57]. Dermatan sulfate is composed of N-acetyl-β-d-galactosamine and uronic acids[159]. Heparan sulfate contains α- or β-d-glucosamine and uronic acids[160].

Synthesis of GAGs begins by linking four core monosaccharides together[160]. Subsequent disaccharide addition to this core elongates the chain. Two glycosyl transferases located in the Golgi apparatus are responsible for this process, EXT1 and EXT2[161,162]. These two enzymes work as a heteromeric complex. Next, several sulfotransferases and epimerases associate to form oligomeric complexes that modify the polysaccharide chain[163,164]. HS undergoes C4 or C6 sulfation on α- or β-d-glucosamine and C2 or C3 sulfation on the uronic acid. For DS, there is sulfation of the C2 carbon of α-l-iduronic acid as well as C4 and C6 carbons of N-acetyl-β-d-galactosamine[165]. GAGs are biosynthesized while attached to the core protein, forming a proteoglycan. DS and HS are attached at a serine residue of core proteins, such as syndecans and glypicans[158,165]. Proteoglycans can vary greatly, as variable place of monosaccharides, chain length, and sulfation levels results in complex structures[164].

HS is a core component of the extracellular matrix (ECM). There, HS plays a role in several cellular processes, such as water accumulation, mechanical support, cell signaling, growth, immune cell regulation, and viral cell entry[166-169]. DS is a part of cartilage, connective tissues, bones, and skin[86,170]. In these tissues, DS plays a role in water accumulation, mechanical support, cell growth and signaling, pathogen infectivity, and inflammation[171]. The complex structures contribute to their wide-ranging involvement in biological processes.

Heparan and Dermatan Sulfate Degradation and Pathology

HS and DS are removed from the core protein by heparanase and chondroitinase B, respectively[57,172]. Once the polysaccharide is free of the core protein, degradation occurs in a stepwise fashion from the non-reducing end (Figure 1)[57]. HS degradation is carried out by 3 glycosidases, 1 acetyltransferase, and 3-4 sulfatases[57]. The order of these enzymes for degradation is iduronate-2-sulfatase, α-L-iduronidase, heparan-N-sulfatase, acetyltransferase, α-N-acetyl glucosaminidase, glucuronate sulfatase, β-glucuronidsase, and N-acetyl glucosamine 6-sulfatase[57]. Deficiencies in these enzymes lead to MPS II, MPS I, MPS IIIA, MPS IIIC, MPS IIIB, no known disease, MPS VII, and MPS IIID[58]. 3 glycosidases and 2 sulfatases are needed to degrade DS[57]. The enzyme sequence for degradation is iduronate-2-sulfatase, α-L-iduronidase, N-acetylgalactosamine 4-sulfatase, β-hexosaminidase, and β-glucuronidase[57]. Hyaluronidase may also play a role in DS degradation. Deficiencies in these enzymes lead to MPS II, MPS I, MPS VI, Sandhoff disease and Tay-Sachs disease, and MPS VII[58].

MPS II patients accumulate more HS than DS (that is, the ratio of HS to DS is >1)[86,173]. This is reflected in CSF GAG analysis, and indicates the brain accumulates more HS than DS[174]. HS has been implicated in the CNS manifestations of MPS II, including neurodegeneration and seizures[86]. Patients with lower levels of sulfated HS have less severe CNS manifestations[175]. Elevated HS contributes to dysfunction in neuronal growth, differentiation, neurotransmission, and glial cell scaffolding[165]. In the ECM, HS binds to growth factors, such as fibroblast growth factors (FGFs) the signaling of which is likely altered[108,176]. FGF1 activation by HS may be a possible explanation for

the papular skin eruptions in MPS II [99]. Improper HS sulfation leads to abnormal neuronal proliferation and survival. Increased HS activates inflammatory responses in the CNS, such as toll-like receptors (TLRs) and interleukin receptors[101]. There is also evidence for inflammasome activation in the brain[177]. HS binds tau and alpha-synuclein, and is associated with several other neurological diseases, such as Alzheimer's disease and Parkinson's disease[178-180]. Clearance of HS from the brains of MPS II mice was reported to prevent neurocognitive impairment[181]. Thus, HS accumulation may contribute to aging related neurodegeneration.

DS is associated with somatic manifestations, such as coarse facial features, dysostosis multiplex, joint stiffness, and arthropathy. It likely also plays a role in liver pathology of MPS II patients[182]. DS binds growth factors and cytokines, which is disrupted in MPS patients[171]. DS induced inflammatory cytokines, nitric oxide production, and innate immunity activation contribute to arthropathy in MPS II patients[183]. DS may potentially activate adaptive immunity through CD3+ T cells[184]. Increased chondrocyte apoptosis from inflammatory and mechanical stresses exacerbates bone and joint problems[185]. Aberrant transforming growth factor-β (TGF-β) and bone morphogenetic protein (BMP) signaling may contribute to skeletal manifestations as well[186]. Evidence for tumor necrosis factor-α (TNF-α) induced pain and physical disability has also been reported[187]. Overall, levels of HS and DS are about six times higher in MPS II patients than controls[188]. The pathology of elevated HS and DS on a cellular level is so far understudied in MPS II.

Palliative Interventions

Palliative treatments for MPS II center on supportive interventions related to the signs and symptoms of the disease[87]. Management is typically challenging due to the complex nature of the disease, which requires monitoring and management in several arenas[189,190]. Following a thorough diagnosis, several specialists are generally required to address patient symptoms[87]. Disease monitoring and management accomplished through medications, surgical interventions, and physical/occupational therapy[170].

Somatic manifestations require palliative interventions, especially those that are unaddressed by ERT. MPS patients often undergo surgery at a young age. The Hunter Outcome Survey reported 83.7% of MPS II patients received surgical interventions, with a median age of 2.6 years of age[191]. Inguinal and umbilical hernias require clinical examination and are treated surgically[170,190]. Diarrhea can be controlled with diet and antimotility agents[87]. Because daily activity and walking is impaired with MPS II, monitoring is accomplished with range of motion tests, the 6-minute walk test (6MWT), and clinical examination[170,189]. Generally, joint and skeletal manifestations can be combated with physical/occupational therapy[170]. Issues with knee ligaments, such as the genu valgum, may need surgery[170]. Splints can be used to treat joint contraction[170,190]. Skeletal manifestations are monitored with clinical examinations. Abnormal ossification and thickened joints mean surgical interventions are difficult[189,192]. Surgery for hip dysplasias is particularly challenging, due to pelvis deformation[87]. Nevertheless, hip replacements, knee replacements, arthroscopy, and dental procedures are occasionally undertaken[100,170]. Cardiac manifestations are monitored by echocardiogram and MRI[170].

Valve disease is addressed by valve replacements in about 50% of MPS II cases[170,193]. Monitoring of respiratory manifestations and airway obstructions is accomplished by sleep studies and clinical examinations of the airway[87,170]. CPAP machines are suggested for those struggling with sleep apnea[104]. Tonsillectomy and adenoidectomy are commonly performed in cases of MPS II[87]. Respiratory physical therapy can also be considered, and those with severely progressed disease can be placed on ventilation[87,94,170].

Neurological manifestations can be evaluated by cognitive testing[170]. Seizures, hydrocephalus, and spinal cord compressions can be monitored by MRI[170]. Several palliative care options are available for MPS II CNS manifestations. Patients can be placed into stimulating environments, speech therapy, and special schooling[194,170]. Behavioral issues can be tackled with antipsychotics and behavioral therapy[194]. Seizures can be treated with anticonvulsants[195]. Shunts can be implanted to address hydrocephalus[170]. Spinal cord compression requires decompression surgery to prevent loss of motor function[196]. Ultrasound and nerve studies can be carried out to monitor carpal tunnel syndrome and decompression surgery is required to relieve pressure on the median nerve[197,198]. Left untreated, loss of hand sensation or function is possible. Hearing loss and otitis can be tracked by audiological and otological assessments[170]. Hearing aids and drainage tubes are supportive interventions for these symptoms[199]. While ocular manifestations are rare in MPS II, retinopathy can manifest and is corrected by surgery[57,114].

Enzyme Replacement Therapy (ERT)

Enzyme replacement therapy is the administration of recombinant enzyme to compensate for enzyme deficiency in a patient. The idea of administering exogenous enzyme for metabolic disorders goes back to the 1960s and 1970s[200,201]. Isolation of protein from human tissues, such as placental tissues, proved difficult for MPS II because of degradation and low enzyme abundance[189]. Early attempts of replacement therapy included plasma, serum, and leukocyte infusions[202,203]. After the development of recombinant DNA technology, ERT for MPS II became an FDA approved treatment option in 2006[76,77]. The approved enzyme is idursulfase (Elaprase®) and is administered weekly by intravenous infusion at 0.5 mg/kg[204,205]. Another recombinant IDS enzyme, idursulfase beta (Hunterase), was approved for treatment in South Korea in 2012[170,189].

Idursulfase is produced in the HT-1080 human cell line[87,94]. These cells were transfected with an expression plasmid encoding the full 550 amino acid *IDS* cDNA[76,77]. Analysis of the purified protein reveals that the 8 *N*-linked glycosylation sites contain M6P motifs, crucial for host cellular uptake of the administered enzyme[76,77,87]. Further analysis confirmed modification of Cys84 to a formylglycine residue[76,77].

ERT with idursulfase is beneficial in alleviating some systemic manifestations of MPS II. Improvements in spleen and liver volumes, cardiopulmonary function, gastrointestinal control, epidermal manifestations, coarse facial features, joint mobility, ambulation, and sleep have been reported[86,76,77,204,206-212]. Phase I/II trials showed reduced urine GAG excretion and hepatosplenomegaly after 24 weeks[77].

Treatment with ERT for 1 year in phase II/III trials demonstrated decreased urine GAG excretion, reduced hepatosplenomegaly, and increased walking during the 6MWT[76]. A following study confirmed these 6MWT improvements seen with ERT[206]. Further early studies of ERT revealed improved respiratory function, a reduction in the frequency of respiratory diseases, and cardiac valve disease in MPS II patients[208-210]. There is evidence that ERT can increase survival in MPS II patients[170,204,212]. ERT with idursulfase is accepted as safe and well tolerated in MPS II patients[189]. The most common side effects are infusion related adverse reactions[211,213].

Despite improved outcomes in MPS II patients, ERT has several limitations. Families face practical burdens associated with the ERT protocol. Weekly hospital visits for enzyme infusions are time consuming for families, although in some countries home treatment with idursulfase is becoming more feasible[170,189,215]. Additionally, the annual cost of ERT is exceptionally high, at around $500,000 USD[170,214]. An efficacy issue in patients is immunoreactivity to the recombinant enzyme. Patient immune systems will recognize idursulfase as a foreign antigen and mount an immune response that neutralizes the enzyme and prevents it from exerting its therapeutic effect. Reports on immunoreactivity show 50% of treated patients generated anti-idursulfase IgG antibodies, a third of which were neutralizing[216,217]. These neutralizing antibodies were associated with lower treatment efficacy[217]. Contrary to some early evidence, a 9-year follow-up study showed no benefit to respiratory function, skeletal dysplasias, or neurocognitive function[211]. Why does ERT fail to improve of some systemic manifestations, such as those found in skeletal, cardiac, and connective

tissues[218]? A proposed explanation for this suggests the low vascularity of these tissues means low bioavailability of the infused enzyme[8,189]. A secondary explanation is that differential tissue expression of the M6PR leads to lower enzyme uptake in some tissues[170,219]. A central challenge for ERT is addressing the CNS manifestations. Idursulfase administered intravenously does not cross the blood-brain barrier (BBB), and thus is not available for metabolic cross correction in the CNS[8,170]. As such, cases of neuronopathic MPS II receive no benefit from ERT neurologically[220,221]. Studies in the MPS II mouse model have suggested a small percentage of recombinant IDS can cross the BBB, but that the dose administered by ERT is too low for the this to occur[318].

Modified ERT Protocols

Modified ERT consist of alternative routes of administration (ROA) and fusion proteins. CNS directed ROAs, such as intrathecal (IT) and intracerebroventricular (ICV) administrations have been tested in animal models. Positive data for addressing the CNS manifestations was observed, including improved cognitive function and GAG reduction[222,223]. Recently, a clinical trial extension (NCT01506141) evaluated IT administration of idursulfase for neuronopathic MPS II[224]. While CSF GAG content was decreased, patients showed no cognitive stabilization[224,414]. Other similar trials evaluating IT administration of idursulfase resulted in little to no beneficial effects[86]. In contrast, a Japanese clinical trial showed promising results by ICV administration of idursulfase-beta[225]. Worth noting here is the side effects of frequent IT or ICV administration, which have caused nearly half of enrolled patients to leave trials[189,226]. These are unrelated to the enzyme but rather the drug delivery devices. BBB penetrable ERT fuses IDS to

another protein that can induce receptor mediated transcytosis in endothelial cells, releasing the fusion protein into the brain parenchyma[170,227]. Clinical trials involving the fusion of IDS to an anti-transferrin receptor antibody or transferrin peptide were initiated by two companies, JCR Pharmaceuticals and Denali Therapeutics. In mice, JCR Pharmaceuticals reported transferrin-based fusions showed detectable brain IDS activity and a concomitant GAG reduction[228]. A JCR Pharmaceuticals phase I/II clinical trial reported decreased HS levels in the CSF of MPS II patients[229]. Phase II/III trials also demonstrated improved neurocognition in MPS patients[230,231]. The Denali Therapeutics trial is still ongoing[170]. ArmaGen Technologies conjugated IDS to an anti-insulin receptor antibody for its clinical trial. It showed promising results in rhesus monkeys, but no trial results have been published as of yet[232,233].

Hemopoietic Stem Cell Transplantation

Cellular therapy as a source of IDS for MPS II patients has taken several forms. Implantation of IDS overexpressing myoblasts, fibroblast transplantation, human amnion membrane implantation, leukocyte infusions, and hematopoietic stem cell transplantation have all been tested in animal models and/or clincally[203,235-238]. Most of the research has focused on HSCT, with hematopoietic stem cells sourced from either bone marrow or umbilical cord blood[189]. Essentially, HSCT for Hunter syndrome relies on engrafting donor-derived cells (which are enzymatically competent) as a permanent source of functional IDS[213]. In addition, it has been shown that donor-derived cells can transit the BBB and differentiate into microglia that become a source of functional IDS in the CNS[38,239]. Donor cell localization to the brain has been reported in mice and humans,

with cells located in the perivascular spaces and brain parenchyma[38,239]. A successful transplant would result in a lifelong and durable treatment from a onetime procedure[170]. This would reduce time and financial costs for patient families significantly by reducing the reliance on ERT[189]. Unfortunately, HSCT comes with a myriad of safety concerns. An inherent disadvantage to allogeneic HSCT is the possibility of graft vs. host disease (GvHD)[62,240]. GvHD can result in organ failure and subsequently a patient's death[62]. Immunosuppressive regimens given to ensure donor cell engraftment can result in damage to other tissues and even oncogenic events[62,240]. Recurrent infections are also an issue[62]. Lastly, disease progression can place MPS II patients at risk of death from transplant[62]. However, in recent years, the safety of HSCT procedures has improved and death rates have dropped to below 5%[192,241]. Some studies have reported 100% survival for HSCT in MPS II patients, albeit with a GvHD rate of 41%[62,242].

Initial reports of HSCT in neuronopathic MPS II patients were not positive[58,87,243,244]. In particular, the neurological outcomes were poor[243,244,245]. This combined with risks associated with transplantation means HSCT is not considered a standard treatment for MPS II, as least in Western countries[86,189]. However, there is renewed interest in HSCT for MPS II. After evidence of donor-derived cells reaching the brain, several case studies evaluated the treatment of MPS II with HSCT[239]. HSCT treated many systemic manifestations, including reduced urine GAG excretion, reduced hepatosplenomegaly, increased growth, amelioration of epidermal manifestations, improved cardiopulmonary function, decreased apnea, and a higher level of daily activity[242,245-253]. The impact of HSCT on the joint stiffness, arthropathy, and skeletal

manifestations for MPS II is unclear, with some cases reporting improvements, while others do not[242,247,253]. More recent studies detail HSCT as an effective treatment for stabilizing neurocognitive function in MPS patients. One long term study reported decreased brain atrophy and reduced brain lesions[250]. Importantly, these findings only held true for patients who had no established neurocognitive deficits. One report showed cognitive stabilization in patients treated early, but that HSCT toxicities and musculoskeletal problems persisted[251]. A 2017 combined study and meta-analysis described 146 MPS II patients that received HSCT[254]. Most patients were found to improve or show no progression neurologically by brain MRI. Based on these new data, HSCT is an approved treatment option for MPS II in Brazil, China, and Japan[62,242,246,248,250,254]. Why the difference in outcomes between older and newer studies? Recent advances in the safety of HSCT have certainly impacted this[62]. Additionally, earlier studies may have used suboptimal cell sources[238,244,245]. Patient age and disease progression may have also played a role, as treating later does not reverse neuronal damage, and only stabilizes neurodegeneration[170]. Treating MPS II with ERT and HSCT is potentially more effective than either alone. In one study, ERT/HSCT combination led to a greater GAG reduction than either ERT or HSCT exclusively in dried blood samples[254]. ERT is also unlikely to alter donor cell engraftment in transplant recipients, based on data from an MPS I study[255]. In fact, one investigation described a case where an IgG antibody response nullified the therapeutic effects of ERT[254]. The patient displayed improved somatic outcomes after treatment with HSCT. Thus, HSCT is a possible treatment option for those unable to receive on ERT[62,254].

Substrate Reduction and Other Possible Treatments

Substrate reduction therapy (SRT) aims to prevent the accumulation of storage material, HS and DS for MPS II, by partially inhibiting the rate of their biosynthesis[170,189]. Often SRT takes the form of a synthetic analog of synthesis intermediates to inhibit GAG biosynthesis[170,189,256]. SRT is an approved treatment option for other LDs, but is not for MPS II[170,189]. In 2006 a soy isoflavone, genistein, showed efficacy in reducing GAG storage in MPS II fibroblasts[257]. Genistein may exert its substrate reduction effects either by epidermal growth factor receptor inhibition or correction of cell cycle dysfunction[258,259]. A mouse model of MPS II given genistein showed reduced GAG levels in a variety of tissues[260]. A small MPS II clinical study showed improvement in joint stiffness[261]. However, poor results in a related trial of MPS III patients has stymied development for MPS II[213,262]. Inventiva Pharma has developed Odiparcil, a substrate analog that inhibits DS synthesis[263]. However, trials are only being run for MPS VI patients[170].

Other possible treatments include pharmacological chaperone therapy (PCT), anti-inflammatory therapy, umbilical cord blood derived myeloid cells, and encapsulations. Some IDS mutations lead to misfolded proteins, their subsequent ER/Golgi aggregation, and eventual degradation by the ER-associated degradation pathway[53,189,264]. PCT avoids this by introducing a small molecule that interacts with misfolded proteins and assists in proper folding and/or trafficking[53]. MPS disorders have been considered good candidates for PCT, as modest increases in enzyme activity can improve outcomes[265]. One PCT has been investigated for MPS II, D2S0, a sulfated

disaccharide derived from heparin[266]. A study of D2S0 reported a minute increase in enzyme activity in fibroblasts expressing mutant IDS[266]. Anti-inflammatory therapy suppresses the role of inflammation as a mechanism of disease[183-185,192]. Little work has been done in this area for MPS II, but some drug studies have been carried out for related MPS diseases[192,267,268]. Transplantation of umbilical cord derived myeloid cells, also known as oligodendrocyte-like cells and DUOC-01, are under investigation for MPS II. Central to HSCT as a therapy for MPS diseases is microglia reconstitution in the CNS[38]. This process can take up to six months in mice and perhaps even longer in humans, meanwhile neurocognitive decline can continue during this period[38,269]. Decreasing the time required to engraft cells in the brain could stave off neurological deficits. DUOC-01 cells are CD14+ monocytes that resemble oligodendrocytes in morphology with remyelinating properties[270,271]. In conjunction with HSCT, these DUOC-01 cells are given IT to shrink the aforementioned gap in CNS reconstitution[271]. A clinical trial, (NCT02254863), is underway and recruiting patients to test this potential therapy for MPS II[86]. Cell encapsulations have also been given some attention as a potential therapy for MPS II. With this technology, cells are placed within a semipermeable matrix. This prevents immune cell interference, but also permits the exchange of nutrients and proteins, such as IDS[272]. Previously, implantation of encapsulated IDS overexpressing myoblasts in MPS II mice showed modest IDS activity and a concomitant GAG reduction[236]. However, the transplanted cells died within a few months[236]. More recently, MPS II mice implanted with alginate capsules containing cells overexpressing IDS exhibited continuous plasma IDS activity and tissue GAG reduction[273].

Models of MPS II

Many *in vitro* cell models of MPS II are available, either patient derived or lab generated[189]. Historically, patient derived fibroblasts were the model of choice to study MPS II[66-68]. The fibroblasts exhibit increased GAG levels and were used to establish both the biochemical basis of the disease and metabolic cross correction[65-68,274,275]. More recently, MPS II pathophysiology research and drug testing utilized the fibroblasts[259,276]. Other important cell models include neural stem cells (NSC) and induced pluripotent stem cells (iPSC). NSCs were derived from an MPS II mouse for studying the mechanisms of neurodegeneration[277]. Use of the model has identified abnormal neuronal differentiation, oxidative stress, impaired mitochondrial function, and increased apoptosis as mediators of neurodegeneration[277,278]. iPSC technology allows the reprogramming of differentiated cells to a more naïve state[279]. Several iPSC lines have been derived for studying disease pathology[280-286,319]. The first use of iPSCs to study MPS II was accomplished in 2016, with 4 distinct lines derived from patient peripheral blood mononuclear cells (PBMCs)[280-283]. These lines were differentiated into NSCs and further to cortical neurons to investigate storage vacuole pathology[284]. A separate group also used PBMCs to derive an MPS II iPSC line. The line was differentiated into neurons and glial cells that maintained increased GAG and lysosomal-associated membrane protein 1 (LAMP1) phenotypes[285]. Most recently, a third group derived NSCs from patient iPSCs with the purpose of evaluating small molecule drugs that can reduce storage material[286].

The mouse *IDS* gene shares high sequence similarity (86%) to the human gene and is located in a similar position on the X chromosome[147]. The mouse *IDS* gene is 22

kb in length and, like the human gene, the coding regions consist of 9 exons[147,302]. Murine IDS has 2 fewer *N*-linked glycosylation sites. The enzyme is 2 amino acids longer than human IDS, at 552[147].

MPS II mice have been the most widely used and important model of the disease. Four MPS II mouse models have been generated on a C56BL/6J background. The first was produced in 1999 by replacing a portion of exon 4 and the entirety of exon 5 with a neomycin resistance gene[293]. Further work in 2006-2007, highlighted both biochemical and pathological features of the mice[294,295]. Characterization revealed the absence of IDS activity, elevated urine GAG excretion, GAG accumulation in tissues, increased organ weight, skeletal manifestations, neurobehavioral deficits, and a shortened lifespan[293-295]. Neuronal vacuolization and death, along with increased LAMP1 and LAMP2 expression is seen in the brain[293-295]. Another MPS II mouse was generated in 2010 by deleting exons 2 and 3 and inserting a neomycin resistance gene[189,296]. Phenotypically, it is comparable to the first mouse model, and hearing loss was observed in the mice[296,297]. One study used it to interrogate neurological disease pathology and found reducing autophagy may prevent neuronal vacuolization[298]. A third model with exons 2 and 5 deleted was generated in Japan by JCR Pharmaceuticals[299]. It was characterized similarly as the previous mice and used to study ICV delivery of ERT[299]. Lastly, a fourth model was generated by Taconic Biosciences, with exons 2 and 5 knocked out[300]. This model was used to evaluate intracisternal administration of an *IDS* encoding adeno-associated virus vector 9 (AAV9)[300]. Recently, a novel NOG mouse model was developed in Japan to test human hematopoietic stem cell therapies for MPS II[301]. The authors engrafted

human CD34+ cells transduced with a lentiviral vector (LVV) encoding human *IDS* and observed amelioration of biochemical pathology.

Over the last 23 years, MPS II mouse models have been used to investigate disease pathology and carry out preclinical studies for therapeutics development. Using the mouse strain, one study reported that oxidative damage to glial cells contributes to neurodegeneration[278]. The impact of inflammation in the brain has been studied and shows undegraded GAGs activate the inflammasome[177]. Brain RNA-seq profiling of IDS deficient mice showed altered gene expression in several pathways, such as axon guidance, calcium homeostasis, circadian rhythm, inflammation, and Wnt signaling[303]. FGF dysregulation was associated with skeletal abnormalities in MPS II mice[290]. Because a great deal of research centers on addressing CNS disease manifestations, extensive neurobehavioral characterization has been carried out in at least one mouse strain[304]. MPS II mice were used in the preclinical studies that developed ERT, where they were dosed 0.1-1 mg/kg idursulfase[305]. Treatment with ERT reduced GAG accumulation and resulted in clinical trials that ultimately garnered ERT approval from the FDA[76,77]. Mouse models have also evaluated HSCT for MPS II[306-308]. One study assessed the impact of donor chimerism on treatment and observed a high level of engraftment was necessary to impact disease manifestations[307]. A second study evaluated anti-c-kit antibody mediated preconditioning for HSCT in MPS II mice and found it efficient for bone marrow transplants[308]. A third study administered hematopoietic stem and progenitor cells (HSPCs) ICV rather than IV and showed robust microglia engraftment in brain[309]. Other studies have examined micro-encapsulations, nanoparticles, SRT, and modified ERT as

potential therapies in MPS II mouse strains[228,231,234,236,260]. The MPS II mouse model has been invaluable for investigating potential gene therapies, both *ex vivo* LVV and *in vivo* AAV approaches, as well as gene editing and are discussed below[295,296,300,310-318].

Several other animal models of MPS II have been identified or generated. A naturally occurring canine model of the disease was discovered in 1998, showing elevated urine GAGs, hepatosplenomegaly, coarse facial features, osteopenia, corneal dystrophy, and neurological deterioration[287]. However, it was never used because it was euthanized before offspring were generated. Two zebrafish models have been developed to study MPS II. The first employed a morpholino based knockdown of the *IDS* ortholog in the fish. Morphants had altered TGF-β, SOX-10, and crestin signaling that mediated altered cartilage pattering[288]. Further, they found abnormal cardiac development in the fish was due to disruptions in the sonic hedgehog and Wnt/β-catenin signaling pathways caused by GAG accumulation[288,289]. A CRISPR/Cas9 *IDS* ortholog knockout zebrafish model was generated recently[290]. They found dysregulation of the FGF pathway that led to skeletal manifestations[290]. Lastly, wildtype zebrafish models have been used to study overexpression of mutant IDS by microinjection of mutant *IDS* mRNA[291]. The authors noted defective phenotypes and a dominant negative effect from the mutant IDS[291]. Lastly, a drosophila model of MPS II was generated in 2019[292]. RNAi was used for specific knockdown of global, neuronal, or glial cell populations. The model did not produce a phenotype, likely due to the incomplete abrogation of enzyme activity[292].

Gene Therapy for MPS II

Introduction to Gene Therapy

Gene therapy is any product or technology that mediates a therapeutic effect through the transcription and/or translation of genetic material that has been edited or transferred into the host cell[320]. Gene therapies necessarily require safe and efficient introduction of genetic material and/or editing reagents. To accomplish this, there are a wide variety of delivery modalities. There are two groups of delivery methods, viral and non-viral delivery[321,322]. Viral methods rely on a recombinant viral vector to deliver genetic material, either through chromosomal integration or existing as episomes. This includes, among others, retroviral vectors, LVV, adenoviral vectors, and AAV[321,323]. Nonviral modes of delivery depend upon either physical or chemical methods[324,325]. Physical methods include microinjection or electroporation of the genetic cargo[324,325]. Chemical methods take the form of lipid, polymer, or gold nanoparticles to encapsulate and deliver material[324,325]. Virus like particle systems are being developed that utilize minimal viral components to transduce cells but lack the viral genetic material present in viral vectors[326]. Nonviral vectors are used to deliver a variety of gene or gene expression modifying tools, such as DNA plasmids, minicircles, transposons, siRNA, and antisense oligonucleotides[322]. These methods all have advantages and disadvantages related to safety, production costs, cargo capacity, transduction/transfection efficacy, expression level, and activation of host immune response[327]. Besides delivery vehicles, the gene therapy can be administered through several ROAs depending on the target tissue. These include, but aren't limited to, intravenous (IV), intramuscular, intranasal, IT, intracisternal, and ICV[391-397]. Viral vectors have historically been the tools used for

therapeutic gene transfer. They have robust transduction efficiencies and the ability to target both dividing and non-dividing cells[321,327]. In addition, many viral vectors have been engineered to have improved safety[328]. These attributes aside, viral vectors suffer from several disadvantages. These include the difficulty and cost of manufacture, packaging limitations, immune reactions to the virus, and insertional mutagenesis (oncogenesis) and are discussed below[321,327].

LDs and MPS diseases have long been thought of as ideal candidates for gene therapy[213,329,330]. As monogenic disorders, they have a well-established molecular etiology. In addition, gene therapies for MPS diseases make use of metabolic cross correction through the M6P pathway which benefits cells not directly modified by the gene therapy (Figure 2)[213,329,330]. Lastly, only a small percentage of wild type enzyme is sufficient to improve clinical manifestations[213,329,330]. Gene therapy for MPS II transfers recombinant nucleic acids encoding a functional *IDS* gene to supplement the disrupted endogenous gene in a host cell. Gene therapies for MPS II have been tested using two main approaches, *ex vivo* gene therapy and *in vivo* gene therapy[331].

Ex Vivo Gene Therapy for MPS II

Ex vivo gene therapy entails the derivation of patient cells, genetically modifying them *in vitro*, and administering them back into the patient[331]. Strictly speaking, this approach is a cell therapy, a subset of gene therapy, as it relies on the infusion of genetically modified cells rather than delivering nucleic acids directly into cells *in vivo*. Most often these cells are lymphocytes or HSPCs transduced by retroviral vectors or

LVV[331,332]. Retroviral vectors and LVV are both based on viruses from the family *Retroviridae*[333-335].

Retroviral virions are spherical and enveloped, with a diameter of 80-100 nm[333]. Structurally, the virus particle is comprised of 2 envelope proteins, a transmembrane protein and a glycoprotein receptor, which can be glycosylated. The interior core structure of the virus is made up of matrix, capsid, and nucleocapsid proteins[333]. Other interior proteins include a protease, reverse transcriptase, and integrase. Inside the virion, the viral genome exists as a dimer of linear, positive sense, single-stranded RNA. The ssRNA has a 5' cap and 3' poly(A) tail, as it is synthesized by host RNA polymerase II. The RNA structure includes long terminal repeats (LTRs) at each end[333-335]. LTRs are several hundred base pairs in length and composed of U3, R, and U5 regions. U3 contains a promoter-enhancer that controls viral RNA transcription from the 5' LTR. R is a repeat sequence and can contain the poly(A) signal. U5 is positioned between R and a primer binding site. On the RNA is a primer binding site, where a tRNA binds to initiate reverse transcription[333,334]. The packaging signal (ψ) is a cis-acting element that regulates the incorporation of retroviral RNA into the capsid. The polypurine tract plays an important role in proviral DNA synthesis. Lastly, there is a rev response element which aids in nuclear export of RNA. The coding features of the provirus are ordered 5'-*gag-pro-pol-env-3'*[333-335]. The *gag* polyprotein encodes the matrix, capsid, and nucleocapsid structural proteins. *Pro* codes for the protease, essential for maturation of *gag* and *pol* proteins. The third coding domain, *pol*, includes the reverse transcriptase critical to viral DNA synthesis and an integrase required for viral DNA integration into the host genome. *Env*

encodes the glycoprotein receptor and transmembrane proteins. *Gag-pro* or *Gag-pro-pol* are often encoded as one polyprotein[334]. Viral entry is based on the viral surface glycoprotein and host cell receptors[333]. After endocytosis, the viral particles uncoat and reverse transcription of the viral RNA produces the provirus. Host machinery and possibly nuclear membrane breakdown are needed for nuclear entry of the provirus and proteins. Once in the nucleus, integrase inserts the provirus into the host genome[333-335]. Host RNA polymerase II then uses the provirus as a template to transcribe full-length genomic RNA. For lentiviruses, transactivators also play a role in transcription and nuclear export of RNA[334]. Following this, there is translation of viral proteins and nascent polyproteins are matured by proteolytic cleavage of the viral protease. Capsids assemble at the plasma membrane and are exocytosed from the cell in a budding process[333]. Retroviral vectors for gene therapy are based on the Moloney leukemia virus[336,337]. One potential disadvantage related to gamma retroviral vector efficacy is the need for nuclear envelope breakdown to complete integration. Thus, retroviral vectors require cell cycling to complete transduction[337,338]. Safety concerns for gamma retroviral vectors are related to preferential insertion near regulatory elements and transcription start sites[332].

Lentiviral vectors are derived from human immunodeficiency virus 1 (HIV-1) and have become a fundamental gene transfer tool. In addition to the aforementioned general retrovirus characteristics, lentiviruses have their own distinct morphology and accessory proteins. Structurally, their virion core structure is cone shaped. The lentivirus genome codes for several additional proteins: tat, rev, vpr, vpu, vif, and nef[333,334]. Tat is a transactivator that promotes transcription by binding to a tat responsive element located

in the R region[334]. Rev binds to the rev response element to aid in the exportation of viral RNA to the cytoplasm[334]. Vpr, vpu, vif, and nef are either regulate viral RNA or combat host antiviral factors[333]. Lentiviruses also have specific characteristics with regards to cell entry and integration. For cellular entry, lentiviruses bind to CD4 or CCR5 surface receptors and can efficiently transduce dividing and non-dividing cells because they are imported into the nucleus by the nuclear pore complex[332]. For integration, lentiviruses have shown preference to insert within transcriptional units of open chromatin[332]. The packaging capacity of lentiviruses is ~9 kb[333]. In the creation of modern LVV, the HIV-1 genome has undergone extensive engineering to improve safety[339-342]. Current third generation LVV production utilizes 4 plasmids to generate the necessary components[332]. Accessory proteins tat, vpr, vpu, vif, and nef have been removed for their nonessential role in lentiviral vector production[343]. The transfer plasmid encodes the promoter and gene of interest for gene therapy. Also on the transfer plasmid, the 5' LTR is chimeric and is fused to a heterologous promoter, such as CMV[332,343]. This eliminates the need for tat or the tat response element. The 3' U3 region is deleted to ensure transcription of the full-length provirus is abolished and the LVV is rendered replication incompetent and self-inactivating[343]. The transfer plasmid also incorporates a packaging signal and polypurine tracts. Packaging machinery is split into two plasmids[332,343]. The first contains *gag-pol* with a rev response element and the second encodes *rev*. The fourth plasmid codes for *env*, but is often pseudotyped with a sequence encoding vesicular stomatitis virus G (VSV-G). VSV-G binds the low-density lipoprotein (LDL)-receptor and confers broad tropism[344]. In addition, VSV-G can withstand the ultracentrifugation required to

concentrate the viral vector to high titers. LVV transduction of target cells provides long lasting expression of the therapeutic gene of interest[330-332].

Initial gene therapy studies for MPS II used Moloney murine leukemia retroviral vectors[345-347]. The first of these evaluated the transduction of patient derived lymphoblastoid cell lines by an *IDS* encoding retroviral vector[345]. They achieved supraphysiological levels of enzyme (10-70x) compared to wild type lymphoblastoid cells. GAG accumulation was also normalized in co-cultured MPS II fibroblasts, the first demonstration of metabolic cross correction using genetically engineering cells[345]. The same vector was used to transduce patient lymphocytes in a preclinical study[346]. Transfer efficiency was low (<5%), but enzyme levels were comparable to wild type lymphocytes and reduced cellular GAG accumulation was observed[346]. Transduced cell conditioned media was also used to demonstrate the potential for metabolic cross correction[346]. This work led to a clinical trial (NCT00004454) that was ultimately terminated. A second group also evaluated gamma retroviral vector transduction of human CD34+ cells[347].

Subsequent investigations of *ex vivo* gene therapy for MPS II utilized LVV based hematopoietic stem cell gene therapy (HSCGT). HSCGT relies on the engraftment of HSPCs that were transduced with a LVV encoding *IDS* cDNA[331]. HSCGT for MPS II is predicated on three key advantages. First, donor-derived cells will overexpress IDS and produce supraphysiological levels of IDS enzyme[348]. Importantly, this enzyme will be available for metabolic cross correction. Second, donor-derived cells of the monocytic lineage traffic to the brain and differentiate into microglia[38,348]. These genetically modified microglia secrete IDS for uptake by resident neurons. Third, the autologous

nature of HSCGT means it does not rely on an HLA-matched donor for HSPCs and avoids risks associated with GvHD[348]. A major limitation of HSCGT is that the integrative nature of the therapy poses the potential risk of insertional mutagenesis and subsequent oncogenesis[349]. Previous work has shown insertional mutagenesis in patients treated with genetically modified HSPCs can activate genes like *LMO2*, *MECOM/EVI1*, and *HMGA2* [350-355]. Patients with these mutations developed serious adverse events, including myelodysplastic syndrome and acute leukemia.[350-355.389].

Preclinical studies of HSCGT for MPS II began in 2015, when a Japanese group found HSCGT to improve most biochemical outcomes in MPS II mice[310]. This included supraphysiological levels of IDS and normalized GAG content in the liver and heart. An IDS level in the brain of 2.9% wild type mice was observed, and improvements in short term spatial memory were measured by the Y-maze[310]. However, some GAG content remained in the brain and many manifestations remained unstudied, such as skeletal abnormalities[310]. In 2018, one group evaluated HSCGT using a LVV encoding *IDS* under the control of a myeloid specific promoter, hCD11b[311]. In addition, they investigated fusing the IDS protein to an ApoEII receptor binding domain to assist in crossing the BBB. Mice exhibited supraphysiological levels of IDS activity and reduced GAG content in a variety of peripheral tissues. Reduction in the zygomatic arch, humerus, and femur diameters was seen. HS levels in the brain were reduced with the IDS construct and normalized with fusion construct. Brains of mice from both groups recorded lower levels of LAMP1, GFAP, and inflammatory cytokines. Mice showed better coordination and spatial working memory. Lastly, anti-hIDS antibodies likely did not impact the therapy,

as no increase in antibody production was measured[311]. This is consistent with a previous study that showed MPS II mice do not mount an immune response to hIDS[316]. In 2020 two HSCGT studies were reported. The first examined engraftment efficiency and its impact on the therapeutic efficacy of HSCGT[312]. By modulating the precondition regimen, the authors found supraphysiological IDS levels and reduced GAG content in several peripheral tissues. However, neurocognitive improvements were only seen in mice given a lethal dose of irradiation, suggesting the need for a high level of donor cell engraftment to treat neuronopathic MPS II[312]. The second study examined the pathology of the skeletal manifestations in MPS II mice and their amelioration by HSCGT[313]. Bone volume, density, strength, and trabecular number were significantly increased in MPS II mice. GAG accumulation interfered with bone metabolism in osteoblasts and osteoclasts[313]. HSCGT restored bone remodeling by these cells, and subsequently reduced bone density, strength, trabecular number, zygomatic arch diameter, and intermaxillary width[313].

In Vivo Gene Therapy for MPS II

Adeno-associated viruses are of the *Dependovirus* genus within the family *Parvoviridae*[358]. Productive viruses are dependent on co-infection of a helper virus, such as herpes simplex virus or adenovirus to complete their lifecycle[55,359]. Morphologically the virions have a nonenveloped, icosahedral capsid that is 20-26 nm in diameter[55,358]. In total, 60 viral capsid proteins (VP) comprise the entire capsid[358,359]. Three VP proteins comprise the capsid, VP1, VP2, and VP3, arranged in a 1:1:10 ratio. Four nonstructural proteins, Rep40, Rep52, Rep68, and Rep78, are involved in viral replication and virion

assembly[358,359]. The virus also encodes an assembly-activating protein (AAP), which provides a scaffolding function for capsid assembly[360]. The virus genome is a ~4.7 kb single-stranded DNA molecule of either positive or negative sense, as packaging shows no strand preference[359]. The genome has three coding regions, *cap, rep, and aap*[358,359]. These regions code for the VP proteins, Rep proteins, and AAP, respectively. At either end of the genome are hairpin regions called inverted terminal repeats (ITRs)[359]. ITRs are 145 bp in length and contribute as *cis*-acting elements for gene expression and packaging signals[358,359]. Viral entry is accomplished through receptor-mediated endocytosis[361]. The primary and possibly secondary receptors for AAV cell entry vary by serotype. The viral particle is the trafficked to endosomal compartments and eventually released from late endosomes or lysosomes[361]. Virions transit to the nucleus where they uncoat and release their ssDNA genome[358,361]. Host DNA polymerases then synthesize the second-strand of DNA. Worth noting here is that AAV genomes tend to exist as an episome in the cell nucleus[360]. However, studies have indicated that wildtype virus can integrate, particularly into the AAVS1 locus[359]. Integration may occur in the absence of a helper virus or in the presence of DNA damage[359,362]. After second-strand synthesis, Rep proteins are expressed to facilitate replication. Viral replication may require host cells to enter S-phase and requires host machinery, Rep proteins, and helper virus proteins E1, E2a, E4, and VA[358,415]. AAP and VP proteins are synthesized, and ssDNA is packaged into the viral particle[359]. Finally, cell lysis releases the mature virions. There are 12 naturally occurring AAV serotypes and >100 variants[361,363]. The 12 serotypes use different cell entry mechanisms, and thus have different tissue tropisms[361]. Around 80% of the human

population is seropositive for anti-AAV antibodies[359]. However, no discernable pathology is associated with infection[359,361].

Recombinant AAV vectors are generated by transfecting cells with three plasmids, a transfer plasmid, a Rep/Cap plasmid, and a helper plasmid[55,360]. Although AAV genomes are small, up to 96% of their sequence can be removed or placed on the Rep/Cap plasmid[361]. Thus, on the transfer plasmid, only ITR sequences are kept. The *rep*, *cap*, and *aap* genes are all replaced with an expression cassette of choice, generally a promoter, gene of interest, and poly(A) sequence[55,360,361]. A separate plasmid codes for the Rep and Cap proteins[55]. The third plasmid fulfills the role of a helper virus, encoding the E1, E2a, E4, and VA proteins required for AAV replication[360,361]. For production, HEK293 cells are typically transfected with these plasmids and recombinant AAV collected from cell lysates[55]. Density gradients, affinity columns, or ion exchange columns are used to purify the recombinant AAV[55,364].

Recombinant AAV vectors have several beneficial attributes as gene therapy tools. AAV9 vectors enter both dividing and non-dividing cells by binding galactose and/or a secondary receptor, laminin receptor 1 or AAV receptor[361]. Thus, AAV9 vectors exhibit broad tropism, including transduction of CNS[361,365]. AAV9 has been shown to cross the BBB and transduce both neurons and glial cells by both IV and CNS-directed ROAs[365-370]. AAV transduction also confers long-lasting transgene expression. In mice, EGFP expression persisted for at least one year[371]. A long-term AAV gene therapy study in hemophilia A canines showed factor VIII expression lasting 10 years[372,374]. Human trials of hemophilia A have reported multiyear factor VIII expression after gene transfer

with an AAV vector [373]. However, AAV mediated gene therapy has several drawbacks. With a packaging capacity of ~4.7kb, often times dual or even triple vector systems are required[318,359]. Self-complementary systems, which aim to skip the rate limiting step of second-strand synthesis, have half that compacity at around ~2.5kb[317,361,367]. The administration of high (or low) doses of AAV vectors can elicit a host immune response which can interfere with the effectiveness of the gene therapy[375,376]. Innate immune reactions to AAV vectors through TLR9 and cytokine production have been observed in mice and human cell lines[375,377]. Humoral response via neutralizing antibodies can block transduction completely[3778,379]. Capsid presentation on transduced cells can mediated a cytotoxic T-cell response that eliminates the cell[380].

All *in vivo* viral vector gene therapy work for MPS II has utilized recombinant AAVs. The first reported preclinical work was done in 2006[295]. An AAV2/8 vector carrying *IDS* cDNA regulated by a liver specific promoter, TBG, was dosed IV at $4x10^{12}$gc. Peripheral tissues showed complete normalization of GAG content and supraphysiological levels of IDS activity. Correction of skeletal manifestations and locomotion abnormalities was also observed. However, neurological data was poor[295]. Subsequently, the group evaluated an AAV2/5 CMV-h*IDS* vector by systemic administration in 2-day old pups[314]. Again, peripheral tissues were corrected, and a small but noticeable level of IDS activity was seen in the brain. Markers of neurodegeneration, astrogliosis, and inflammation were normalized in the brains of treated mice[314]. An AAV2/8 EF1α-h*IDS* vector administered IV reported similar results to the 2006 study[296]. A study examined AAV9 CAG-h*IDS* vector administered ICV at 3 different doses

($3x10^{8,9,10}$gc)[315]. Dose-dependent IDS and GAG reduction was observed, peripherally and in the CNS. Brain lesions were resolved, and memory was improved in treated mice[315]. Another study investigated an AAV9 CAG-m*IDS* vector, and thoroughly characterized the therapy after administration into the cisterna magna at a dose of $5x10^{10}$gc[300]. Four months post-administration, IDS activity in the brain was 40% of wild type and GAG content was normalized. Lysosome-associated membrane protein 2 (LAMP2), Glial fibrillary acidic protein (GFAP), and microgliosis were all reduced in the brains of treated mice. The enzymatic activity of other lysosomal hydrolases was also restored to homeostatic levels. Treated mice had an extended lifespan and showed correction of locomotion and exploratory behaviors compared to controls[300]. One report detailed extensive analysis of vector biodistribution and IDS activity in the brain of mice treated with an AAV9 CB7-h*IDS* vector by ICV administration at a dose of $5x10^{10}$gc[316]. In addition, the study evaluated co-expressing SUMF1 with hIDS. A previous study had shown post-translational modification by SUMF1 was a rate limiting step in the activities of five sulfatases[381]. Co-expression increased the activity of the sulfatase SGSH in MPS IIIA mice[382]. However, the MPS II study showed no benefit to including SUMF1 in the vector with hIDS compared to hIDS alone. IDS activities were high, and GAGs normalized in peripheral tissues of treated mice. Biodistribution in the same peripheral tissues was low, except for the liver at 44gc/ge. This suggests that the vector was escaping the CNS and transducing the liver, where IDS was synthesized and secreted into the circulation. Brain distribution was varied from ~1gc/ge to 47gc/ge. Regardless, through brain microdissection, the authors found the treatment conferred IDS activity 7-40% of wild type and normalized GAG levels. Treated mice showed improved spatial

navigation and memory when assessed in the Barnes maze compared to controls[316]. Overall, these studies showed AAV9 vectors encoding m*IDS* or h*IDS* can transduce the CNS and subsequently ameliorate CNS manifestations in MPS II mice when delivered by a CNS-directed ROA. More recently, an investigation of a self-complementary AAV9 CMV-*hIDS* vector administered IV was carried out in MPS II mice[317]. Administration of higher doses ($2.5x10^{12}$-$2x10^{13}$gc) conferred IDS activity of 6-14% of wild type and significant GAG reduction in the brain. AAV9 vector positive cells were observed in the brain by qPCR analysis and neurocognitive impairment was prevented in treated mice. These results were key, as they proved AAV9 can cross the blood brain and express IDS in the CNS of MPS II mice[317]. It has been observed that systemic administration of AAV vectors generates supraphysiological levels of circulating lysosomal hydrolase activity[295,318]. Consequently, some studies have noted minimal brain transduction by AAV, while achieving low, but detectable hydrolase activity in the brain[295,318,383]. Thus, the hypothesis of a "high dose effect" has been put forth. This hypothesis states that when consistently high levels of circulating enzyme are present, a small fraction can enter the CNS. For MPS II, since as little as 1.5% of wild type activity levels are needed in the brain to ameliorate CNS manifestations, this "high dose effect" may be enough to achieve those levels[314,318].

Gene Editing and Non-Viral Vector Based Gene Therapies for MPS II

Gene editing is any method that institutes an insertion, deletion, or alteration of an endogenous DNA locus in a living cell[324]. This includes zinc finger nucleases (ZFN), transcription activator-like effector-based nucleases (TALENs), and most recently

CRISPR/Cas9 and its derivatives[325]. For MPS II, a single study has been done utilizing ZFNs[318]. Three AAV 2/8 vectors were administered IV to mice that ultimately delivered ZFNs and a functional h*IDS* cDNA sequence at the albumin locus of hepatocytes. At a dose of $1.5x10^{12}$gc, supraphysiological IDS enzyme levels were observed in circulation and in most peripheral organs. GAG content was normalized in peripheral tissues as well. Although a low level of IDS activity and a small reduction of GAG levels were observed in the brain, this was sufficient to prevent neurocognitive deficits in the mice[318]. These results prompted the launching of a clinical trial (NCT03041324), but it was ultimately terminated from lack of efficacy[464].

Non-viral vector-based gene therapies have low cost, low immunogenicity, and high cargo capacity[327]. Hurdles for this approach include low efficiency, low expression, and material toxicity[327]. For Hunter syndrome, a 2002 paper studied non-viral gene therapy *in vitro* using electro-gene transfer (EGT)[356]. Plasmid carrying the h*IDS* sequence was injected into mouse quadriceps and stimulated by EGT. Mouse muscle cells were transduced, resulting in 10x increase in IDS activity for 5-week post administration. The same group more thoroughly characterized muscle directed EGT in MPS II mice[357]. While they found elevated enzyme in the muscle, little to no circulating IDS was measured.

Gene Therapy Clinical Trials for MPS II

The first clinical trial (NCT00004454) of a gene therapy for MPS II was in the 1990s using a retroviral vector, based on *in vitro* preclinical data[345,346]. In the trial, patient

T cells were transduced with a retroviral vector encoding h*IDS*. No results have been published from the trial. The next trial, sponsored by Sangamo Therapeutics, used a gene editing approach with ZFNs. The clinical trial (NCT03041324) was based on positive results from the preclinical ZFN work done in the mouse described above[318,464]. Patients were dosed with the AAV8 vectors, but a lack of detectable IDS activity in patient plasma ended the trial[384]. Encouraging preclinical results from CNS directed administration of AAV9 prompted REGENXBIO to launch two clinical trials[316]. The first trial (NCT04571970) enrolled older patients (5-17 years of age) with neuronopathic MPS II and were administered a dose of $6.5x10^{10}$gc/g brain mass. Positive outcomes on safety and efficacy led to the launch of second trial (NCT03566043). This pediatric dose escalation study is evaluating intracisternal administration of AAV9 encoding h*IDS* at doses $1.3x10^{10}$, $6.5x10^{10}$, $2.0x10^{11}$, and $2.9x10^{11}$gc/g brain mass. Primary outcomes are safety, GAG reduction in the CSF, and neurodevelopment function. Secondary outcomes include plasma IDS activity levels and urine GAG reduction. Both trials are still recruiting patients. Most recently a phase 1 clinical trial (NCT05238324) sponsored by Homology Medicines was launched. The purpose of their trial is to investigate the safety and efficacy of IV administration of their h*IDS* encoding AAV-HSC vector, which is a human hematopoietic stem cell derived AAV vector[385,386]. No results have been communicated for this trial yet.

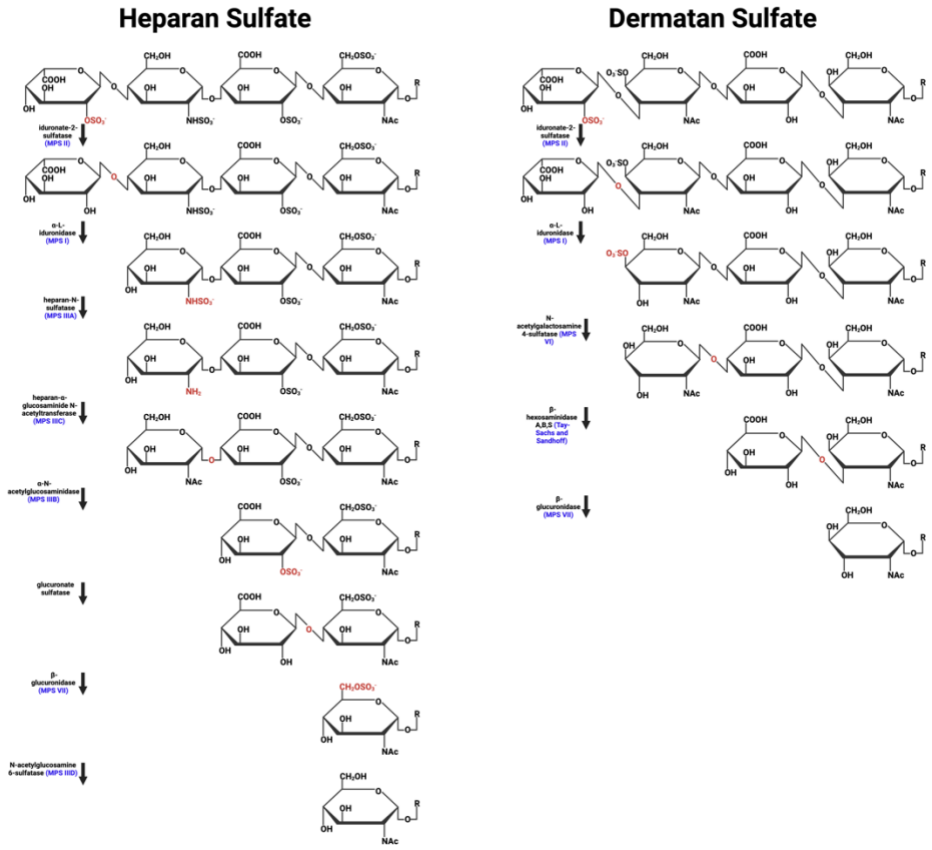

Figure 1. Stepwise degradation of heparan sulfate and dermatan sulfate. Each arrow represents the reaction carried out by the labeled enzyme. The label also includes the lysosomal disease (in blue) that arises from deficiency of said enzyme. Red labeling on GAG structures indicates the moiety upon which a given enzyme acts. At the non-reducing end of both heparan sulfate and dermatan sulfate, iduronate-2-sulfatase hydrolyzes the C2-sulfate ester bond of α-L-Iduronic acid. Adapted from Neufeld and Muenzer, 2001[57] and made with BioRender

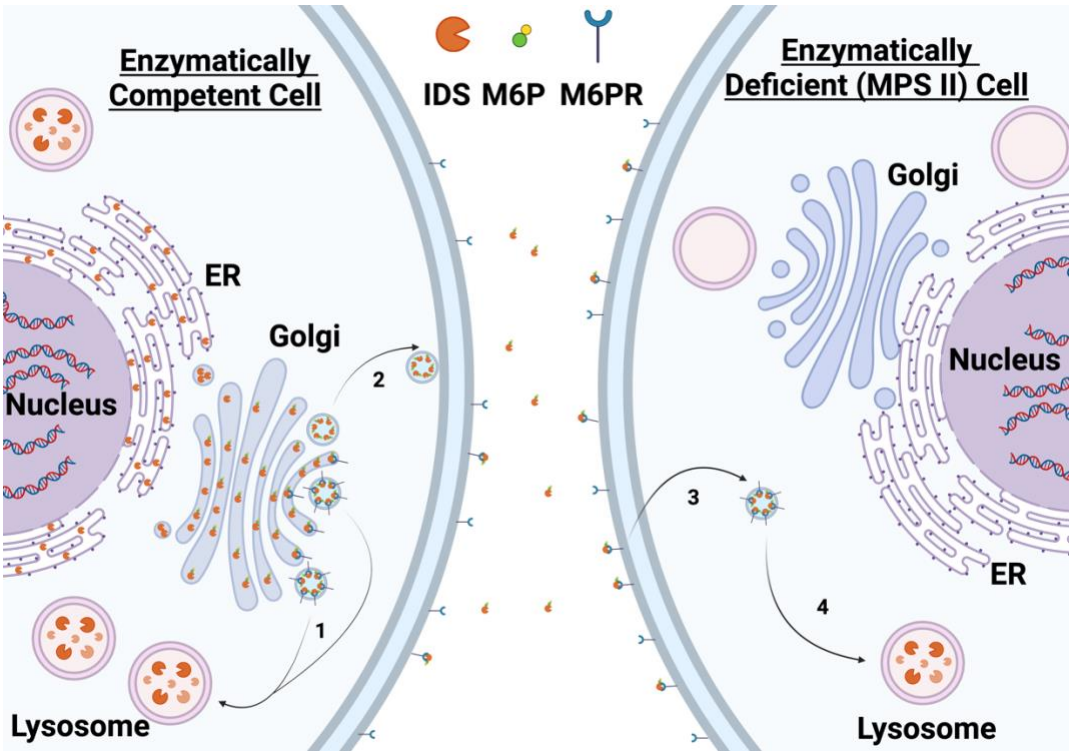

Figure 2. Metabolic cross correction by trafficking of IDS via the mannose-6-phosphate pathway. Nascent IDS (orange circle) is translated into the lumen of the ER where it is glycosylated and modified by SUMF1. IDS enzyme then transits to the Golgi by COPII coated vesicles where it obtains a mannose-6-phosphate (M6P, green and yellow circles) modification. In the trans Golgi network a mannose-6-phosphate receptor (M6PR, blue crescent) binds to the enzyme. IDS is then trafficked to mature lysosomes (1). A subset of enzyme is instead secreted from the cell (2). Extracellular IDS can enter a deficient cell through M6PR mediated endocytosis (3). Lastly, the exogenous enzyme is trafficked to the lysosome where it can carry out its catabolic reaction on heparan sulfate and dermatan sulfate (4). Made with BioRender.

Thesis Statement

Mucopolysaccharidosis Type II (Hunter syndrome, MPS II) is an X-linked recessive disease caused by deficiency in IDS, the first enzyme required for the stepwise degradation of the GAGs heparan and dermatan sulfates. The accumulation of undegraded heparan and dermatan sulfate leads to a progressive and multisystemic disease. Hunter syndrome cases exhibit a wide range of disease manifestations including hepatosplenomegaly, joint stiffness and arthropathy, skeletal abnormalities, cardiopulmonary dysfunction, neurodegeneration, and death by adolescence. Current treatments for Hunter syndrome include ERT, with HSCT conducted on a trial basis. However, these treatments fall short in addressing the whole disease and importantly do not ameliorate the CNS manifestations. Thus, there is an unmet need to develop a therapy that can not only treat the peripheral and CNS disease manifestations. The following chapters describe two preclinical studies dedicated towards the development of gene therapies for MPS II, as well as the characterization of a novel MPS II mouse model for use in future research of MPS II.

Chapter II: Phenotypic Correction of Murine Mucopolysaccharidosis Type II by Engraftment of *Ex Vivo* Lentiviral Vector-Transduced Hematopoietic Stem and Progenitor Cells

Previous preclinical LVV mouse work described in *Ex Vivo* Gene Therapy for MPS II (Chapter I) has not comprehensively characterized the approach with a strong, constitutively active promotor. Using an established C57BL/6 mouse model of MPS II, this project evaluated *ex vivo* transduction of hematopoietic stem and progenitor cells

using LVV carrying a codon optimized human IDS coding sequence regulated by a strong, constitutively active MNDU3 promoter. The extensive analysis of the therapy included biochemical, histological, skeletal, and neurocognitive assessments. The radiographical and neurologic testing are of particular relevance to clinical translation, as ERT shows no improvement in these functional outcomes.

Chapter III: Comparative Minimal Dose Effectiveness of Intravenous and Intrathecal AAV9.CB7.hIDS (RGX-121) in a Murine Model of Mucopolysaccharidosis type II

In vivo AAV mouse work for MPS II has included both systemic and CNS-directed ROAs to treat the disease. Previous CSF-directed preclinical work showed it can address the CNS, but it is unknown if a CSF-directed approach with RGX-121 can address both the CNS and peripheral disease manifestations or if supplementation with systemic administration is required. Additionally, the relative effectiveness of any given dose is not known for addressing the CNS and/or peripheral disease manifestations. Thus, this project compared IT and IV administration of an AAV9 encoding human IDS at varying doses and found that a dose of 10^{11}gc by IT ROA can address both peripheral and CNS disease manifestations in a mouse model of MPS II.

Chapter IV: Generation and Characterization of an Immunodeficient Mouse Model of Mucopolysaccharidosis type II

An extensively characterized immunodeficient MPS II mouse strain is currently not available as a research model. The immunodeficient background allows for the engraftment human cells, such as human hematopoietic stem cells. Thus, *ex vivo* gene therapies for MPS II can be evaluated in human cells with this mouse. For this reason,

this project generated an NSG-MPS II mouse model using CRISPR/Cas9 knockout of m*IDS*. The mice recapitulate the biochemical, skeletal, and neurological disease manifestations associated with MPS II.

Chapter II: Phenotypic correction of murine mucopolysaccharidosis type II by engraftment of *ex vivo* lentiviral vector transduced hematopoietic stem and progenitor cells

Miles C Smith[1] Lalitha R Belur[1], Andrea D Karlen[1], Olivia Erlanson[1], Kelly M. Podetz-Pedersen[1], Jessica McKenzie[2], Jenn Detellis[2], Khatuna Gagnidze[2], Geoffrey Parsons[2], Nicholas Robinson[2], Shelby Labarre[2], Saumil Shah[2], Justin Furcich[3], Troy C. Lund[3], Hsing-Chen Tsai[2], R. Scott McIvor[1*], Melissa Bonner[2]

[1]Center for Genome Engineering, Department of Genetics, Cell Biology and Development, University of Minnesota, Minneapolis, MN, United States

[2]bluebird bio, Inc., Cambridge, MA, United States

[3]Department of Pediatrics, University of Minnesota, Minneapolis, MN, United States

* Corresponding Author:
R. Scott McIvor
mcivo001@umn.edu

Published Work Citation:

Smith MC, Belur LR, Karlen AD, et al. Phenotypic correction of murine mucopolysaccharidosis type II by engraftment of ex vivo lentiviral vector transduced hematopoietic stem and progenitor cells. Human Gene Therapy 2022; doi: 10.1089/hum.2022.141.

Summary

Mucopolysaccharidosis type II (MPS II, Hunter syndrome) is an X- linked recessive lysosomal disease caused by deficiency of iduronate-2-sulfatase (IDS). Absence of IDS results in the accumulation of the glycosaminoglycans (GAGs) heparan sulfate and dermatan sulfate. Currently the only approved treatment option for MPS II is enzyme replacement therapy (ERT), Elaprase®. However, ERT is demanding for the patient and does not ameliorate neurological manifestations of the disease. Using an IDS deficient mouse model that phenocopies the human disease, we evaluated hematopoietic stem and progenitor cells (HSPCs) transduced with a lentiviral vector (LVV) carrying a codon optimized human IDS coding sequence regulated by a ubiquitous MNDU3 promoter (MNDU3-IDS). Mice treated with MNDU3-IDS LVV transduced cells showed supraphysiologic levels of IDS enzyme activity in plasma, peripheral blood mononuclear cells (PBMCs), and in most analyzed tissues. These enzyme levels were sufficient to normalize GAG storage in analyzed tissues. Importantly, IDS levels in the brains of MNDU3-IDS engrafted animals were restored to 10-20% that of wild-type mice, sufficient to normalize GAG content and prevent emergence of cognitive deficit as evaluated by neurobehavioral testing. These results demonstrate the potential effectiveness of *ex vivo* MNDU3-IDS LVV transduced HSPCs for treatment of MPS II.

Introduction

Mucopolysaccharidosis type II (MPS II, Hunter syndrome) is an X-linked recessive metabolic disorder caused by deficiency of the lysosomal hydrolase iduronate-2-sulfatase (IDS). Incidence of the disorder is approximately 1:160,000 male births[86].

Loss of IDS leads to disruption in the catabolism of the glycosaminoglycans (GAGs) heparan sulfate and dermatan sulfate, which accumulate in lysosomes leading to progressive and multisystemic disease[323]. Manifestations include organomegaly, cardiopulmonary dysfunction, skeletal dysplasias, and in the most severe cases neurodegeneration and death by adolescence[57].

The current standard of care for MPS II is enzyme replacement therapy (ERT), consisting of recombinant IDS (Elaprase®) infused intravenously[416]. Patients on ERT show several improvements that correlate with reduced urine GAG levels, including reduced organomegaly and improved performance on the six-minute walk test[417]. However, ERT fails to address some of the systemic disease burden. A 9-year follow-up of patients on ERT showed no improvements in pulmonary, ocular, skeletal or central nervous system (CNS) manifestations,[189,211] which has been attributed to low bioavailability of the enzyme in some tissues[189]; for example, the administered enzyme does not cross the blood brain barrier (BBB), leaving the neurologic manifestations of the disease unaddressed[418]. In addition, the treatment is expensive and requires weekly enzyme infusions.

Allogeneic hematopoietic stem cell transplantation (HSCT) has been considered as a possible treatment for MPS II. Potential benefits of HSCT include a consistent level of enzyme for patients, avoiding the peaks and troughs common to periodic enzyme infusions, thereby replacing expensive and time-consuming weekly ERT infusions with the prospect of addressing CNS manifestations of the disease[43,189]. However, HSCT is not a standard treatment for MPS II, as initial clinical testing met with poor outcomes due to low enzyme levels, graft vs. host disease, sepsis, and patient death[251]. Recent reports on

HSCT for MPS II have shown some neurologic benefit, but also low levels of IDS activity and continued musculoskeletal problems[251,254]. Thus, MPS II patients still have significant unmet need for a treatment that can address the limitations of ERT and allogeneic HSCT.

Successful gene therapy for lysosomal diseases relies on the production of bioavailable enzyme at a sufficient and consistent level both systemically and in the CNS that is not achieved by currently available treatment options. Bioavailable enzyme secreted from genetically modified cells containing the transgene would be available for metabolic cross-correction of unmodified cells by mannose-6-phosphate receptor mediated endocytosis[419]. For MPS II, strategies have been developed that employ either adeno-associated virus (AAV) for *in vivo* IDS gene delivery to target tissues, like the CNS, or lentiviral vector (LVV) for *ex vivo* IDS gene delivery to hematopoietic stem and progenitor cells (HSPCs).

CNS directed AAV administration has shown effectiveness in transducing cells in the brain, leading to sustained IDS expression, GAG reduction and improvement in neurobehavior[300,315,316]. Systemic approaches have also shown improvement in neurobehavior[317,318]. However, AAV-based approaches face several challenges including the invasiveness of direct CNS administration, pre-existing anti-AAV immune response, and scaling up to clinical doses[189,311,375].

Autologous, *ex vivo* LVV-based approaches look to improve upon allogeneic HSCT by providing higher levels of bioavailable systemic IDS, addressing CNS manifestations, and reducing the possibility of graft vs. host disease[43,311,312,313]. In this study, we sought to develop a therapy that provides high and sustained levels of

bioavailable IDS to address the systemic, including skeletal, and CNS manifestations of MPS II. Using an MPS II mouse model, we evaluated the efficacy of *ex vivo* LVV gene-modified HSPCs encoding a codon-optimized human IDS under the control of a strong, constitutively active MNDU3 promoter (MNDU3-IDS) for treatment of MPS II.

Materials and Methods

Animal Husbandry. Animal care and procedures were compliant with and approved by the University of Minnesota Institutional Animal Care and Use Committee (IACUC). Animals were maintained at University of Minnesota Research Animal Resources facilities under specific pathogen free conditions. C57BL/6 iduronate-2-sulfatase knockout (IDS-KO) mice were graciously provided by Dr. Joseph Muenzer, and offspring were genotyped by PCR[294]. These mice were backcrossed with C57BL/6 CD45.1 mice to generate IDS-KO animals on a congenic C57BL/6 CD45.1 background. Heterogeneity at CD45 was used for determination of donor chimerism in transplant recipients. Animals were fed food and water *ad libitum*.

MNDU3-IDS and MNDU3-GFP Lentiviral Vector Production. Self-inactivating and replication deficient third generation MNDU3-IDS and MNDU3-GFP LVVs were produced by transient transfection of HEK293T cells. The transfection included several packaging plasmids encoding GAG/POL, REV, and VSV-G as well as a plasmid transfer vector. Purification of LVVs was carried out by chromatography and formulated before storage at ≤ -65°C[420].

Lentiviral Transduction and Transplant Procedures. Whole bone marrow was harvested, red blood cells (RBCs) were lysed using ammonium chloride, and nucleated

cells were enriched for the HSPC population by lineage depletion using Miltenyi Biotec's murine Direct Lineage Cell Depletion Kit as previously described[421]. For LVV transduction, lineage depleted cells were suspended in Dulbecco's modified Eagle medium (Gibco) with 10% fetal bovine serum (EquaFETAL, Atlas Biologicals) and supplemented with penicillin-streptomycin (10,000U/mL), protamine sulfate (600μg/mL), and stimulatory cytokines (mouse stem cell factor [mSCF, 50 ng/mL], mouse interleukin-3 [mIL-3, 20 ng/mL], and human interleukin-6 [hIL-6, 50 ng/mL]). Lineage depleted cells were transduced with either MNDU3-IDS or MNDU3-GFP LVV at a multiplicity of infection (MOI) of 50 and plated onto non-treated suspension plates for 24 hours at 37 ^{o}C, 5% CO_2. One day before transplantation, MPS II male recipient animals 6 to 8 weeks of age were myeloablated by lethal irradiation at a dose of 900 cGy X-ray. Lethal irradiation was chosen as the method of myeloablation after busulfan treatment (25mg/kg daily for 4 days) resulted in low levels of donor cell engraftment. 24 hours later, transduced cells were harvested by centrifugation for 10 minutes, resuspended in phosphate-buffered saline (PBS), and then irradiated recipient mice were infused with 0.84-1.0x10^6 cells via the lateral tail vein. Animals were observed daily for any clinical signs of declining health or unscheduled deaths and blood and urine collections were done monthly.

Flow Cytometry. Peripheral blood was collected from the submandibular vein into heparinized tubes and the RBCs were lysed using RBC lysis buffer (Stem Cell Technologies, #07850). The leukocytes were stained with phycoerythrin (PE)-conjugated anti-murine CD45.1 and allophycocyanin (APC)-conjugated anti-murine CD45.2 (all antibodies from BioLegend) and then evaluated by flow cytometry using a BD

Biosciences Canto cytometer. The data were analyzed using FlowJo software (BD Biosciences) and donor cell engraftment was determined as the percentage CD45.1+ or CD45.2+ cells present.

Vector Copy Number (VCN) Analysis in Peripheral Blood Cells. The VCN, or number of vector copies present in diploid genomic DNA (gDNA), was assessed based upon identification of the Psi-Gag sequence and normalization to a mouse house-keeping gene, TERT. PBMCs were isolated following RBC lysis using ACK Lysing Buffer (ThermoFisher-Cat-A1049201) and gDNA was extracted using Qiagen DNA Extraction Kit (Cat # 51331) followed by quantitative Polymerase Chain Reaction (qPCR) amplification of the Psi-Gag and mouse TERT (ThermoFisher Cat # 4458369) sequences[422].

Tissue Processing. Animals were euthanized at 8 months of age by CO_2 asphyxiation and transcardially perfused with 50 mL of PBS. A necropsy was performed, and tissues (liver, spleen, kidney, brain, heart, lung, spinal cord, ileum, cecum, colon, eye, and bone marrow) were harvested, frozen on dry ice and stored at -20 °C until processed. A wide range of tissues was collected due to the multisystemic nature of MPS II, relevance to patient disease manifestations, and relevance to therapeutic approach. A portion of each tissue was fixed overnight in 10% neutral buffered formalin (VWR) at a ratio of 1:10-20 tissue to formalin and then after 24 hours transferred to 70% ethanol for storage until paraffin embedding. Tissues stored at -20 °C were processed for biochemical analysis by homogenization in 0.9% saline using a Bullet Blender bead mill (Storm 24 Homogenizer, NEXT ADVANCE) as previously described[316] and clarified by centrifugation in a 5424R Eppendorf centrifuge. The supernatants were termed tissue

lysates and were used for protein, IDS, and GAG assays. After clarification, the tissue lysates were stored at -20 °C until analyzed.

Iduronate-2-sulfatase (IDS) Enzyme Assay. Plasma and tissue lysates were assayed for IDS activity in a fluorometric assay using 4-methylumbelliferyl α-l-iduronide 2-sulfate disodium salt (4-MU2S) as substrate (Cat #: M334715, Toronto Research Chemicals) as previously described[318]. 4-MU2S (5 mg) substrate was dissolved in 8.33 mL distilled water to yield a 1.25 mM working solution. 20 μL aliquots of working substrate were mixed with 10 μL aliquots of plasma or tissue lysates and incubated at 37 °C for 1.5 hours. Then, 20 μL of PiCi Buffer (0.2M Na2HPO4 + 0.1M Citric Acid, 0.02% Na-Azide, pH 4.5) was added to stop the IDS reaction. 10 μL of 5 μg/mL alpha-L-iduronidase (IDUA) (Cat #: 4119-GH, Bio-Techne) was added and the mixture was incubated at 37 °C overnight. The reaction was terminated by the addition of 200 μL stop buffer (0.5 M Na2CO3 + 0.5 M NaHCO3, pH 10.7). Tubes were then centrifuged at ~13,000 rpm for 1 minute. Supernatant was transferred into a black 96-well round bottom plate and the resulting fluorescence was measured using a Bio-Tek Synergy Mx plate reader with excitation at 355 nm and emission at 460 nm. IDS catalyzes the reaction of 4-MU2S into non-fluorescent 4-MU iduronide, and then IDUA catalyzes cleavage of the non-fluorescent 4-MU iduronide into fluorescent product 4-methylumbelliferone (4-MU). A 4-MU (Sigma #M1381) standard curve was used for the calculation of 4-MU generated in the reaction. Protein was measured using the Pierce protein assay reagent (Cat #: 22660, ThermoFisher). Enzyme activity is expressed as nmol 4-MU released per mg protein per hour (nmol/h/mg) for tissues extracts, and as nmol/h/ml for plasma. All reactions were assayed in duplicate.

Glycosaminoglycan (GAG) Assay. Tissue lysates were incubated with proteinase K (20 mg/mL) at a ratio of 1:10 (ProK:tissue lysate) at 55 °C overnight, followed by heat inactivation of the proteinase K by boiling for 10 minutes. Tissue lysates were further digested with 200 units of DNase and 2 mg of RNase per 50 μL tissue lysate at room temperature overnight with gentle mixing. DNase and RNase were heat inactivated by boiling for 10 minutes. GAG levels were then determined using the Blyscan Sulfated Glycosaminoglycan Assay kit (Biocolor Life Science Assays, Accurate Chemical, NY Inc. Cat # CLRB1000) according to the manufacturer's protocol. For tissue GAGs, protein was measured using the Pierce protein assay (Cat #: 22660, ThermoFisher) and results were expressed as μg GAG/mg protein. For urine, GAG levels were also assessed using the Blyscan assay, normalizing to urine creatinine levels and expressed as μg GAG/mg creatinine. Creatinine levels were determined using a creatinine assay kit (Sigma, MAK080).

Histology. For Alcian blue staining of GAGs, formalin-fixed, paraffin embedded (FFPE) tissues were deparaffinized, rehydrated, and then exposed to 1% Alcian blue in 3% acetic acid. Tissues were rinsed with distilled water and counter stained with 0.1% Nuclear Fast Red Kernechtrot. The tissues were then dehydrated and mounted. Semiquantitative Alcian blue staining was scored as previously described[423].

For immunohistochemistry of lysosomal associated membrane protein-1 (LAMP-1), dry FFPE slides were loaded onto a Leica BOND Rx instrument and baked at 60 °C, placed in BOND Dewax Solution (Leica #AR9222) at 72 °C, rinsed with ethanol, and rinsed in BOND Wash Solution 10x Concentrate (Leica #AR9590). Slides were then pretreated with HIER Solution, BOND Epitope Retrieval Solution 2 and 1 (Leica

#AR9961) before being washed with BOND Wash Solution. Slides were then blocked and stained using a peroxidase block, Rodent Block "M" (Biocare Medical #RBM961L), Primary LAMP-1 at a final concentration of 0.25 μg/mL (Biorad #MCA497G), Rat Probe (Biocare Medical #RTP629L), Rat Polymer (Biocare Medical #RTH630L), Mixed DAB Refine (Leica #DS9800), and Hematoxylin, with BOND Wash Solution used between each. Finally, slides were mounted after dehydration with ethanol and xylene. LAMP-1 scoring was based on the average percentage of LAMP-1 positive cells and their average intensity for each location. Scoring was calculated by multiplying the proportion of stained cells by the intensity of staining.

In situ hybridization was performed using RNAscope® 2.5 LS Probe- BBB-Lenti-G-sense (ACD Cat# 519048) to identify the LVV provirus integrated into genomic DNA. The tissues were stained on a Leica BOND Rx robot using ACD RNAscope 2.5 LSx Reagent kit – RED (ACD Cat# 322750) according to the manufacturer instructions. A mouse Brain Slicer Matrix (AgnThos, Lidingö, Sweden, Brain Matrice Stainless Steel, mouse, coronal, 1 mm cut, Cat# 69-2175-1) was used to section the brains into 6 coronal slices and images were scored based on the number of dots per cell and number of positive cells per 200x field.

Radiography and Image Analysis. One week before mouse euthanasia, experimental mice were sedated with 5% isoflurane and whole-body X-ray or Micro-CT images were acquired using a Bruker Xtreme or Siemens Inveon PET/CT machine, respectively. The acquired DICOM files were exported from the machines and converted to Imaris image files using the Imaris File Converter software. This conversion resulted in an X-ray or Micro-CT file that could be analyzed using the Imaris 3D Analysis

software. Imaris 3D Analysis software was then utilized to obtain body measurements of the X-ray or Micro-CT scans, including zygomatic arch diameter.

Barnes Maze. The Barnes maze is a measure of spatial navigation and memory[424]. It consists of a circular platform with twenty holes positioned around the periphery, all of which are blocked except for one hole which has an escape box positioned underneath that the mouse can access using an inclined ramp. Visual cues are placed on the walls around the maze for spatial navigation. The animal is released into the center of the maze with the lights dimmed, bright overhead lights are then turned on, and the mouse is given 3 minutes to explore the maze. If the mouse does not enter the escape box within 3 minutes, it is guided to the escape hole and left there for 30 seconds before returning to its home cage. The mice were trained on the Barnes maze for 4 days at 4 trials a day, with an interval of 12-15 minutes between any two consecutive trials for each animal. The time taken by the animal to escape was recorded as latency to escape.

Fear Conditioning. This associative learning task assesses a fear response (i.e., time spent freezing) to a conditioned stimulus (cue) that is predictive of an unconditioned stimulus (mild foot shock) introduced during training trials[425]. Data collection and analysis were semi-automated via video-monitoring (Med Associates, Inc.). On the conditioning day (training day; day 1), the test chamber was sprayed with a solution of Simple Green as an olfactory cue, and mice were exposed to a series (five pairings; 1-minute intertrial interval) of cue (80-dB white noise tone and light) presentations (15 seconds in duration) that co-terminated with a mild foot shock (0.7 mA, 1 second in duration). Twenty-four hours later, a cued fear test was performed in a test chamber with altered contextual elements (floor, wall, and odor) and consisted of three 1-minute

baseline (nonspecific freezing behavior) and three 1-minute light and sound cue exposure (cued fear) periods. Freezing response was assessed during both the baseline and cue testing sessions. Percent difference in freezing during the cued fear test was taken as:

*(average freezing during cue – average freezing in baseline) *100*.

Statistics. GraphPad Prism was used for all graphing and statistics. Error bars on graphs represent group mean ± standard deviation (SD). Multiple group comparisons were evaluated by one-way or two-way ANOVA for IDS activity, urine and tissue GAGs, and Barnes maze. Fear conditioning data were analyzed by nonparametric comparisons using the Mann-Whitney U test. Histological data were analyzed by one-way ANOVA and Tukey's multiple comparisons test. *P* values of < 0.05 were considered statistically significant for all tests. Radiographic data were grouped into mouse treatment types and evaluated using the student's t-test.

Results

Ex vivo LVV gene therapy study design

To test the potential of MNDU3-IDS LVV transduced HSPCs in treating MPS II, donor HSPCs from MPS II knockout mice ($IDS^{Y/-}$) were transduced *ex vivo* with an LVV carrying a codon optimized IDS encoding gene regulated by a strong, constitutive MNDU3 promoter (Figure 3A). This MNDU3-IDS group was compared to three control groups: (i) MNDU3-GFP LVV transduced group (affected control), (ii) a group transplanted with wild-type $IDS^{Y/+}$ bone marrow from congenic C57BL/6 littermates (HSCT control), and (iii) an untreated wild-type group (unaffected control). For the MNDU3-IDS and MNDU3-GFP transplantation groups, lineage-depleted $IDS^{Y/-}$ bone

marrow was transduced overnight with either the MNDU3-IDS or MNDU3-GFP LVV at an MOI of 50. For the HSCT group, $IDS^{Y/+}$ HSPCs were similarly harvested and enriched, then transplanted without transduction or *ex vivo* culture. Donor HSPCs were injected into 6- to 8-week-old myeloablated (900 cGy X-ray) $IDS^{Y/-}$ C57BL/6 mice at a dose of 0.84-1.0x10^6 cells/mouse. Mice at 6- to 8- weeks of age are presymptomatic and have been used in past studies to evaluate the prevention of skeletal and neurobehavioral manifestations[311,312,316].

Peripheral blood and urine were collected every month (except for month 4 post-transplant when the mice underwent neurobehavioral testing) to evaluate donor cell engraftment, IDS enzyme activity in both the plasma and PBMCs, VCN in PBMCs, and urine GAG excretion. At 4 months post-transplant, the mice underwent neurobehavioral evaluation consisting of Barnes maze and fear conditioning. Approximately one week after neurobehavior testing, the mice underwent full body skeletal analysis by X-ray or Micro-CT imaging. At 5 months post-transplant the animals were euthanized, perfused, and necropsied. Tissue samples were collected for measuring IDS enzyme activity and GAG accumulation, as well as histologic evaluation. Tissues assayed included liver, spleen, kidney, heart, lung, brain, spinal cord, eye, ileum, cecum, colon, and bone marrow.

Donor chimerism in transplant recipients

Donor cell engraftment vs. recipient cell repopulation post-transplant was evaluated by distinction of CD45.1 vs CD45.2 via flow cytometry. All three transplant groups showed high levels (>60%) of engraftment at one-month post-transplant (Figure 3B). In the following months, engraftment increased 10-20% and then stabilized in all

three transplant groups. By 5 months post-transplant, MNDU3-IDS and HSCT groups showed engraftment of >90%, while the MNDU3-GFP group showed engraftment of approximately 80%. PBMCs from MNDU3-GFP treated animals were on average 75% GFP positive, comparable to the level of engraftment shown by CD45 donor chimerism analysis (Figure 3C). Overall, these analyses revealed high levels of stable donor cell engraftment in all 3 transplant groups, and specifically in the MNDU3-GFP group stable engraftment of gene-modified cells, as assessed by GFP+ PBMCs.

VCN analysis in PBMCs

VCN in PBMCs of MDU3-IDS and MND-GFP transplanted groups was determined by qPCR throughout the 5-month time course of the experiment. The MNDU3-IDS group had PBMC VCN between 1-6 c/dg and the MNDU3-GFP group had similar values of 2-8 c/dg during in-life collections (Figures 3D, E). One animal in the MNDU3-GFP group initially had PBMC VCN of 13 c/dg at 1-month post-transplant but VCN decreased to 4 c/dg by 5 months post-transplant (Figure 3E). Throughout the study period, the average VCN in the MNDU3-GFP group trended higher compared to the MNDU3-IDS group (shown in black lines in Figures 3D and 3E), but this difference was not statistically significant ($p=0.1320$). Taken together with the donor chimerism results, groups receiving gene-modified HSPCs exhibited stable engraftment of gene-modified cells.

Peripheral blood IDS enzyme activity and urine GAG excretion

Expression of the MNDU3-IDS transgene was assessed by IDS enzyme activity assay both in the peripheral blood plasma and in PBMCs. The following in-life means are a combined post-transplant average of all samples collected monthly by group. Wild-type

mice had a mean of 30.5 nmol/h/ml IDS in the plasma (Figure 4A) and 31.5 nmol/h/mg protein in PBMCs (Figure 4B). The MNDU3-GFP group showed no detectable activity above background in the plasma and low-level background activity in PBMCs. Remarkably, MNDU3-IDS treated animals had an average of 8.2×10^3 nmol/h/ml IDS activity in plasma, 269 times higher than the wild-type level of activity ($p<0.01$-0.0001) and a mean of 5.7×10^3 nmol/h/mg protein in PBMCs, 180 times the wild-type level of activity ($p<0.01$-0.001). MPS II mice engrafted with wild-type HSPCs (HSCT group) had a mean of 4 nmol/h/ml IDS in plasma and a mean of 15 nmol/h/mg protein in PBMC extracts, both below wild-type levels, although this was statistically significant only for plasma IDS ($p<.001$). These IDS enzyme activity levels were maintained from 1-month post-transplant to the end of study at 5-months post-transplant. In summary, supraphysiological levels of IDS enzyme activity were seen in both plasma and PBMCs in the MNDU3-IDS transplant group.

Prior to treatment, all groups showed elevated levels of urine GAG excretion (~2900 µg GAG/mg creatinine) when compared to wild-type mice (~600 µg GAG/mg creatinine) and were not significantly different from one another. After transplant, the MNDU3-GFP group maintained a high level of ~3000 µg GAG/mg creatinine for the duration of the study, which was significantly higher compared to all other groups throughout the remainder of the study ($p<0.05$-0.001) (Figure 4C). In contrast, the MNDU3-IDS and HSCT groups showed normalization of excreted GAGs that was not significantly different from wild-type. The reduction in excreted GAGs was maintained throughout the study for both the MNDU3-IDS and HSCT groups.

Tissue IDS enzyme activity and GAG normalization in MNDU3-IDS treated mice

The potential for IDS cross-correction was evaluated by assaying for enzyme activity in non-hematopoietic peripheral and CNS tissues collected at end of study 5 months post-transplant. Wild-type mice showed varying levels of IDS activity by tissue, ranging from a mean of 15 nmol/h/mg protein in the heart to 278 nmol/h/mg protein in the brain (Figure 5A). The MNDU3-GFP group showed little to no IDS activity in any peripheral or CNS tissues. MNDU3-IDS treated mice had IDS activities that far exceeded those of normal unaffected controls in peripheral tissues and were significantly greater than those of MNDU3-GFP treated mice. Tissues with resident hematopoietic cells showed the highest IDS levels, with a 140-fold increase over wild-type levels in the liver ($p<0.0001$) and a 52-fold increase over wild-type levels in the spleen ($p<0.0001$). Cross-correction of non-hematopoietic tissues was also observed; there was a 14-fold increase in IDS enzyme activity over wild-type levels in the kidney ($p<0.05$) and 18-fold increase over wild-type levels in the heart ($p<0.0001$) (Figure 5A). In contrast, MPS II animals engrafted with wild-type HSPCs generally showed IDS enzyme activity levels lower than wild-type levels in the liver ($p<0.001$), spleen ($p<0.001$), kidney ($p<0.05$), and lung ($p<0.01$), but not heart ($p=0.179$).

A key goal of potential therapeutics for MPS II is achieving high levels of IDS in the CNS to address neurologic manifestations of the disease. Consistent with previous reports[311,316], in wild-type mice we observed a high level of IDS enzyme activity in the brain at an average of 278 nmol/h/mg. Animals engrafted with MNDU3-IDS transduced HSPCs had a mean of 35.6 nmol/h/mg IDS activity in brain tissue, approximately 13% that of wild-type on average ($p<0.01$) (Figure 5A) and this level of IDS activity was sufficient to normalize GAG accumulation in the CNS (Figure 5B). In the spinal cord,

MNDU3-IDS treated mice exhibited physiological levels of IDS activity (162.6 nmol/h/mg. MPS II animals engrafted with wild-type HSPCs had less than 1% of wild-type IDS activity in the brain ($p<.01$). In the spinal cord, the HSCT group showed only 3% of wild-type IDS activity (4.5 nmol/h/mg) ($p<.0001$).

Collected tissues were analyzed for GAG accumulation. In the MNDU3-GFP affected control group, levels of GAG were consistently higher than wild-type animals in all organs; the liver, kidney, and spleen in the MNDU3-GFP group had 36x ($p<0.0001$), 36x ($p<0.0001$), and 16x ($p<0.05$) significantly increased GAG compared to wild-type animals, respectively. In CNS tissues, MNDU3-GFP mice exhibited GAG levels 2.3x higher in the brain ($p<.001$) and 9.7x higher in the spinal cord ($p<.0001$) compared to wild-type controls. In contrast, the MNDU3-IDS group showed normalization of GAG levels in all peripheral tissues analyzed. In the CNS, GAG levels were normalized in the brain and not significantly different from wild-type levels ($p=0.1214$) (Figure 5B). Interestingly, the spinal cord in MNDU3-IDS transplanted animals had significantly higher GAG accumulation than wild-type mice ($p<0.05$), even though wild-type levels of IDS were observed (Figures 5A, B). However, GAG accumulation was nonetheless reduced when compared to the affected ($p<0.001$) or HSCT control groups ($P<0.05$). For the HSCT group, GAG levels were higher than wild-type in all tissues ($p<0.01$ to $p<0.001$) except the ileum. There was major improvement in hemopoietic resident tissues such as the liver and spleen, but complete GAG normalization was not observed. Lastly, HSCT mice showed no reduction of storage material in the brain or spinal cord, which were not significantly different from affected controls. MNDU3-IDS LVV transduced

HSPC transplanted recipients with significantly increased tissue IDS enzyme activity thus exhibited concomitant reduction in tissue GAG accumulation, including in the CNS.

Histologic Analysis

GAG content in the liver, kidney, bone marrow, and spleen was additionally evaluated by Alcian blue staining. Large amounts of GAG accumulated in the bone marrow and the spleen in the MNDU3-GFP control group, with resident macrophages contributing to the majority of GAG accumulation in these tissues. Staining in the MNDU3-IDS and HSCT groups revealed a substantial reduction in GAG content compared to the MNDU3-GFP group (Figure 6C, G & Supplemental Figure 9A, D). In MNDU3-GFP mice, GAG content in the liver was mainly located in the cytoplasm of hepatocytes, leading to large amounts of cytoplasmic vacuolization. The HSCT group showed a reduction of GAG content in the liver but retained a small amount of storage material in the perivascular region. GAG levels in liver and kidney of the MNDU3-GFP group were significantly higher than the MNDU3-IDS group ($p<0.0001$), which was normalized to wild-type levels. In the kidney, GAG content of the HSCT group was not significantly different from the MNDU3-GFP group, but scored significantly different from the MNDU3-IDS and wild type groups. Accumulation in the kidney was largely in the interstitium and glomeruli. (Figure 6A, B, E, & F).

Lysosomal associated membrane protein-1 (LAMP-1) is upregulated in cells with persistent GAG accumulation, such as IDS deficient cells. Therefore, LAMP-1 can be used as a marker for cellular damage[292]. The MNDU3-GFP group showed significantly higher

levels of LAMP-1 in the myocardium and aortic valve compared to wild-type mice ($p<0.05$). The MNDU3-IDS group showed normalized LAMP-1 staining in the myocardium. In the aortic valve, however, there was a reduction in LAMP-1 staining but this was not significantly different when compared to the MNDU3-GFP group. In the myocardium, the HSCT group was not significantly different than wild-type but did show low levels of LAMP-1 positivity in the aortic valve (Figure 6D, H & Supplemental Figure 9B, E). LAMP-1 positive macrophages were detected only in the colons of the MNDU3-GFP group (Supplemental Figure 9C, F). Taken together with the GAG assay results, this histological analysis shows that MNDU3-IDS can effectively reduce storage material to or near wild-type levels in the tissues analyzed, with the exception of the aortic valve and spinal cord.

LVV transduction was detected by *in situ* hybridization (ISH) for both the MNDU3-IDS and MNDU3-GFP groups. LVV positive cells were seen in the spleen and bone marrow, but not in the liver (Supplemental Figure 10C, D). In the brain, LVV positive cells were seen in the meninges, as well as the perivascular regions (Supplemental Figures 10A, B, & D), supporting a mechanism of gene-modified hematopoietic cell engraftment in the CNS. Additionally, ISH was employed to evaluate two multicentric lymphomas that occurred in two mice from the MNDU3-IDS group. LVV ISH performed on the spleen and liver was negative in the neoplastic lymphocytes. Thus, the two instances of lymphoma were considered spontaneous and unrelated to the vector.

Skeletal analysis

This MPS II mouse model exhibits a skull enlargement phenotype, which includes an increase in the cross-sectional area of the zygomatic bones[294.] To assess the impact of this therapy on skeletal manifestations, mice were imaged by either full body X-ray or Micro-CT to evaluate zygomatic arch thickening at 4 months post-transplant. An additional control group of untreated MPS II $IDS^{Y/-}$ mice (n=8) was also imaged. Figure 7A shows representative microradiographs from all 5 groups, with arrows indicating the location of the zygomatic arch. In these images, thickness of the zygomatic arch was measured as the diameter of the bone at this location. MNDU3-IDS and HSCT groups showed thickness similar to that of normal wild-type mice. However, mice from the MNDU3-GFP or untreated MPS II mice had significantly more bone thickening than untreated wild-type mice ($p<0.01$, $p<0.0001$) (Figure 7B). MNDU3-GFP treated mice showed significantly thicker zygomatic bones compared to the MNDU3-IDS treated mice ($p<0.05$), although not to the same extent as untreated MPS II controls ($p<0.0001$). These data thus reveal a trend toward normalization of the zygomatic arch skeletal defect in MNDU3-IDS as well as HSCT mice.

Neurobehavioral Analysis

At 4-months post-transplant (6 months of age), mice from all 4 groups underwent neurobehavioral testing to assess neurocognitive function. A 20-hole Barnes maze was used as a test of spatial navigation and memory and consisted of 4 three-minute trials a day for 4 days. On day one, all groups scored ~180s latency to escape. On day 3, the MNDU3-GFP group performed worse than the wild-type group ($p<0.05$), demonstrating a latency to escape of 105s compared to 69s. In contrast, the MNDU3-IDS and HSCT groups performed similarly to the wild-type group with a day 3 latency to escape of 58s

for each (Figure 8A). Fear conditioning is an associative learning task measuring fear responses to a conditioned stimulus, in this case a cue (light and sound). In this test, the MNDU3-IDS group exhibited a fear response that was similar to wild-type controls in % freezing during cue induction. Both the wild-type and MNDU3-IDS groups had a significantly better fear response compared to the HSCT group ($p<0.05$). Wild-type and MNDU3-IDS groups also trended with a higher percent freezing than the MNDU3-GFP group, but this difference was not statistically significant (Figure 8B). In conclusion, transplantation of MNDU3-IDS HSPCs into MPS II mice showed a trend towards normalization of neurobehavioral outcomes, indicating the potential for prevention of neurocognitive deficiency.

Discussion

In this study, we evaluated *ex vivo* transduction of HSPCs using an LVV carrying a codon optimized IDS encoding gene that is transcriptionally regulated by a strong, constitutively active MNDU3 promoter with subsequent transplantation into MPS II mice as a potential therapeutic. Circulating IDS enzyme activity was found to be >100 times higher than wild-type levels in the plasma and in PBMCs of MNDU3-IDS transplanted mice, indicating a high level of IDS was secreted from gene-modified hematopoietic cells and was bioavailable for cross-correction of unmodified host tissues. Tissue analysis confirmed supraphysiological levels of IDS enzyme activity in all analyzed peripheral tissues. In the CNS, IDS activity levels were ~13% of wild-type, sufficient to result in normalized GAG levels as observed both biochemically and histologically. Neurobehavioral evaluation showed that MNDU3-IDS engrafted mice performed as well

as wild-type mice in Barnes maze and fear conditioning analyses. Finally, skeletal analysis determined that MNDU3-IDS mice had significant reduction in zygomatic arch thickness.

Initial studies of *ex vivo* LVV-transduced HSPCs for MPS II showed correction of disease in peripheral tissues, but without improvement in CNS manifestations[310]. Other more recent studies have evaluated use of a tissue specific promoter, effectiveness against skeletal manifestations, and the need for a high level of engraftment[311-313]. Here we investigated the use of a ubiquitously expressed promoter in a comprehensive evaluation of biochemical, skeletal, histological, and neurobehavioral outcomes in MPS II mice. Circulating levels of IDS observed in our study were much higher than those reported in recent studies[312,313]. Reasons for these differences could include transduction efficiency, overall levels of engraftment achieved, or vector design. The sustained, supraphysiological levels of circulating IDS observed in this study facilitated metabolic cross-correction of tissues, with greater than wild-type levels of IDS observed in all analyzed peripheral tissues and commensurate normalization of GAG accumulation in these tissues. Previous reports of both *ex vivo* and *in vivo* IDS gene transfer approaches have similarly shown supraphysiological levels of IDS with GAG normalization[311,317]. We observed no toxic effect resulting from the high levels of IDS expressed in MNDU3-IDS treated $IDS^{Y/-}$ mice. One concern regarding supraphysiological levels of IDS expression is the potential impact on post-translational modification and trafficking of other lysosomal hydrolases[426]. However, recent reports have shown that elevated levels of IDS in IDS deficient mice restore other lysosomal hydrolases to normal levels of activity[300,315].

As previously reported, IDS levels measured in the brains of wild-type mice were higher than any other analyzed tissue[311,316,317]. Overall, these preclinical studies suggest that regardless of gene therapy modality, achieving wild type levels of IDS in the mouse brain remains a significant challenge[311,316,317]. What it is that limits IDS expression has not been reported. By comparison, MPS I preclinical gene therapy studies generally achieve higher than wild type levels of IDUA enzyme activity in the brain[395,427.428]. Conversely, preclinical gene therapy studies of MPS IIIA have also been unable to achieve wild-type levels of *N*-sulfoglucosamine sulfohydrolase[429.430]. Although in this study normal levels of IDS in the brain were not reached, MNDU3-IDS mice achieved IDS levels in the brain that were ~13% of wild-type IDS mice and were sufficient to normalize brain GAG levels. Previous studies have suggested that only a fraction (<5%) of wild-type IDS is needed to impact GAG accumulation in the CNS[314,316]. Similar results have been reported in conjunction with both AAV and LVV based therapies for MPS II. AAV based therapies both systemic[317] and CNS directed[300,316] have shown that increased IDS levels in the brain between 5-40% of wild-type significantly reduced GAG content. A similar finding was reported in an *ex vivo* LVV based study where ~5% of wild-type brain IDS activity normalized brain GAG content[311]. Additionally, Laoharawee et al[318] showed that as little as 1.5% of wild-type IDS reduced GAG accumulation and positively impacted neurocognitive function. Our data are consistent with these studies, as we observed normalization of brain GAGs to wild-type levels, and no significant differences were seen between MNDU3-IDS and unaffected controls in tests of spatial learning and memory in the Barnes maze as well as learning and memory in fear conditioning. Additionally, the MNDU3-IDS group performed significantly better than the MNDU3-

GFP affected control group in the Barnes maze on Day 3 and the HSCT group in fear conditioning. While we observed that the MNDU3-GFP affected control mice failed to show as much of a deficit as expected based on previous neurobehavioral analyses of similarly aged MPS II mice[315,316], the differences between the HSCT, MNDU3-IDS and wild-type groups highlight the potential effectiveness of LVV gene therapy over allogeneic HSCT to impact neurological manifestations of MPS II.

The mechanism of action of allogeneic HSCT for treatment of the mucopolysaccharidoses, especially MPS I, is thought to be, in part, through donor-derived monocyte trafficking to the brain followed by differentiation into resident microglia[38]. These cells can then metabolically cross-correct neurons via mannose-6-phosphate receptors to reduce GAG levels and impact CNS manifestations associated with the disease[43]. This concept also applies to autologous LVV transduced HSPCs, whereby the progeny of transduced HSPCs traffic to the CNS, differentiate into microglia and mediate metabolic cross-correction. To support this mechanism, we used *in situ* hybridization to demonstrate the presence of LVV positive cells in the choroid plexus, perivascular regions of the brain, and in the brain meninges. However, we did not see any LVV positive cells in the brain parenchyma. Another possible mechanism of enzyme delivery to the brain is by circulating enzyme crossing the blood brain barrier or blood CSF barrier[300,383]. Systemic based studies have provided evidence that sufficiently high levels of circulating IDS enzyme can impact the CNS. A liver directed therapy using AAV 2/8 vectors encoding zinc finger nucleases targeting the albumin locus for liver-specific expression showed a moderate level of circulating IDS, a low level of brain IDS activity, a reduction in GAG accumulation, and neurobehavioral correction[318]. Similar

results have been shown in studies focusing on MPS I and IDUA expression in a liver directed strategy using intravenously administered AAV[383,431]. However, the mechanism by which circulating enzyme accesses the CNS has not been elucidated. Given the extremely high levels of systemic IDS achieved in our study, it is thus possible that circulating IDS contributed to the observed IDS levels in the brain of MNDU3-IDS mice.

Patients with MPS II exhibit a variety of skeletal manifestations termed dysostosis multiplex. MPS II mice also display skeletal evidence of disease, such as thickening of the zygomatic arch[294]. To evaluate the impact of autologous HSCT with gene-modified cells on skeletal manifestations associated with MPS II, we employed full body X-ray and Micro-CT. Wada et al[313] recently showed that *ex vivo* gene therapy in MPS II mice can resolve bone lesions, including the zygomatic arch, by remodeling. Our skeletal analyses showed similar results in which we saw a reduction in zygomatic arch diameter, suggesting engraftment of MNDU3-IDS transduced cells could prevent the emergence of skeletal manifestations in MPS II mice.

Allogeneic HSCT is not considered a standard treatment option for MPS II due to the lack of evidence that it can effectively address CNS manifestations, as well as safety issues associated with allotransplant such as graft vs. host disease[62,251]. This contrasts with other lysosomal diseases, such as MPS I, where allogeneic HSCT is considered standard of care and there is evidence that engraftment following allogeneic HSCT can impede the onset of CNS manifestations. Given that MPS I and MPS II exhibit similar disease manifestations, why is it that only MPS I shows neurologic stabilization following allogeneic HSCT? Currently, one difference is that the time to diagnosis has been faster for MPS I than for MPS II; diagnosing and transplanting MPS II patients at an

earlier age could lead to increased neurologic stabilization[170]. Indeed, some recent evidence suggests that allogeneic HSCT, particularly when administered early, could be a viable treatment option for MPS II[251,254]. It's also possible that the amount of IDS expressed by engrafted cells may be insufficient to achieve therapeutic effectiveness. If this is the case, *ex vivo* gene transfer may be a better option for delivering more gene-modified cells capable of producing supraphysiological levels of enzyme compared to allogeneic HSCT.

Here we report that MPS II mice engrafted with MNDU3-IDS transduced HSPCs exhibit supraphysiological levels of circulating, bioavailable IDS enzyme capable of tissue cross-correction as evidenced by normalization of GAGs. In the CNS, increased levels of IDS activity with concurrent GAG normalization was observed as well as a benefit to neurocognitive function. Overall, this study supports the potential therapeutic efficacy of *ex vivo* MNDU3-IDS LVV transduced HSPCs for MPS II patients.

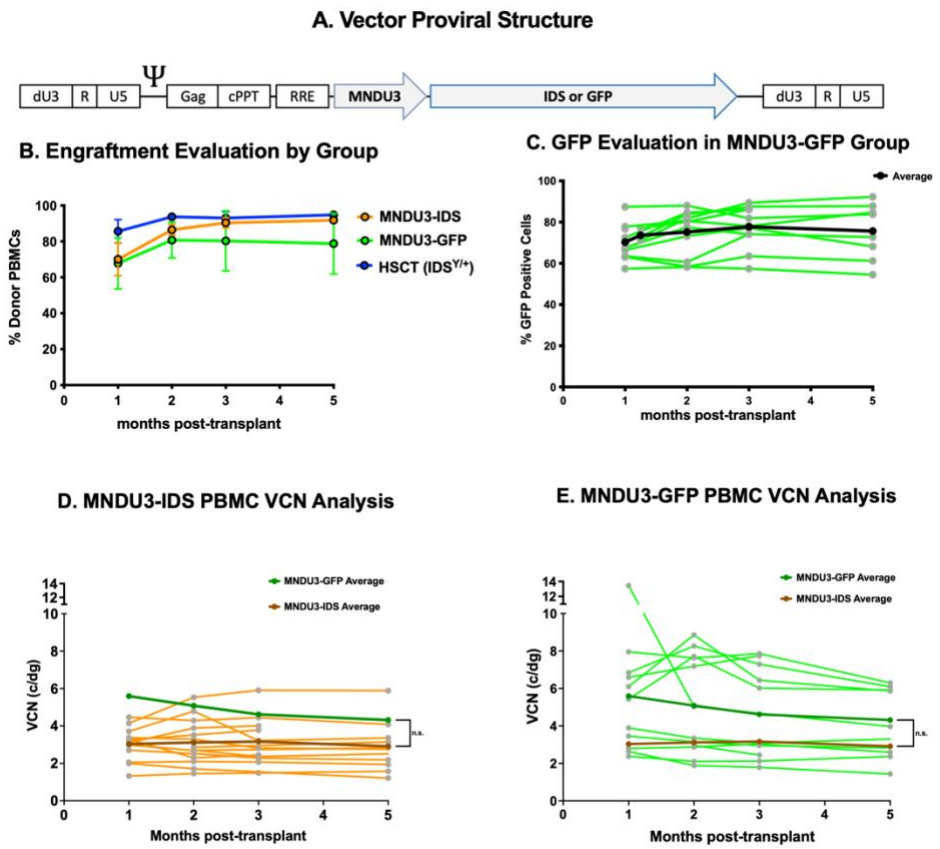

Figure 3. Donor chimerism and VCN analysis in transplant recipients. (A) Diagram of the lentiviral vector proviral construct containing a codon optimized IDS or GFP sequence regulated by the MNDU3 promoter. dU3- deleted U3 region (self-inactivating), R- repeat region, U5- unique 5' region, Y- packaging signal, gag- group specific antigen sequence, cPPT- central polypurine tract, RRE- rev response element, MNDU3- myeloproliferative sarcoma virus U3 region with negative control elements deleted and dl587rev primer binding site added[432], IDS- codon optimized human IDS. (B) Mean donor engraftment for the three transplant groups as indicated in the key. (C) Percentage of GFP positive cells for each animal in the MNDU3-GFP group. Green lines show individuals, while the black line indicates GFP+ average over time. In D and E, PBMCs were analyzed by qPCR to determine VCN per cell (c/dg) post-transplant. The dark orange and dark green lines on each graph represent the MNDU3-IDS and MNDU3-GFP average VCNs by month, respectively. (D) MNDU3-IDS LVV transplant group VCN evaluation. Orange lines show individual animal VCN by month. (E) MNDU3-GFP LVV transplant group, VCN evaluation. Green lines show individual animals VCN by month. Some time points were not collected due to COVID-19 lockdown. (For donor chimerism data this includes two month 2, two month 3, and four month 5 MNDU3-IDS samples; one month 2, one month 3, and three month 5 MNDU3-GFP samples; and one month 2, one month 3, and one month 5 HSCT samples. For VCN this includes two month 3 and two month 5 MNDU3-IDS samples, and one month 3 and two month 5 MNDU3-GFP samples.) Sample size for group engraftment: MNDU3-IDS N=9-14, MNDU3-GFP N=8-12, HSCT N=10-11. Sample size for GFP evaluation: MNDU3-GFP: N=12. Sample size for VCN analysis: MNDU3-IDS N=14 and MNDU3-GFP N=12. Error bars show mean +/- S.D. for B-E.

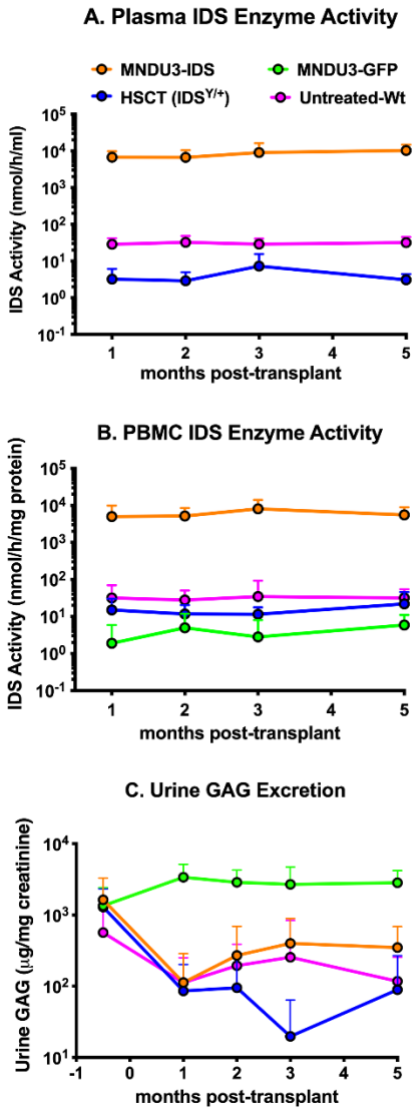

Figure 4. Plasma IDS, PBMC IDS and urine GAG excretion. (A, B) Plasma and PBMC mean IDS enzyme activities by month for each group indicated in the key. All MNDU3-GFP plasma samples have been omitted, as the activity measured was below limit of quantification (LOQ). (C) Mean excreted GAGs in urine collected 2 weeks before the study and then monthly thereafter for the groups indicated in the key. Some time points were not collected due to COVID-19 lockdown (for plasma, PBMC, and urine GAGs; two month 3 and two month 5 MNDU3-IDS samples, one month 3 and two month 5 MNDU3-GFP samples, and two month 3 and two month 5 Untreated-Wt samples). Sample size for IDS activity assays: MNDU3-IDS N=11-14, MNDU3-GFP N=9-12, HSCT N=10, and Untreated-Wt N=9-12. Sample size for Urine GAG assays: MNDU3-IDS N=4-9, MNDU3-GFP N=6-10, HSCT N=1-9, and Untreated-Wt N=1-5. Error bars show mean +/- S.D.

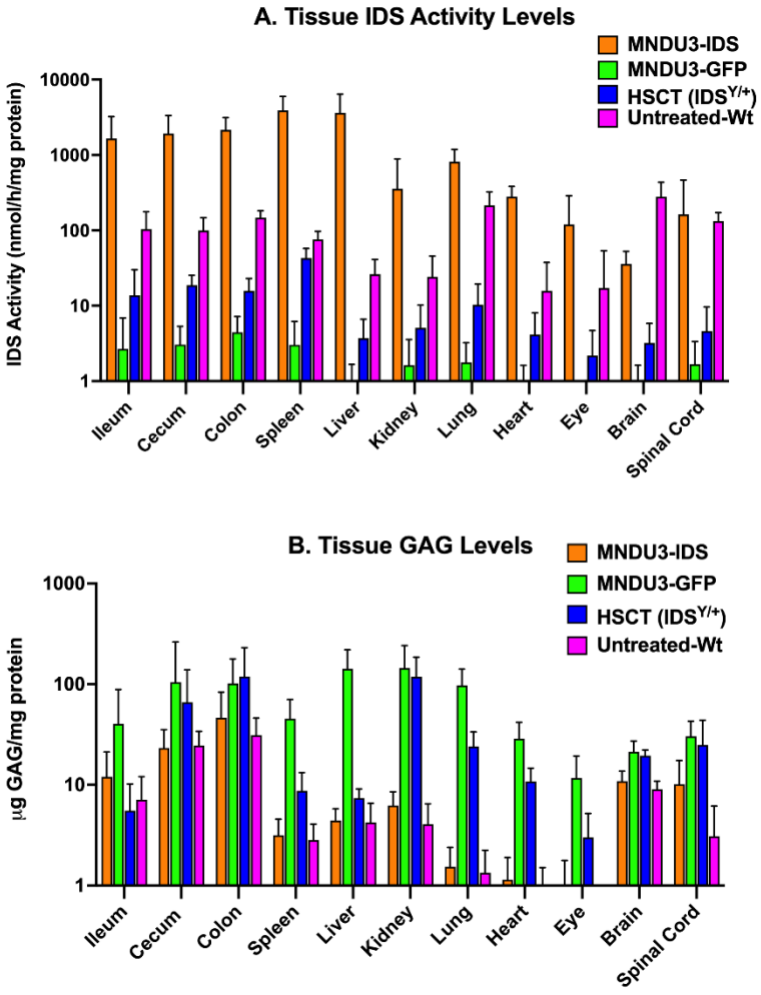

Figure 5. Tissue IDS enzyme and GAG levels for Chapter II. (A) Mean IDS activity in each indicated tissue for each experimental group shown in the key. (B) Mean GAG levels in the indicated tissue and for animal groups shown in the key. Sample size for IDS activity and GAG assays: MNDU3-IDS N=9-12, MNDU3-GFP N=8-11, HSCT N=7-10, and Untreated-Wt N=8-11. Error bars show mean +/- S.D.

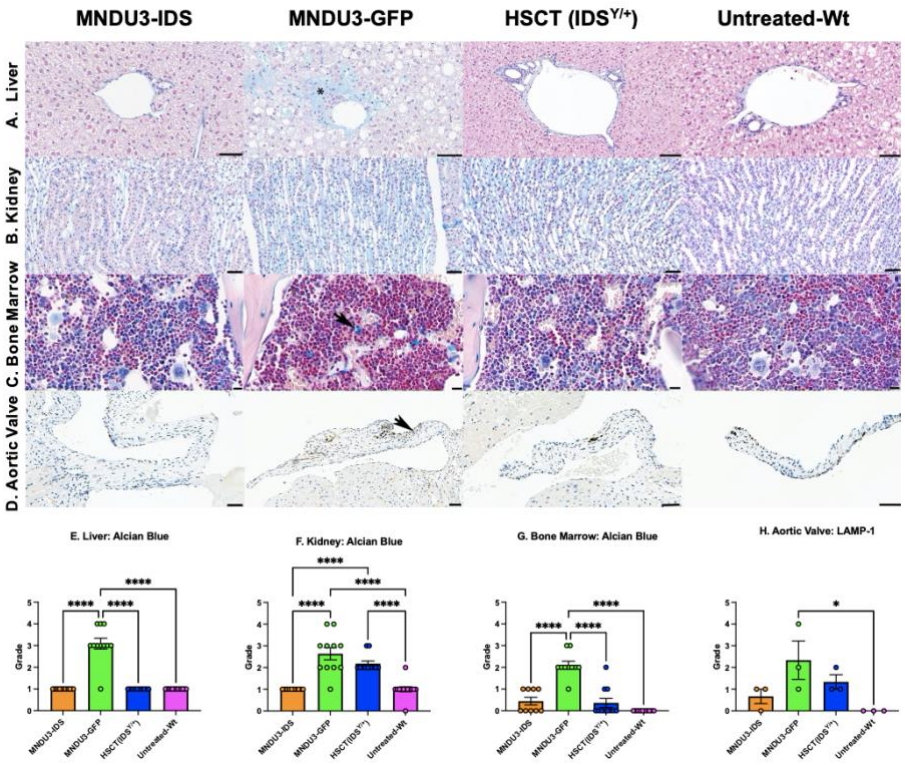

Figure 6. Histological evaluation. Micrographs are presented by group, left to right: MNDU3-IDS, MNDU3-GFP, HSCT, and Untreated-Wt. (A) Liver, Alcian blue (AB) staining. The MNDU3-IDS and Untreated-Wt groups are both AB negative. The MNDU3-GFP group has extensive deposition of AB positive material in the perivascular region extending out into the acini disrupting the architecture (asterisk). There is extensive vacuolation of the hepatocytes with variable amounts of cytoplasmic AB positive material in hepatocytes. The HSCT shows a small amount of AB positive material in the perivascular regions. Scale bars = 50 µm. (B) Kidney, AB staining. The MNDU3-IDS and Untreated-Wt groups both have a normal amount of AB positive material. The MNDU3-GFP and HSCT groups both have AB positive material within the collecting duct epithelial cell cytoplasm. Scale bars = 50 µm. (C) Bone marrow, AB staining. The MNDU3-IDS, HSCT and Untreated-Wt groups are AB negative. The MNDU3-GFP group has numerous macrophages with abundant cytoplasmic AB positive material (black arrow). Scale bar = 10 µm. (D) Aortic valve, LAMP-1 IHC. The MNDU3-IDS group has scant LAMP-1 positivity within the valvular stroma. The MNDU3-GFP group has extensive LAMP-1 positivity throughout the valvular stroma (black arrow). The HSCT group has a small amount of LAMP-1 positivity throughout the valvular stroma. The Untreated-Wt group is LAMP-1 negative. Scale bar = 50 µm. Semiquantitative scoring of AB staining in the (E) liver, (F) kidney, and (G) bone marrow. (H) LAMP-1 IHC quantitative scoring of the aortic valve. Error bars show SEM. Statistics done by one-way ANOVA. *: P<.05, ****: P<.0001.

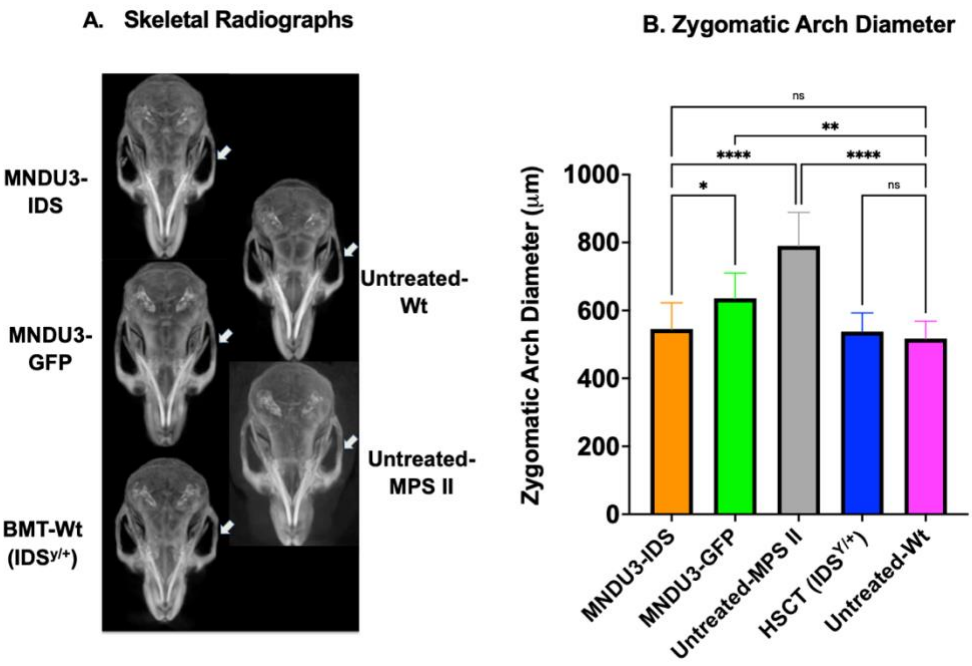

Figure 7. Skeletal analysis. (A) Example radiographs of mouse skulls obtained by Micro-CT analysis for the indicated experimental group. Arrows indicate zygomatic arch location. (B) Comparison of zygomatic arch diameter by group. Significance was determined by one-way ANOVA with Tukey's multiple comparisons test. Sample sizes: MNDU3-IDS N=13, MNDU3-GFP N=11, Untreated-MPS II N=8, HSCT N=10, and Untreated-Wt N=11. Error bars show SEM. ns: no significance, *: P <.05, **: P<.01, ****: P<.0001.

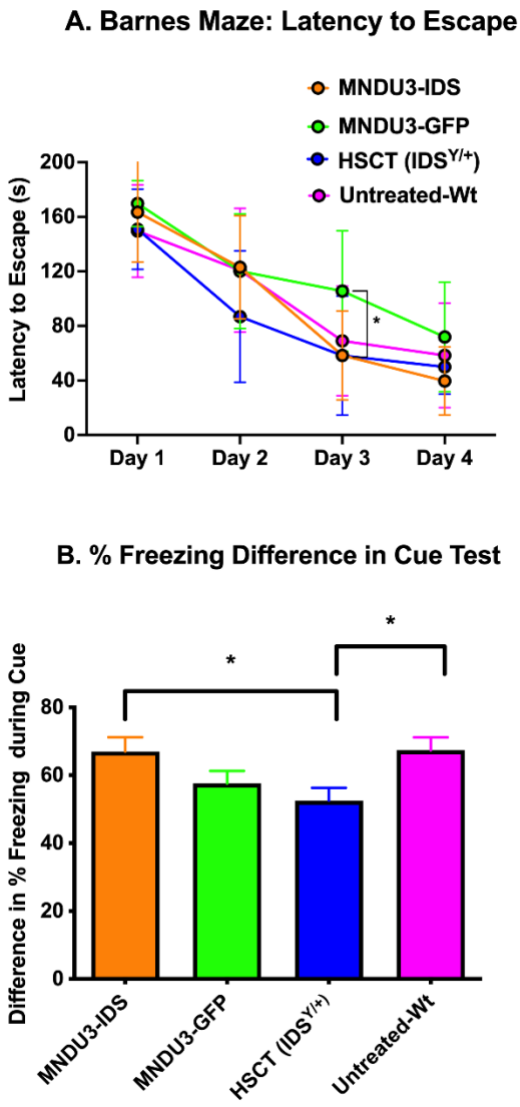

Figure 8. Neurocognitive evaluation by Barnes maze and fear conditioning cue. All four groups were evaluated neurobehaviorally at 4 months into the study. (A) Barnes maze as a long-term spatial memory test. Results are reported as the mean latency to escape over four trials per day for each group. Significance was assessed by 2-way ANOVA. *: P<.05. (B) Fear conditioning cue test, run as a test of learning, memory, and anxiety. Results are reported as percent difference in freezing time between mean of 3 cued vs mean of 3 baseline timepoints per mouse. Significance was determined by Mann-Whitney U Test. *: P<.05. For A and B, error bars show mean +/- S.D. Sample size for both tests: MNDU3-IDS N=12, MNDU3-GFP N=11, HSCT N=10, and Untreated-Wt N=11.

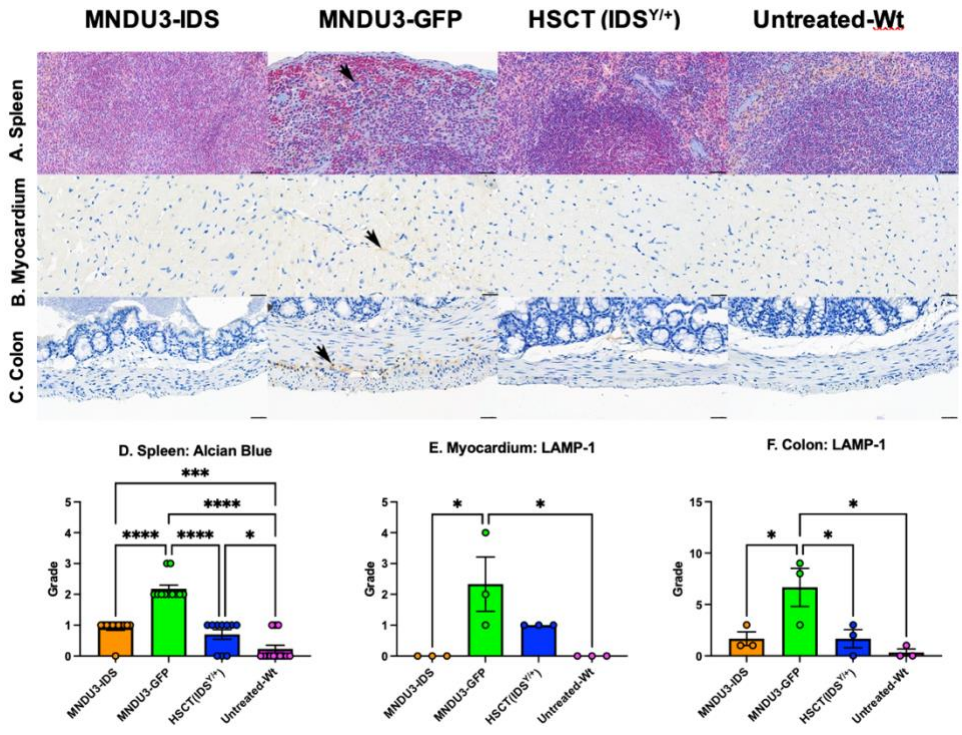

Figure 9. Spleen Alcian blue staining; heart and colon LAMP-1 IHC. Micrographs are presented by group, left to right: MNDU3-IDS, MNDU3-GFP, HSCT, and Untreated-Wt. (A) Spleen, AB staining. The MNDU3-IDS, HSCT and Untreated-Wt groups are AB negative. The MNDU3-GFP group has numerous macrophages with abundant cytoplasmic AB positive material (black arrow). Scale bar = 40µm. (B) Myocardium, LAMP-1 IHC. The MNDU3-IDS, HSCT and Untreated-Wt groups are LAMP-1 negative. The MNDU3-GFP group has extensive mild LAMP-1 positivity within cardiac myocytes (black arrow). Scale bar = 40µm. (C) Colon, LAMP-1 IHC. MNDU3-IDS, HSCT and Untreated-Wt groups are LAMP-1 negative. The MNDU3-GFP group has numerous LAMP-1 positive macrophages throughout the tunica muscularis and submucosa (black arrow). There is mild multifocal LAMP-1 positivity within smooth muscles cells of the tunica muscularis. Scale bar = 40µm. (D) Semiquantitative scoring of spleen AB staining. LAMP-1 IHC quantitative scoring of the myocardium (E) and colon (F). Error bars show SEM. Statistics done by one-way ANOVA. *: P<.05, ***: P<.001, ****: P<.0001.

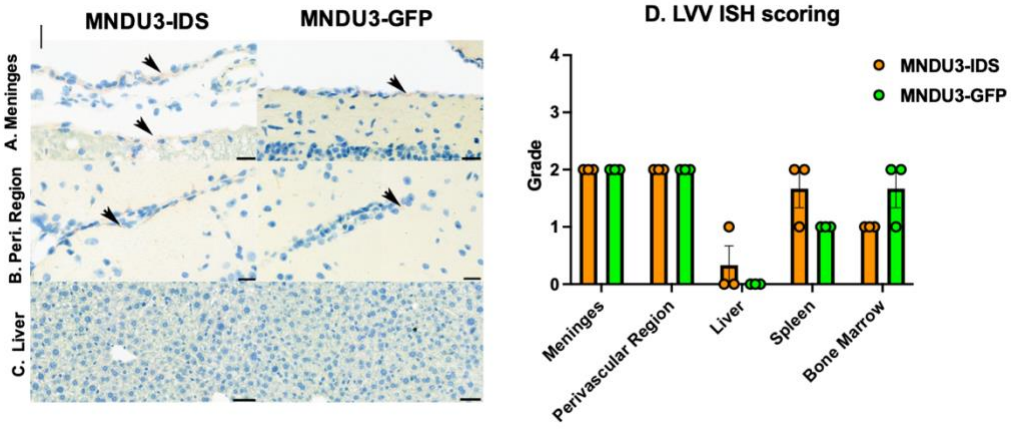

Figure 10. LVV detection by in situ hybridization (ISH). Micrographs are presented by group, left to right: MNDU3-IDS, MNDU3-GFP. (A) LVV ISH in meninges of both the MNDU3-IDS and MNDU3-GFP groups have extensive moderate LVV ISH positivity (black arrows). Scale bars = 20 µm. (B) LVV ISH in the perivascular region of the cortical grey matter in both the MNDU3-IDS and MNDU3-GFP groups has multifocal moderate LVV ISH positivity (black arrows). Scale bars = 20 µm. (C) LVV ISH in the liver is diffusely negative in both the MNDU3-IDS and MNDU3-GFP groups for LVV ISH. Scale bars = 40 µm. (D) Quantitative ISH scoring based on positive cell rate. Errors bars show SEM.

Chapter III: Comparative minimal dose effectiveness of intravenous and intrathecal AAV9.CB7.hIDS (RGX-121) in a murine model of mucopolysaccharidosis type II

Miles C Smith[1], Lalitha R Belur[1], Andrea D Karlen[1], Olivia Erlanson[1], Justin Furcich[2], Troy C. Lund[2], Davis Seelig[3], Kwi Hye Kim[4], Nick Buss[4], R. Scott McIvor[1*]

[1]Center for Genome Engineering, Department of Genetics, Cell Biology and Development, University of Minnesota, Minneapolis, MN, United States

[2]Department of Pediatrics, University of Minnesota, Minneapolis, MN, United States

[3]Comparative Pathology Shared Resource, University of Minnesota, St. Paul, MN, United States

[4]REGENXBIO Inc

* Corresponding Author:
R. Scott McIvor
mcivo001@umn.edu

Summary

Mucopolysaccharidosis type II (MPS II, Hunter syndrome) is an X-linked recessive lysosomal disease caused by iduronate-2-sulfatase (IDS) deficiency. Insufficient IDS leads to the accumulation of glycosaminoglycans (GAGs) in tissues and the emergence of disease manifestations that include cardiopulmonary dysfunction, dysostosis multiplex, neurological impairment, and in severe cases death by early adolescence. Currently, the only approved treatment for MPS II is enzyme replacement therapy (ERT), Elaprase®. However, systemically delivered enzyme does not readily cross the blood brain barrier, leaving the neurological manifestations of MPS II unaddressed. An alternative strategy for the treatment of MPS II is CSF-directed administration of AAV9.CB7.hIDS (RGX-121). However, it is not known whether CSF-directed administration of AAV9.CB7.hIDS will improve both neurologic and systemic manifestations of MPS II or if supplemental systemic administration will be necessary. In this study we compared the effectiveness of a CNS-directed intrathecal (IT) route of administration (ROA) with a systemic intravenous (IV) ROA at a range of vector doses. Doses of $1x10^{7}$gc and $1x10^{8}$gc were ineffective when administered by either ROA. A dose of $1x10^{9}$gc by either ROA resulted in plasma IDS activity at or above wild type levels but was insufficient to achieve wild type levels of IDS or reduced GAGs in most tissues, including the CNS. Doses of $1x10^{10}$gc and $1x10^{11}$gc by either ROA, resulted in plasma IDS activity >100-1000 times the wild type level, and nearly all tissues showed at or above the wild type IDS levels, with a commensurate reduction of GAGs. These same doses by either ROA showed normalization of the zygomatic arch diameter compared to untreated controls or animals administered vector at lower doses, thereby demonstrating

the effectiveness CSF-administered vector in addressing peripheral manifestations of disease. In the brain, the highest quantifiable levels of IDS activity, greatest reduction in GAG content, and prevention of neurocognitive deficits was achieved by administration of $1x10^{11}$gc IT. We conclude that IT or IV administration of AAV9.CB7.hIDS at a dose of $1x10^{10}$gc normalized metabolic and skeletal outcomes in MPS II mice, but that neurologic improvement required IT administration of $1x10^{11}$gc, suggesting the prospect of a similar direct benefit in humans.

Introduction

Mucopolysaccharidosis type II (MPS II or Hunter syndrome) is an X-linked recessive lysosomal disease that affects approximately 1:160,000 male births[86]. The disease is caused by mutation in the *IDS* gene, which leads to deficiency of iduronate-2-sulfatase (IDS). IDS is required for the stepwise degradation of glycosaminoglycans (GAGs) heparan sulfate and dermatan sulfate[57]. Insufficient IDS thus leads to lysosomal accumulation of fully or partially undegraded GAGs in practically all tissues, including cardiac, skeletal, and nervous tissue. Patients with MPS II manifest organomegaly, joint stiffness, arthropathy, hearing loss, cardiopulmonary dysfunction, and skeletal dysplasias[87]. In addition to peripheral disease symptoms, 2/3^{rds} of patients exhibit central nervous system (CNS) manifestations that begin around the age of 2. This neuronopathic form of MPS II includes aggressive behavioral problems, seizures, developmental delay, neurocognitive decline, and death by adolescence[57,87,88,94].

Enzyme replacement therapy (ERT), intravenously administered recombinant IDS (Elaprase®), is the current standard of care for MPS II[77,212,305]. Both non-neuronopathic

and neuronopathic forms of MPS show benefit from ERT in the periphery, such as reduced urine GAG excretion, reduced organomegaly, and improved walking performance[76,206]. ERT can thus manage some aspects of the disease with weekly infusions, but some peripheral and all neurological disease manifestations are left unaddressed. Patients followed for 9 years on ERT did not improve in respiratory, ocular, skeletal or CNS outcomes[211]. It is widely held that ERT provides no CNS benefit for neuronopathic MPS II because the administered enzyme does not cross the blood brain barrier (BBB)[189]. A recent clinical evaluation of intrathecally (IT) administered ERT showed promise by stabilizing neurocognitive function in some patients but failed to do so in others[224]. ERT is also problematic with regard to high cost (>$500,000 USD) and time-consuming weekly infusions. Due to its effectiveness in other lysosomal diseases such as MPS I, allogeneic hematopoietic stem cell transplantation (HSCT) has also been considered as a treatment for MPS II. However, due to early reports of uncertain CNS benefit and transplant complications HSCT is not currently a recommended treatment for MPS II[43]. Although more recent reports on HSCT for MPS II have shown some neurologic benefit, so far there is insufficient and variable clinical outcome[251,254,348]. There is thus an unmet need for treatment that can overcome the limitations of those currently available for MPS II, particularly the neuronopathic form of the disease.

The monogenic nature of MPS II means metabolic correction is achievable by supplying a functional copy of the *IDS* sequence via gene transfer. In addition, cells supplied with a functional gene copy can secrete enzyme via the mannose-6-phospahte pathway to metabolically cross correct other defective cells[329]. For *in vivo* gene transfer purposes, AAV vectors have several advantageous properties for treating lysosomal

diseases in general, such as a variety of tropisms, the potential for strong and lasting expression, and safety[55,371,454,455]. AAV serotype 9 (AAV9) has been of particular interest for MPS II gene therapy owing to its neurotropic properties and potential for systemic transduction[361,456]. Delivery of AAV for MPS II has been accomplished through both systemic and CNS-directed routes of administration (ROA) in MPS II mice. The earliest reports consisted of systemic administration of an AAV2 vector, which showed correction of skeletal and locomotor abnormalities[295,314]. More recently scAAV9 was introduced intravenously (IV) showing brain IDS activity, brain GAG reduction, and improved neurobehavior using vector doses between $2.5x10^{12}$gc-$2x10^{13}$gc[317]. Several studies have explored CSF-directed AAV9 administration either intracisternal or intracerebroventricular (ICV). Lower doses of $3x10^{10}$gc-$5x10^{10}$gc achieved widespread CNS transduction, IDS activity and GAG reduction in the brain, with normalized neurocognitive function[300,314,315]. These results suggest that unlike ERT or HSCT, gene therapy can address the CNS disease manifestations in MPS II patients. Previously conducted MPS II clinical trials involving transduction of patient lymphocytes *ex vivo* with a retroviral vector or liver directed gene editing did not achieve significant IDS expression. Currently, AAV9.CB7.hIDS (RGX-121) is in clinical trials where it is administered intracisternally (NCT03566043, NCT04571970) to address the CNS disease manifestations. However, it is not known whether RGX-121, when administered intrathecally, is sufficient to remedy both peripheral and CNS manifestations of MPS II. In this study, IT and IV ROAs were compared for their effectiveness and dose-response in remedying both peripheral and CNS manifestations of murine MPS II as a model for genetic therapy of the human disease.

Materials and Methods

Animal husbandry

All animal husbandry and procedures were compliant with and approved by the University of Minnesota Institutional Animal Care and Use Committee (IACUC). Wild-type C57BL/6 mice were purchased from the National Cancer Institute or Envigo and C57BL/6 iduronate-2-sulfatase knockout (IdS-KO) mice were graciously provided by Dr. Joseph Muenzer of the University of North Carolina[294]. Offspring were genotyped by PCR and maintained at University of Minnesota Research Animal Resources facilities under specific pathogen free conditions. Animals were provided food and water *ad libitum*.

AAV vector design and production

RGX-121 was designed, constructed, and packaged by REGENXBIO, Inc., Rockville, Maryland. The vector plasmid consisted of; (i) the CB7 promoter sequence (chicken β-actin promoter and cytomegalovirus immediate-early enhancer) and chimeric intron (chicken β-actin intron with intron 2 splice acceptor, rabbit β-globin exon 3). (ii) a codon-optimized *hIDS* coding sequence; (iii) a rabbit B globin polyadenylation signal. (iv) AAV2 ITR's (inverted terminal repeats) flanking the IDS transcription unit. This AAV vector construct was packaged[316] by co-transfection with an AAV2/9 rep/cap plasmid along with adenovirus helper plasmid pAdDF6 into HEK293 cells. Vector product was purified from cell supernatant by affinity chromatography as previously

described[457]. For potency assessment the vector which was titered by digital droplet PCR[457].

AAV vector administration

Genotyped MPS II mice were administered AAV9 vector doses of 10^7, 10^8, 10^9, 10^{10}, or 10^{11} genome copies (gc) at two months of age. Intravenous injections were given in a 100µL volume through the lateral tail vein. Intrathecal injections were given to conscious animals in a 10µL volume between the L5 and L6 vertebrae as previously reported[395].

Tissue processing

Animals were euthanized at 4 or 7 months of age by CO_2 asphyxiation and transcardially perfused with 0.9% normal saline. A necropsy was performed, and tissues (liver, spleen, kidney, brain, heart, lung, spinal cord, and gonad) were harvested, frozen on dry ice and stored at -20 °C until processed. A section of each tissue was fixed in 10% neutral buffered formalin (VWR) at a ratio of 1:10-20 v/v tissue to formalin, and after 24-48 hours transferred to 70% ethanol for storage and histologic analysis. A Bullet Blender bead mill (Storm 24 Homogenizer, NEXT ADVANCE) was used to process tissues for biochemical analysis by homogenization in 0.9% saline as previously described [316,318] and clarified by centrifugation in a 5424R Eppendorf centrifuge. The clarified supernatants were termed tissue lysates and were used for protein, IDS, and GAG assays. Unclarified homogenates were used for qPCR analysis. Homogenates and lysates were stored at -20 °C until further processing or analysis.

Iduronate-2-sulfatase (IDS) enzyme activity

IDS enzyme activity in plasma and tissue lysates was determined in a fluorometric assay using 4-methylumbelliferyl α-l-iduronide 2-sulfate disodium salt (4-MU2S) as substrate (Cat #: M334715, Toronto Research Chemicals or Cat #: EM03201, Carbosynth) as previously described[316,436]. 5 mg of 4-MU2S substrate was dissolved in 8.33 mL substrate buffer (0.1M Na-Acetate buffer, pH 5.0 + 10 mM Pb-Acetate + 0.02% (w/v) Na-azide) to yield a 1.25 mM working solution. 10 μL aliquots of plasma or tissue lysates were mixed with 20 μL aliquots of working substrate and incubated at 37 °C for 1.5 hours. The IDS reaction was then stopped with the addition of 20 μL of PiCi Buffer (0.2M Na2HPO4 + 0.1M Citric Acid, 0.02% Na-Azide, pH 4.5). 10 μL of 5 μg/mL alpha-L-iduronidase (IDUA) (Cat #: 4119-GH, Bio-Techne) was added and incubated at 37 °C overnight. The reaction was terminated by adding of 200 μL stop buffer (0.5 M Na2CO3 + 0.5 M NaHCO3, pH 10.7) and then the reaction mixture was centrifuged at ~13,000 rpm for 1 minute. The supernatant was transferred into a black 96-well round bottom plate and the resulting fluorescence was measured using a Bio-Tek Synergy Mx plate reader with excitation at 355 nm and emission at 460 nm. A 4-MU (Sigma #M1381) standard curve was used to calculate the amount of 4-MU produced in the reaction. Tissue lysates were also assayed for total protein using Pierce protein assay reagent (Cat #: 22660, ThermoFisher). Enzyme activity is expressed as nmol 4-MU released per mg protein per hour (nmol/h/mg) for tissues extracts, and as nmol/h/ml for plasma. All samples were assayed in duplicate.

Glycosaminoglycan (GAG) assay

Proteinase K (20 mg/mL) was mixed with tissue lysates at a ratio of 1:10 (ProK:tissue lysate) and incubated at 55 °C overnight, followed by proteinase K inactivation by boiling for 10 minutes. 50uL of tissue lysate was then digested with 200 units of DNase and 2 mg of RNase at room temperature overnight. Nucleases were inactivated by boiling for 10 minutes. GAG levels were determined using the Blyscan Sulfated Glycosaminoglycan Assay kit (Biocolor Life Science Assays, Accurate Chemical, NY Inc. Cat # CLRB1000) according to the manufacturer's instructions, with results expressed as μg GAG/mg lysate protein. GAG levels were assayed in unprocessed urine using the Blyscan kit, normalizing to urine creatinine (creatinine levels were determined using a creatinine assay kit; Sigma, MAK080) and expressed as μg GAG/mg creatinine.

Vector biodistribution by quantitative PCR (qPCR)

Tissue homogenates were incubated with Proteinase K overnight at 55°C and then genomic DNA was extracted using phenol-chloroform. For qPCR, each reaction contained 100ng gDNA template, 2x IQ SYBR Green Supermix (Bio-Rad), 5pmol/μL forward primer (5'-CCCTGGTAATCCCCGTGAAC-3'), 5pmol/μL reverse primer (5'-TGGTGCGTATGGAATAGCCC-3'), and nuclease free water to a volume of 25μL. Thermocycler parameters were: 95°C for 5 minutes, followed by 40 cycles of 95°C for 15s, 59°C for 30s, and 72°C for 45s in a Bio-Rad C1000 Touch Thermo Cycler. A standard curve was generated by serial dilution of plasmid

pAAV.CB7.CI.hIDS.RBG.KanR. QPCR results from analysis are expressed as vector copies per genome equivalent.

Radiographic analysis of zygomatic arch

One week before euthanasia, all experimental animals underwent Micro-CT imaging using a Siemens Inveon PET/CT machine. The animals were sedated with 5% isoflurane before imaging. Micro-CT imaging resulted in DICOM files that were converted to Imaris image files using the Imaris File Converter software. This Imaris file was analyzed using the Imaris 3D Analysis software. This analysis obtained whole body measurements from the converted Micro-CT scans, including zygomatic arch diameter.

Histopathology

Processing of formalin-fixed tissues was carried out by a graded series of alcohols. For hematoxylin and eosin (H&E) analysis, tissues were embedded in paraffin and 4 μm sections were cut and stained. For Alcian Blue staining, 4 μm sections were cut, deparaffinized, and hydrated to distilled water. Sections were immersed in a solution of 3% acetic acid for 3 minutes and subsequently stained with Alcian Blue for 30 minutes. After rinsing with running tap water and then distilled water, the slides were counterstained with nuclear fast red. For LAMP1 IHC, 4 μm formalin-fixed, paraffin-embedded (FFPE) sections were deparaffinized, rehydrated, and submitted to heat induced antigen retrieval in EDTA. Slides were incubated with a 1:500 diluted rabbit monoclonal anti-LAMP antibody (ab208943, Abcam) overnight at 4°C. Following this,

slides were incubated with Rabbit Envision (Dako) for 30 minutes and then chromogen 3,3'-diaminobenzidine (DAB) before hematoxylin counterstaining.

Barnes Maze

The Barnes maze is a measure of spatial navigation and memory[437]. The maze is comprised of a circular platform with twenty holes located around the periphery, all of which are blocked apart from the escape hole. The escape hole has a box placed underneath, which is accessible to the mouse. Visual cues are placed on the walls surrounding the maze, which are used by the mice for spatial navigation. The mouse is placed in the center of the maze under bright overhead lights and given 3 minutes to explore the maze. If the mouse does not enter the escape box within 3 minutes, it is gently guided to the escape hole and left there for 15-30 seconds before returning to its home cage. The mice were given trials on the Barnes maze 4 times a day for 4 days, with an interval of 10-20 minutes between any two consecutive trials for each mouse. The time taken by the animal to enter the escape hole was recorded as latency to escape.

Statistics

Microsoft Excel was used for calculations and analysis. GraphPad Prism was used for all graphing and statistics. One-way ANOVA was utilized for group comparisons in radiographic data. Multiple group comparisons were evaluated by 2-way ANOVA for Barnes maze. P values of < 0.05 were considered statistically significant for all tests.

Results

Study Rationale and In-life evaluations

We previously reported the prevention of neurologic deficits and metabolic disease in MPS II mice after either intravenous[465] or CSF-directed[316] (intracerebroventricular) administration of an AAV9.CB7.hIDS vector to achieve systemic or CNS -directed expression of iduronate sulfatase. We also observed in the ICV studies that there was substantial release of AAV9-hIDS vector from the CSF, transduction of the liver and secretion of IDS into the circulation[316]. The current study has been undertaken first of all to determine if the systemic level of enzyme achieved after AAV9-hIDS delivery through the CSF is sufficient to alleviate peripheral manifestations of disease, or if supplemental intravenously administered vector is required for this purpose. Secondly, our previous IV and ICV studies were carried out at very high vector doses (5×10^{10}gc ICV, 1×10^{12}gc IV), so another goal of the current study was to determine the quantitative relationship between vector dose delivered, the level of IDS expression achieved and associated alleviation of disease manifestations. In this study we thus compared CNS directed (IT) and systemically directed (IV) administration of RGX-121 (AAV9.CB7.hIDS) in a murine model of MPS II. A depiction of the AAV9.CB7.hIDS vector is shown in Figure 11A. Briefly, the vector construct consists of the constitutive CB7 promoter regulating expression of a codon optimized human *IDS* sequence. Comparative effectiveness of IT and IV routes of administration (ROA) was further evaluated by dose ranging; MPS II mice at 2 months of age were administered doses of 10^{7}-10^{11}gc per animal.

After vector administration, the effectiveness of gene delivery was assessed by measuring circulating levels of IDS activity (Figures 11B, C). Supraphysiological levels of IDS (150 to 1300 times normal) in the plasma of mice treated at the two highest doses via both ROAs were observed. For doses 10^{10}gc and 10^{11}gc, the mean enzyme activity levels in the plasma by IV ROA were 5702nmol/h/mL and 39,400nmol/h/mL, and by IT ROA they were 4400nmol/h/mL and 27,800nmol/h/mL. In comparison, the average plasma enzyme activity in wild type mice was 33 nmol/h/mL (Figure 11B, C). Interestingly, animals administered 10^{9}gc showed a greater than 10-fold reduction in IDS activity compared to animals administered 10^{10}gc (28-fold for IV administered animals, 93-fold for IT administered animals), with the IV group generating a distinctly higher average level of plasma IDS enzyme (176nmol/h/mL) compared to the 10^{9}gc IT group (47nmol/h/mL). Animals dosed with 10^{7}gc or 10^{8}gc showed diminishingly little (IV administered mice) to undetectable (IT administered animals) levels of circulating IDS activity. In summary, doses of 10^{7}gc and 10^{8}gc via both ROA showed low and inconsistent levels of enzyme, the 10^{9}gc dose gave wild type (IT) or just above wild-type (IV) enzyme levels, while the 10^{10}gc and 10^{11}gc doses given via either ROA conferred supraphysiological levels of circulating IDS enzyme that were consistent over the entire study period.

Urine samples were collected over the 20-week study period to evaluate GAG excretion. Untreated MPS II controls had a demonstrably higher mean level of urine GAG over the study (2010µg GAG/mg creatinine) compared to wild type controls (775µg GAG/mg creatinine). 10^{9}gc, 10^{10}gc, and 10^{11}gc doses given by IV ROA were sufficient to normalize urine GAG levels (Figure 11D). In comparison, only the 10^{10}gc

and 10^{11}gc doses by IT ROA were sufficient to normalize urine GAG levels (Figure 11E). The 10^{9}gc IT group exhibited normalized urine GAG (mean 793µg GAG/mg creatinine) at the 2-week time point, but by the end of the study at 20 weeks urine GAG in this group had increased to affected MPS II levels (mean 2214µg GAG/mg creatinine). Animals given doses of 10^{7}gc or 10^{8}gc via either ROA showed elevated levels of urine GAG throughout the study period. Overall, a minimal dose of 10^{9} IV or 10^{10} IT was needed for normalization of urine GAG excretion in MPS II mice.

Tissue IDS enzyme and GAG levels

At 20 weeks post-administration, all mice were euthanized, and tissues collected to evaluate IDS enzyme, GAG storage, vector biodistribution and tissue pathology as described in Materials and Methods. Wild type mice showed a wide range of IDS enzyme activities depending on tissue type, with the brain showing the highest IDS activity at a mean of 230.5nmol/h/mg protein down to a mean of 4.9nmol/h/mg protein in the heart (Figure 12A, B). In contrast, the affected MPS II mice had no IDS activity detectable in any tissue, with a collective average background for all tissue samples of 0.22nmol/h/mg protein.

Mice given 10^{11}gc IV exhibited IDS activity levels at or exceeding wild type levels in all peripheral tissues. The liver showed the highest levels of IDS activity, with an average of 4315nmol/h/mg protein or 181x wild type. Animals administered 10^{10}gc IV also showed a high level of expression in peripheral tissues, conferring supraphysiological levels of enzyme activity in the liver, spleen, kidney, and heart, with other tissues showing a high percentage of wild type activity, such as 50.5% in the lung.

The 10^9gc dose was less effective, showing supraphysiological levels of enzyme activity only in the liver. Little to no activity was observed in any of the other peripheral tissues of animals administered 10^9gc, similar to animals administered 10^7gc and 10^8gc IV.

Tissues from IT administered animals showed a pattern similar to the IV administered animals at the 10^{11}gc and 10^{10}gc doses. Again, the highest levels of IDS activity in animals dosed 10^{11}gc were found in the liver, with an average of 10,574nmol/h/mg protein or 443x wild type levels. All peripheral tissues at this dose met or exceeded wild type levels except the lung which was 87.4nmol/h/mg protein (85.7% wild type). Supraphysiological levels of enzyme activity were found in the liver, spleen, kidney, and heart of animals dosed 10^{10}gc, with closer to wild type levels found in other major organs, such as 23% wild type in the lung. Only the liver showed an appreciable level of enzyme activity at the 10^9gc IT dose, and the 10^7gc and 10^8gc doses showed little to no activity in any peripheral tissue. Overall, the 10^{10}gc dose conferred similar levels of IDS enzyme activity when comparing IV vs. IT. However, except for the liver, peripheral tissues from mice treated by the IV ROA on average had higher levels of IDS enzyme activity than the IT ROA at the 10^{11}gc dose.

In peripheral tissues, normalization of GAG content was observed in all tissues of animals dosed at 10^{10}gc or 10^{11}gc IV. Reduced storage material was seen at the 10^9gc dose by IV ROA, notably in the liver (98.6%), spleen (84.3%), and heart (82.2%), but other tissues showed little to no correction in GAG content compared to affected MPS II controls (Figure 12C). By IT ROA, 10^{11}gc conferred GAG normalization in all peripheral tissues. 10^{10}gc administered IT also showed GAG normalization in most tissues as well (Figure 12D). The lung and kidney showed incomplete but significant reduction in GAG

to 1.7x wild type levels for both tissues (98.4% and 97.4% correction, respectively). Reduced GAG was seen only in the liver and spleen of animals dosed 10^9gc IT. Animals given 10^7gc or 10^8gc by either ROA showed little to no reduction in GAG content of any tissue. Overall, neither robust IDS enzyme activity nor significant reduction in GAG content was observed in mice treated at the 10^7gc or 10^8gc doses by either ROA. The 10^9gc dose showed IDS activity comparable to wild type in the liver and GAG reductions in some, but not all tissues analyzed. In contrast, at 10^{10}gc and 10^{11}gc doses, most tissues showed high if not supraphysiological levels of IDS enzyme and normalization of GAG content.

An essential part of a genetic therapy for MPS II will be to address neurologic manifestations of the disease. In this study, we examined the IDS activity levels of whole brain and spinal cord. A high level of mean IDS activity was assessed in wild type controls, 230.5nmol/h/mg protein in the brain and 126.2nmol/h/mg protein in the spinal cord. Test animals exhibited average IDS activities of 3.8nmol/h/mg protein in the brain and 38.4nmol/h/mg protein in the spinal cord when administered 10^{11}gc IT (Figure 12B). In contrast, 10^{11}gc administered by IV ROA conferred an average of 2.6nmol/h/mg protein in the brain and 18.2nmol/h/mg protein in the spinal cord (Figure 12A). All other doses by either ROA conferred <2nmol/h/mg protein in the brain and <4nmol/h/mg protein in the spinal cord. Although these levels of IDS activity measured in the brains of treated mice are comparatively low even at the highest dose of 10^{11}gc IT (1.65% wild type levels), previous reports have shown that <5% of wild type activity was sufficient to normalize GAG content in the brain and ~1.5% was needed for significant reduction and prevention of neurocognitive deficits in MPS II mice[314,318]. The same tissue lysates were

also extracted for GAG analysis. MPS II controls had mean GAG content that was 4.8x that of wild type controls in the spinal cord. The 10^{10}gc / 10^{11}gc doses showed an average GAG correction of 55.8% /100% by IT administration and 15.6% / 34.6% by IV administration, respectively, in the spinal cord. Affected MPS II controls showed mean brain GAG levels 3x that of wild type controls. GAG content after 10^{10}gc and 10^{11}gc IV administration was reduced by 26.9% and 55.9% in the brain, while MPS II mice administered these vector doses by IT ROA showed a higher level of correction in the brain, 55.8% and 64.9% (Figure 12C, D).

Tissue biodistribution by qPCR

Peripheral and CNS tissues were extracted for genomic DNA and assayed for vector biodistribution by qPCR for the human IDS-encoding sequence. All tissues were observed to have detectable vector copies in animals administered AAV9-IDS vector by either IV or IT ROA at 10^{10}gc and 10^{11}gc doses, with the 10^{11}gc dose on average showing more copies than the 10^{10}gc dose. The 10^{7}gc, 10^{8}gc, and 10^{9}gc doses showed little to no detectable vector copies, apart from liver (Figure 13A, B). For any dose, the vast majority of vector copies were found in the liver of both IV and IT administered animals, with the 10^{11}gc dose conferring the highest copy number per genome equivalent of 11.3gc/ge and 8.8gc/ge, respectively. These data suggest that the liver was producing a large fraction of the circulating IDS enzyme available for metabolic cross correction in these animals. Although IT injection is a CNS directed ROA, it was found to result in "global" biodistribution, transducing cells systemically as well as in the CNS, which is consistent with previous reports on CNS directed AAV ROA (Figure 13B)[300,315,316]. At

the two higher doses of 10^{10}gc and 10^{11}gc, the IT ROA showed a notably higher vector distribution to the spinal cord (.0064gc/ge and .1612gc/ge) than the IV ROA (.0001gc/ge and .002gc/ge). This result is unsurprising given proximity of the spinal cord to the IT site of injection. In the brains of 10^{11}gc dosed mice, IT injection delivered more copies on average compared to IV injection (.011gc/ge vs. .0035gc/ge). Conversely, at the 10^{10}gc dose IT injection conferred less delivery than IV injection (.001gc/ge vs. .0019gc/ge), although this difference is not statistically significant by one-way ANOVA (P = 0.9984).

Zygomatic arch normalization by IT and IV ROA

This MPS II mouse model exhibits a variety of skeletal manifestations, including a thickening of the zygomatic arch bone diameter[294]. Each dose and ROA combination was evaluated for its impact on skeletal manifestations by computed tomography at 4 months post-administration to measure the thickness of the zygomatic arch. Affected MPS II controls had an average increase of 34.6% in zygomatic arch diameter compared to unaffected littermate controls. Notably, MPS II animals dosed IV with 10^{10}gc or 10^{11}gc showed significant decreases in zygomatic arch diameter compared to untreated MPS II controls and were indistinguishable from wild type controls. The 10^{9}gc group also had significantly decreased zygomatic arch diameter, about 50% reduced compared to affected MPS II controls (Figure 14A). Remarkably, IT administration of RGX-121 at doses of 10^{10}gc and 10^{11}gc into the CSF resulted in systemic delivery that was sufficient to normalize zygomatic arch diameter in MPS II mice. Animals administered the 10^{9}gc dose IT were not significantly different from untreated MPS II controls (Figure 14B). Animals given doses of 10^{7}gc or 10^{8}gc by either ROA showed no decrease in thickness

of the zygomatic arch. In summary, doses of 10^{10}gc and 10^{11}gc normalized zygomatic arch diameter in MPS II mice when delivered by either ROA, while a dose of 10^{9}gc partially reduced zygomatic arch diameter and only when delivered IV.

Histological analysis

Tissue samples were taken for H&E (hematoxylin and eosin) and Alcian blue staining, as well as immunohistochemistry for lysosomal associated membrane protein-1 (LAMP-1). In contrast to wild type mice, widespread intraneuronal vacuolization in Purkinje cells was noted in the cerebellum of MPS II mice by H&E staining (Figure 15A, B). H&E staining also revealed a decrease in intracellular vacuolization of Purkinje cells neurons in cerebellum for the 10^{10}gc IV and 10^{11}gc IT groups (Figure 15C, D). Liver H&E staining of MPS II mice showed large amounts of vacuolization in the cytoplasm of resident macrophages (foam cells), but not in wild type mice (Figure 15E, F). In the 10^{10}gc IV and 10^{11}gc IT groups, this vacuolization is absent in both the hepatocytes and macrophages (Figure 15G, H). When compared to wild type, rarefaction of the smooth muscle and vacuolated macrophages were found within the tunica media in aortas of MPS II mice (Figure 15I, J). While the smooth muscle rarefaction was noted the 10^{10}gc IV and 10^{11}gc IT, vacuolated macrophages were not observed in the aorta (Figure 15K, L). Alcian blue (AB) staining revealed blue positive material in the Purkinje and glial cells in MPS II, but not wild type group (Figure 16A, B). The 10^{10}gc IV and 10^{11}gc IT groups showed blue stained material, but to a lesser degree than MPS II mice (Figure 16C, D). While the MPS II group had AB positive staining in liver foam cells, this was not observed in the other 3 groups (Figure 16E-H). No differences in AB staining were

observed in the aorta between the 4 groups (Figure 16I, L). LAMP-1 is upregulated in the cells of both MPS II mice and patients and is considered a marker of disease pathology[181,442]. LAMP-1 IHC of the cerebellum was mild in the wild type group, but a marked staining in the Purkinje and glial cells was seen in the MPS II group (Figure 17A, B). The 10^{10}gc IV and 10^{11}gc IT groups showed decreased staining in the Purkinje cells, but persistent staining in the glial cells (Figure 17C, D). In contrast to the wild type group, the MPS II mice had widespread LAMP-1 staining in hepatocyte and foam cells (Figure 17E, F). A lesser degree of LAMP-1 staining of observed in the 10^{10}gc IV group, but 10^{11}gc IT mice a similarly high amount of staining to the MPS II group (Figure 17G, H). MPS II, 10^{10}gc IV and 10^{11}gc IT groups had marked increase in LAMP-1 staining in the aorta when compared to the wild type group (Figure 17J-L).

Prevention of neurocognitive deficits in the Barnes Maze analysis

Mice underwent neurobehavioral testing at 4 months post-administration using the Barnes maze to evaluate neurocognitive function, as described in Materials and Methods[437]. All animals were given 4 trials a day over a period of 4 days, assessing the time to escape for each trial. Data for the 10^{11}gc IT and 10^{10}gc IV groups are shown at $N \geq 10$ in Figure 18. On day 1 there were no significant differences in the latency to escape. For all groups the latency to escape the maze decreased over the next 3 days as the animals learned the attendant task. By day 4 however, the affected MPS II controls were performing the task (i.e., escaping the maze) significantly worse (79s) compared to wild type controls (29s). The 10^{11}gc IT group was significantly better at learning to escape the maze by day 4 with a mean latency to escape of 28s, suggesting that this dose

and ROA was sufficient to prevent the emergence of neurocognitive defects as measured by the Barnes maze (Figure 18). The 10^{10}gc IV group showed a trend toward prevention of neurocognitive deficits with a mean latency to escape of 47s but was not significantly different from the affected MPS II controls. We conclude that an IT dose of 10^{11}gc was required to prevent the emergence of neurocognitive deficits in MPS II mice.

Discussion

In this study we compared intravenous and intrathecal routes of vector administration to determine if IT delivery alone can remedy both CNS and systemic disease manifestations. A broad range of AAV9.CB7.hIDS doses was tested to determine the effective in a murine model of MPS II. Mice administered vector by either IV or IT ROA at a dose of 10^{9}gc had circulating levels of IDS at or above wild type. However, this dose was insufficient to achieve wild type levels of IDS and normalize GAG levels in most tissues analyzed. Mice dosed at 10^{10}gc and 10^{11}gc by either ROA exhibited circulating levels of IDS activity several logs higher than wild type, and nearly all tissues assayed met or exceeded wild type levels of IDS activity and normalized GAG storage. While a dose of 10^{10}gc by either IT or IV ROA was sufficient to normalize zygomatic arch diameter, a higher dose of 10^{11}gc administered intrathecally conferred the highest level of IDS activity in the brain, the greatest reduction in GAG content, and prevented the emergence of neurocognitive deficits in the Barnes maze.

The lowest doses administered, 10^{7}gc and 10^{8}gc, showed little enzyme activity, no GAG reduction, and little to no detectable copies in the tissues analyzed. AAV vector doses near this range were also recently reported to be biochemically ineffective in a

mouse model of Pompe disease[458]. The dose ranging revealed a "threshold" effect in the level of transduction and circulating IDS activity that was achieved when comparing lower to higher doses. For instance, when increasing the dose from 10^7g or 10^8gc up to 10^9gc, the expected result would be a 10x stepwise increase in circulating IDS activity. However, little to no circulating IDS was detected at 10^7gc and 10^8gc, with the 10^9gc showing at or above wild type levels of circulating activity. This "threshold" effect is reflected in the liver biodistribution data, which comprises the majority of vector copies for any dose by either ROA. Vector copies were not detectable at 10^7gc and 10^8gc, so the most significant jump in copy number was between 10^8gc and 10^9gc (mean 40x for IV, 44x for IT), greater than any other dose to dose comparison.

Interestingly, it appears that both the ROA and the threshold effect play a role in IDS expression and liver transduction. Measurable plasma IDS activity and detectable vector copies in the periphery at doses of 10^9gc or greater by IT ROA reveal that vector is released from CSF into the circulation (Figure 11C and Figure 13C). When contrasted to wild type controls, these levels of circulating IDS enzyme correspond to an increase of 6.07x for animals administered 10^9gc IV, and animals administered 10^9gc IT showed close to wild type levels at 1.42x. With regard to circulating IDS enzyme levels, these data show that an IT dose at 10^9gc confers 27% that of an IV 10^9gc dose. This is also reflected in the vector biodistribution analysis, where an IT dose at 10^9gc conferred 31% of vector copies in the liver compared to the same dose administered IV. The most obvious explanation is that less vector transduces the liver when the same dose is administered IT vs IV, thereby contributing less IDS to the circulation. Interestingly, increasing the vector dose from 10^9gc to 10^{10}gc resulted in a greater than 10-fold increase

in IDS activity for both IV (28-fold) and IT (93-fold) administered animals. IT administration shows 3.3x increase compared to IV here. When increasing the vector dose from 10^{10}gc to 10^{11}gc, IT and IV administered animals show a 6.3-fold and a 6.9-fold increase in plasma activity levels, respectively. These increases are nearly the same (IV 1.1x increase over IT) and closer to the expected 10x increase for a 10x increase in dose. Overall, two key points emerge from these data. First, it is clear that ROA plays a crucial role in the resultant liver transduction and circulating IDS activity. While IT administration allowed vector to escape into the periphery, primarily transducing the liver and subsequently contributing to circulating IDS activity, the level of transduction and circulating enzyme were always lower than that observed after IV administration for any given dose. Second, the threshold effect is observed in both IT and IV administered animals. Initially it appears the threshold more greatly affects IT- than IV-administered animals. However, a lower level of functional AAV is available for transduction of the liver after IT administration in comparison with IV administration. This threshold impacts a greater percentage of bioavailable AAV for IT vs. IV administered vector for any given dose. It also appears that the impact of this threshold is weakened at much higher vector doses, suggesting that threshold gives way to a saturation effect. One possible explanation for the threshold effect is the existence of pre-existing anti-AAV antibodies. Under these conditions, at lower capsid doses antibody-mediated neutralization will lead to a lack of transduction, which is exactly what was observed in our study[375]. Indeed, previous studies in both mice and non-human primates have demonstrated that neutralizing antibody can completely block or reduce AAV vector transduction in the liver[378,379,460]. Other mechanisms of vector neutralization are possible

as well, such as macrophage-mediated destruction of the vector in the liver. Additionally, this response shows a lessening impact as the dose is increased from 10^9gc to 10^{11}gc, where a smaller percentage of the overall dose is neutralized by the threshold effect.

The 10^9gc dose highlights the differences between IT and IV ROAs in outcomes seen systemically, such as plasma IDS activity, urine GAG excretion, and zygomatic arch diameter. A dose of 10^9gc AAV9.CB7.hIDS IT conferred an overall level of IDS activity 1.4 times that of wild type in the plasma. However, this was insufficient to lower urine GAG excretion or significantly reduce zygomatic arch diameter. In comparison, mice treated with 10^9gc AAV9.CB7.hIDS IV exhibited overall plasma IDS activity levels 6 times that of wild type. These mice also showed normalized urine GAG excretion and significant reduction in zygomatic arch diameter, likely because of this supraphysiological level of circulating enzyme with subsequent contribution to bone development.

Decreasing plasma IDS activity over time was seen in animals given doses of 10^9gc, 10^{10}gc, and 10^{11}gc via both ROA. Except for 10^{10}gc IT, the circulating IDS activity at week 20 was approximately 1/3 that of their respective 2-week time point. As previously reported by this and other laboratories[316,317,396,429,461], much of the circulating enzyme is expressed in the liver, given the vast majority of vector copies found there. Loss of transduced hepatocytes could be one cause for the observed decline in circulating IDS activity over time. It is unlikely that this was due to natural hepatocyte turnover, which takes 200-400 days in mice[459], greater than the 20-week study period. Loss of hepatocytes could be due to a CD8+ T cell response[380,462]. However, the observed effect was not entirely consistent, as the IDS level in any given month was not always lower

than the preceding month, and loss of IDS activity over time was not observed in the aforementioned 10^{10}gc IT group. Additionally, other studies have shown that AAV mediated gene expression can persist in mice for at least a year[371,374], and AAV mediated gene expression in dogs and humans has been reported to persist for at least several years[372-374].

A high level of IDS activity and normalization of GAG was observed in all peripheral tissues of animals administered vector at doses of 10^{10}gc and 10^{11}gc by either ROA. Additionally, at 10^{10}gc IV and 10^{11}gc IT, histological analysis revealed reduced vacuolization and AB staining in the liver. Previous studies of animals administered AAV-IDS vector intracerebroventricularly at similar doses or IV at higher doses reported normalization of peripheral tissues as well[300,315,316,461]. The highest levels of IDS enzyme activity and vector copy number were found in the liver. In contrast, relatively low vector copy number and high levels of IDS enzyme were observed in the other peripheral tissues, arguing that the liver is the primary site for expression and secretion of IDS enzyme into the circulation that consequently becomes available for metabolic cross correction. Notably, this was demonstrated for the intrathecally injected animals, showing that much of the administered vector escapes the CSF to transduce the liver and remedy peripheral disease manifestations. Results from animals administered the two highest doses of 10^{10}gc and 10^{11}gc are contrasted with animals administered a dose of 10^{9}gc, where the level of transduction in the liver did not produce a therapeutic amount of circulating enzyme (i.e., zygomatic arch). At this dose, low levels of enzyme and elevated levels of GAG content were found in most tissues, even though the liver showed normalized GAG content.

An integral part of next generation therapy for MPS II will be to address neurological manifestations of the disease that affects approximately 2/3^{rds} of patients[86]. Animals administered 10^{11}gc IT had the highest levels of IDS activity in the CNS, at 3.8nmol/h/mg protein on average in the brain and 38.5nmol/h/mg protein in the spinal cord. This level of activity in the spinal cord was 30% of the wild type level and was sufficient to normalize GAG content, unlike any other dose given IT or IV. In wild-type mice, IDS activity was highest in the brain compared to any other tissue analyzed. Thus, the level of IDS activity achieved in mice administered 10^{11}gc IT corresponds to a fraction (1.65%) of wild type activity. However, previous studies have shown that as little as 1.5% of wild type activity in the brain is sufficient for a meaningful reduction of GAG content in the brain that prevents emergence of neurocognitive deficits in MPS II mice[311,314,318]. Indeed, mice treated at a dose of 10^{11}gc IT demonstrated a mean correction of 65% in brain GAG content. In addition, this group showed a decrease in cerebellar Purkinje cell vacuolization, AB positive material, and LAMP-1 staining, as well as prevention of neurocognitive deficits as measured in the Barnes maze. Based on these results, there are two questions that emerge for MPS II gene therapy: How is it that endogenous levels of IDS in the brain the highest measured, and why are high levels of IDS activity in the brain so difficult to achieve? Even ICV administration of AAV9-IDS vector at high dose (5×10^{10}) resulted in only 40% of the endogenous level of IDS[300,315,316]. By comparison, we found in a companion study on MPS I that endogenous levels of IDUA activity the brain were 5-10nmol/h/mg protein, 23- to 46-fold lower than the level of IDS activity detected in the brain (230.5nmol/h/mg protein). In MPS I mice, a dose of 10^{10}gc AAV9-IDUA administered either IV or IT produced enzyme levels in the

brain that were greater than wild type, with the IT group achieving a mean level of ~100nmol/h/mg protein, 10 to 20-fold higher than wild-type (L.R. Belur et al, manuscript in preparation). Why is it, given an otherwise identical vector construction and ROA, that AAV9.CB7.hIDS performs relatively poorly in MPS II mice compared to AAV9.CB7.hIDUA in MPS I mice? Further investigation is needed to answer the questions detailed here. The brains of MPS II mice treated at higher doses of AAV9.CB7.hIDS IV or IT show some GAG reduction and, with the exception of 10^{10}gc IT, detectable IDS activity. With such evidence of activity and GAG reduction, what is the source of this IDS enzyme? AAV9 has been shown to cross the blood brain barrier[356], and vector copies were detected in the CNS, suggesting transduction and IDS expression in the brain. Indeed, mice administered AAV9.CB7.hIDS IT had higher vector copies than mice equivalently dosed IV, suggesting a higher level of CNS transduction via this ROA. However, we cannot rule out transduction that is limited to the vasculature by either ROA, as previously reported in IV studies[383]. Another possibility is the so called "high-dose effect" that has been reported in preclinical gene therapy studies for MPS I and MPS II, whereby a small fraction of sufficiently high-level circulating enzyme enters the CNS from the blood[314,318,383]. IDS detected in the brain could also have been derived from a combination of vector transduction in the tissue plus transit of enzyme from the circulation. In this case, IT administered vector transduces cells in the CNS that secrete enzyme available for cross correction. At the same time, a portion of the administered vector is released into the circulation and transduces the liver to provide a robust and consistent level of circulating IDS enzyme that can exert the "high-dose effect" and

transit into the CNS. Additional study is warranted to further characterize the source of enzyme in the CNS after CSF-directed as well as systemic AAV vector administration.

Patients with the severe form of MPS II suffer from a wide range of skeletal dysplasias termed dysostosis multiplex that is left unaddressed by ERT[57,211]. Similarly, MPS II mice display skeletal manifestations that include the thickening of bones, such as the zygomatic arch[294]. We found that mice administered AAV9.hIDS by either ROA at a dose of 10^{10}gc or 10^{11}gc showed normalization of zygomatic arch diameter. This is consistent with previous MPS I and MPS II gene therapy studies[311,313]. A lentiviral vector-based approach to MPS II was used to investigate skeletal complications in-depth and found that a high level of IDS in the serum reduced GAGs and normalized bone metabolism, leading to bone remodeling in the zygomatic arch[313]. The *in vivo* AAV9-based approach reported here likely mediates zygomatic arch normalization through the same mechanism, given the high and consistent levels of circulating enzyme assessed in animals administered 10^{10}gc or 10^{11}gc.

Comparing IV and IT ROA in the context of a dose ranging study provided considerable insight into a prospective minimum effective dose for treatment of MPS II in a murine model of the disease. This study finds that dose to be 10^{11}gc IT, based on effectiveness in addressing both CNS and systemic disease manifestations. A dose of 10^{11}gc administered either IV or IT was minimally sufficient to normalize peripheral manifestations (i.e., tissue GAG and zygomatic arch diameter). Similar dose effectiveness has been reported in studies evaluating intracerebroventricular injection of $3x10^{10}$gc[315] or $5x10^{10}$gc AAV9-hIDS vector[300,316]. These slightly lower doses are similar to our optimal dose of 10^{11}gc IT, as in our hands ICV infusion achieves about a 10-fold higher level of

transduction than IT infusion. IV administration of AAV9-IDS has been previously tested at doses ranging from $2.5x10^{11}$gc up to $2x10^{13}$gc[317,318,465]. In contrast, we find that as little as 10^{10}gc (5×10^{11} gc/kg) AAV9.CB7.hIDS administered IV normalizes GAG in peripheral tissues, prevents a key skeletal manifestation, and even shows improvement in neurocognitive analyses. In clinical trials using targeted delivery of AAV a wide range of total doses have been administered, from $5.8x10^{9}$gc to $7.5x10^{15}$gc[376]. Given the importance of target dosing, studies evaluating dose-dependent outcomes to determine a preclinical minimum effective dose in are essential for clinical trial design and translation. Minimal dosing can also address safety concerns, such as those that emerged in a clinical trial of X-linked myotubular myopathy[402,403], and efficacy, as seen in clinical trials of AAV in the treatment of hemophilia[380,463].

By comparing IV vs. IT ROA at varying doses, this study highlights the use of CNS directed vector administration to address both the neurologic and systemic disease manifestations in a murine model of MPS II. A dose of 10^{11}gc administered IT was found to be minimally effective for these purposes. This dose and ROA provided a high level of circulating IDS, normalized tissue GAGs, and normalized zygomatic arch diameter as a key peripheral manifestation. This impact on the periphery was due to the significant fraction of CSF-delivered vector that was released from the CNS with subsequent transduction of the liver, from which a high level of enzyme was secreted into the circulation and made available for systemic metabolic cross correction. This dose of 10^{11}gc administered IT also conferred brain IDS activity of 1.65% wild type, sufficient to reduce GAG storage by 65%, decrease Purkinje cell vacuolization, and prevent the emergence of neurocognitive deficits as measured by the Barnes maze. Finally, this study

emphasizes the value of investigating the efficacy of a new genetic therapy in a dose-dependent manner. We conclude that this study supports the use of AAV9.hIDS delivered through the CSF as an effective approach to remedy both neurologic and peripheral manifestations of MPS II.

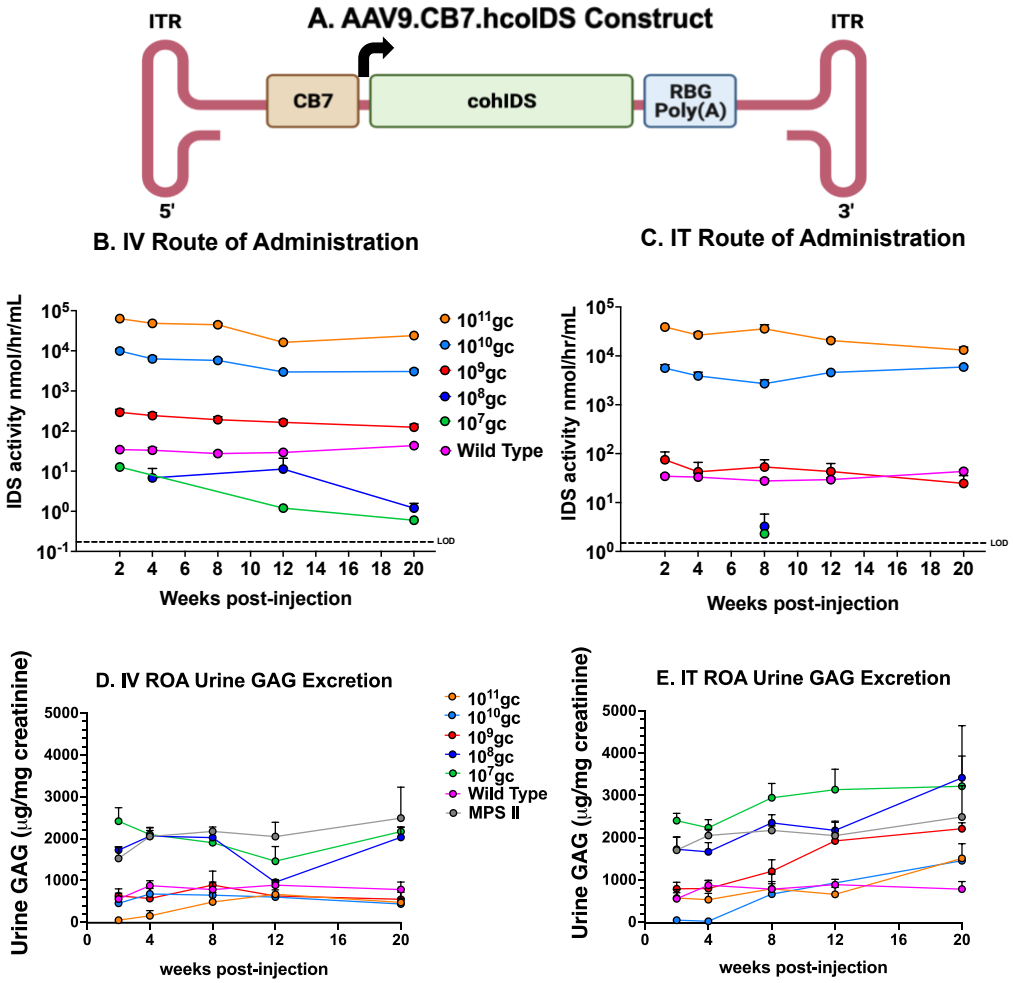

Figure 11. AAV9.CB7.hcoIDS vector, plasma IDS enzyme activity and urine GAG excretion. (A) Illustration depicting the AAV9 vector made with BioRender. CB7; CMV IE enhancer with chicken beta actin promotor, exon 1 and intron 1 with rabbit beta globin splice acceptor. cohIDS; codon optimized human iduronate-2-sulfatase. RBG Poly(A); rabbit beta globin polyadenylation sequence. ITR; AAV inverted terminal repeat. Mean plasma IDS activities by dose and month for IV ROA (B) and IT ROA (C). MPS II and some 10^{7},10^{8} samples were omitted that were below our LOD as determined by 4-MU IDS assay standard curve. Excreted urine GAGs by dose and month for IV ROA (D) and IT ROA (E). For B&C, Wild Type, 10^{9}, 10^{10}, 10^{11} N=3-12. For D&E, Wild Type, Affected MPS II, 10^{9}, 10^{10}, 10^{11} N=1-11. Error bars show SEM.

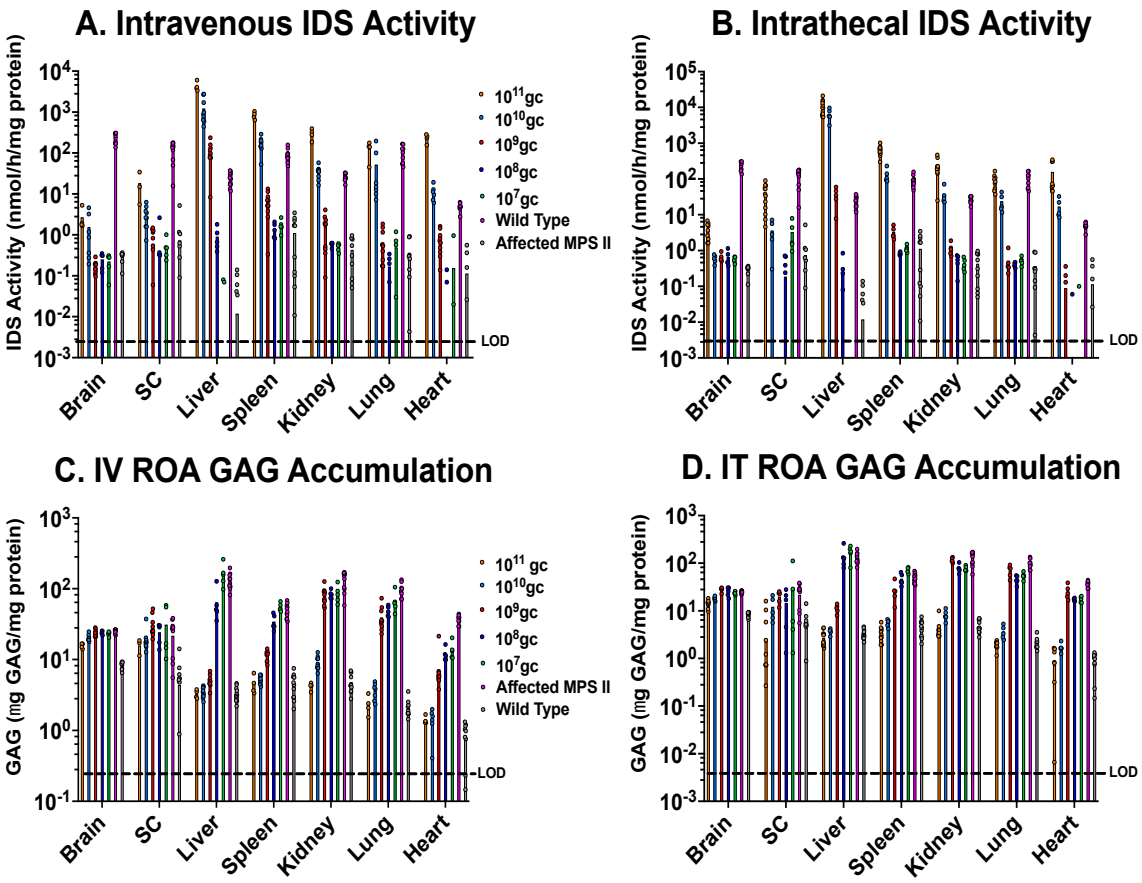

Figure 12. Tissue IDS enzyme and GAG levels in AAV treated animals. Mean IDS activity levels by tissue and dose by IV (A) and IT (B) ROA and mean GAG levels by tissue and dose by IV (C) and IT (D) ROA. Sample sizes are N=4-12. N values vary depending on tissue type and dose, as some tissues were instead taken for histological analysis. LOD (dashed line) was determined based on either IDS assay 4-MU standard curve or GAG assay glycosaminoglycan standard.

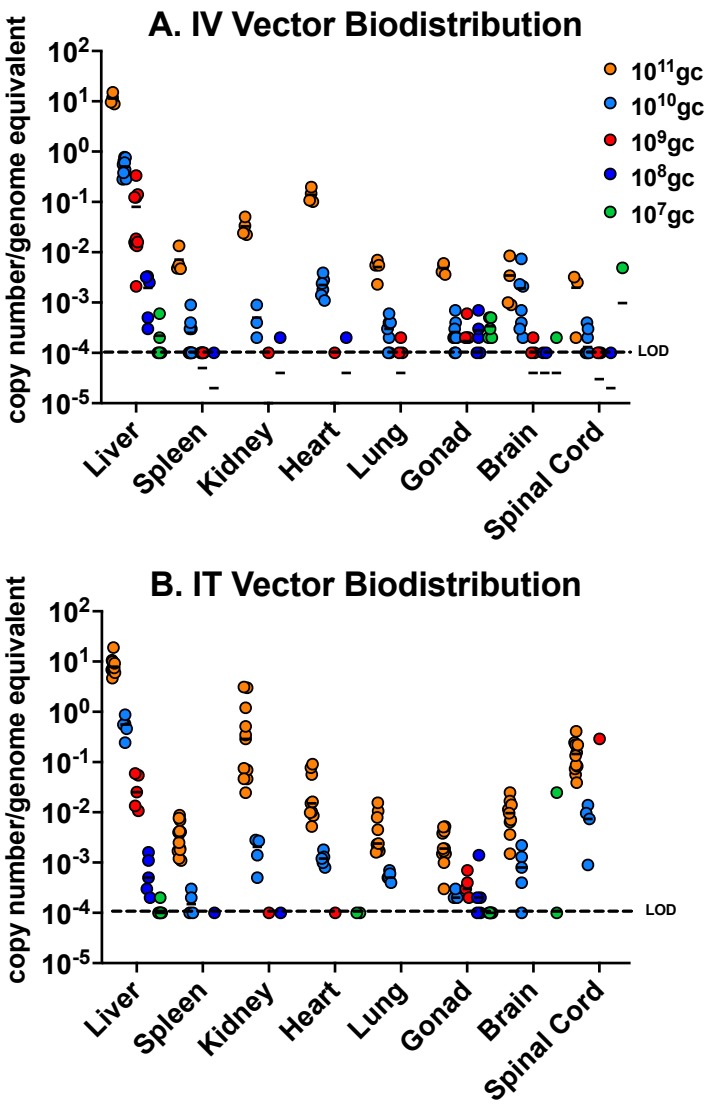

Figure 13. Biodistribution of vector in tissues. Vector biodistribution in tissues by qPCR, analysis by dose and indicated tissue for IV ROA (A) and IT ROA (B). Sample sizes are N=4-12 depending on tissue and dose. LOD (dashed line) was determined by plasmid based standard curve. N values vary depending on tissue type as some tissues were instead taken for histological analysis. Lines show medians by group for each tissue.

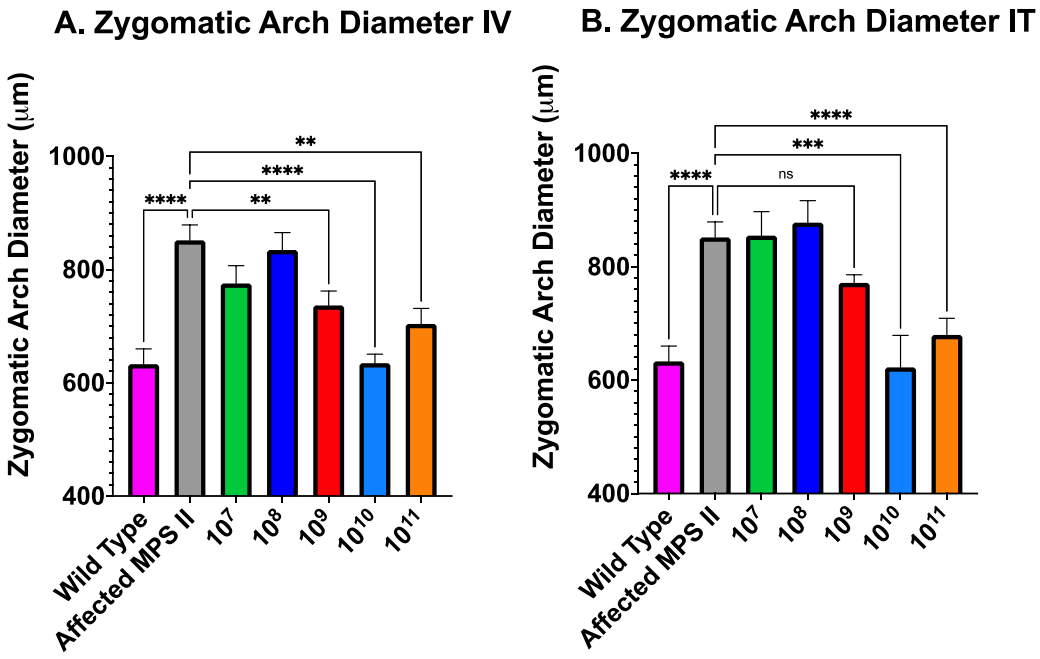

Figure 14. Zygomatic arch analysis. Zygomatic arch diameter measurements by Micro-CT analysis for the IV ROA by dose (A) and IT ROA by dose (B). Significance was determined by one-way ANOVA. Sample sizes: Wild Type N=12, Affected MPS II N=11, IV 10^7,10^8 N= 5, IV 10^9,10^{10} N=10, IV 10^{11} N=4, IT 10^7,10^8,10^9 N=5, IT 10^{10} N=3, IT 10^{11} N=11. Error bars show SEM. ns: no significance, **: P <.01, ***: P<.001, ****: P<.0001.

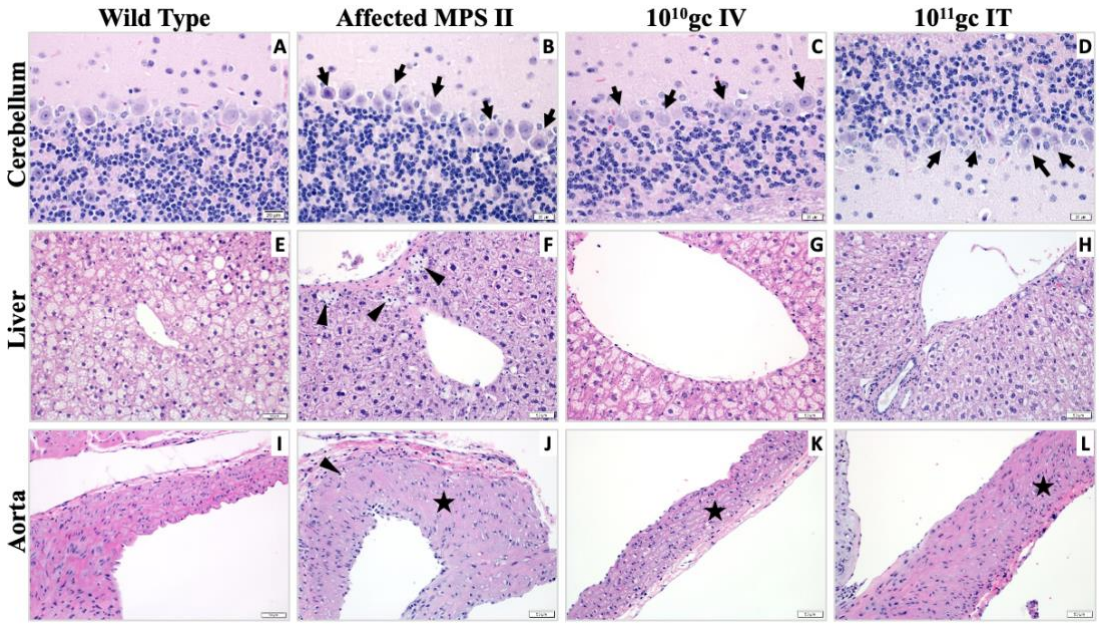

Figure 15. Hematoxylin and Eosin stained sections from 10^{10}gc IV and 10^{11}gc IT mice. (A-D) Cerebellar cortex: In contrast to the wild type mice (A), intracytoplasmic vacuolization (black arrows) was noted in the Purkinje cells from the affected MPS II mice (B). Persistent, but lesser intracytoplasmic vacuolization with noted in the Purkinje cells from the 10^{10}gc IV (C) and 10^{11}gc IT (D) treated mice. (E-H) Liver: In contrast to the wild type mice (E), numerous fine-vacuolated perivascular macrophages ("foam cells", black arrowheads) were seen in the affected MPS II mice (F). Foam cells were not observed in the 10^{10}gc IV (G) and 10^{11}gc IT (H) treated mice. (I-L) Aorta: In contrast to the wild type mice (I), there was extensive rarefaction of the smooth muscle (black star) and few finely-vacuolated macrophages (black arrowheads) within the tunica media of the affected MPS II mice (J). A similar magnitude of rarefaction was noted in the 10^{10}gc IV (K) and 10^{11}gc IT (L) treated mice.

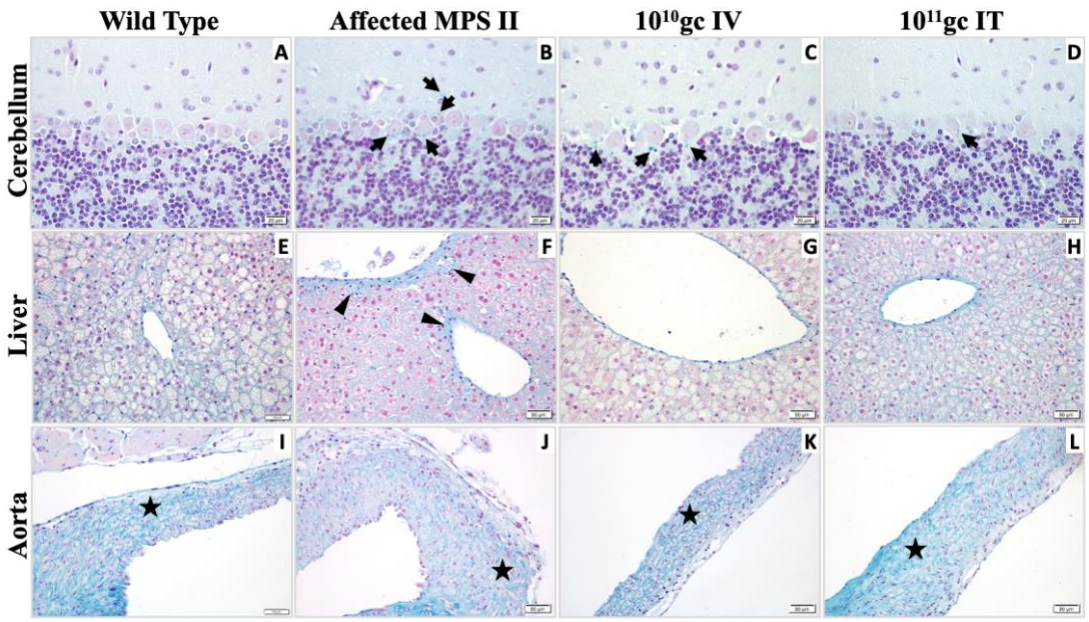

Figure 16. Alcian blue (AB) stained sections from 10^{10}gc IV and 10^{11}gc IT mice. (A-D) Cerebellar cortex: In contrast to the wild type mice (A), intracytoplasmic AB-positive blue material (black arrows) was noted in the Purkinje cells and presumed glia from the affected MPS II mice (B). Persistent, but lesser amounts of material was noted in the Purkinje cells from the 10^{10}gc IV (C) and 10^{11}gc IT (D) treated mice. (E-H) Liver: In contrast to the wild type mice (E), small amounts of AB-positive blue material (black arrowheads) was seen in presumed foam cells in the affected MPS II mice (F). No such material was observed in the 10^{10}gc IV (G) and 10^{11}gc IT (H) treated mice. (I-L) Aorta: No significant differences were noted in the AB-stained aortic tissues from the 4 groups of mice.

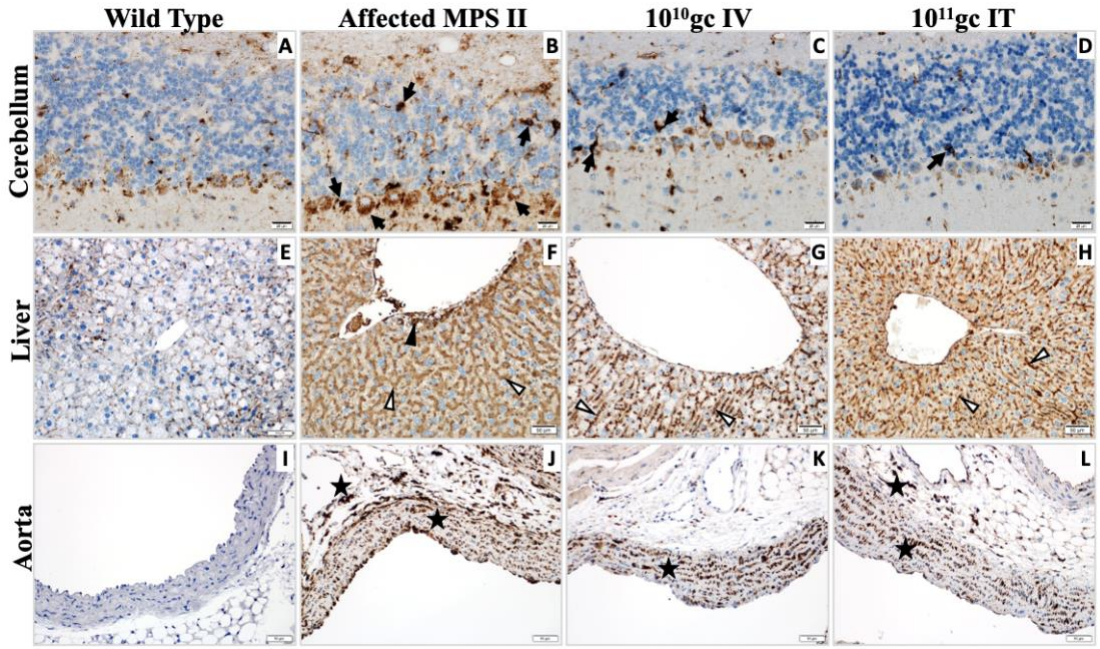

Figure 17. LAMP-1 IHC immunostained sections from 10^{10}gc IV and 10^{11}gc IT mice. (A-D) Cerebellar cortex: In contrast to the mild intracytoplasmic LAMP1 staining in the Purkinje cells and small glia from the wild type mice (A), there was marked intracytoplasmic LAMP1 staining (black arrows) in the Purkinje cells from all and presumed glia from the affected MPS II mice (B). In both the 10^{10}gc IV and 10^{11}gc IT treated mice, lesser amounts of LAMP1 staining was observed in the Purkinje cells, but there was persistent heavy staining within presumed glia (black arrows, C and D). (E-H) Liver: In contrast to the minimal LAMP1 staining in the liver from the wild type mice (E), there was marked LAMP1 staining in the perivascular macrophages (black arrowheads) and hepatocytes (white arrowheads) in all the affected MPS II (F). There was lesser LAMP1 staining in the hepatocytes from the 10^{10}gc IV treated mice (white arrowhead, G), but a similarly high amount of staining in the hepatocytes from the 10^{11}gc IT treated mice (white arrow head, H). (I-L) Aorta: In contrast to the scant LAMP1 staining in the wild type mice (I), there was marked LAMP1 staining within the smooth muscle and macrophages (black stars) from the affected MPSII and 10^{10}gc IV and 10^{11}gc IT mice (J-L).

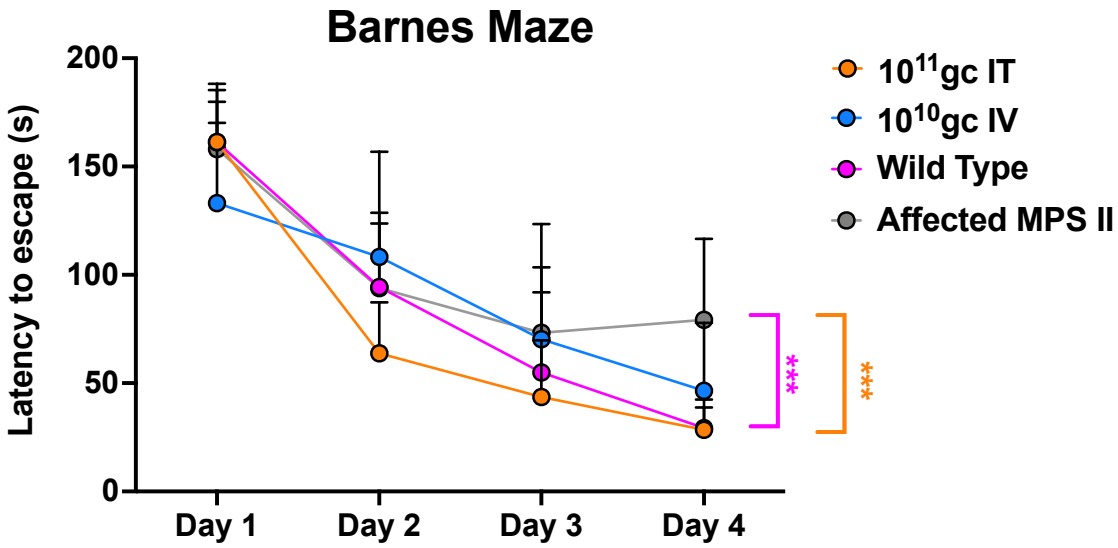

Figure 18. Neurocognitive analysis by Barnes maze. All groups underwent neurobehavioral testing at 6 months of age. **(**A) Barnes maze evaluation for long-term spatial learning and memory. Results are shown as the mean latency to escape of 4 trials per day over 4 days. Significance determined by two-way ANOVA. Sample sizes are Wild Type N=12, Affected MPS II N=11, IT 10^{11} N=12, IV 10^{10} N=10. Error bars shown are mean +/- S.D. ***: P<0.001.

Chapter IV: Generation and characterization of an immunodeficient mouse model of mucopolysaccharidosis type II

Miles C Smith[1,2] Lalitha R Belur[1,2], Andrea D Karlen[1,2], Kelly Podetz-Pedersen[1,2], Olivia Erlanson[1,2], Kanut Laoharawee[1,2], Justin Furcich[3], Troy C. Lund[3], Yun You[4], Davis Seelig[5], Beau R Webber[2,3,6,7], R. Scott McIvor[1,2*]

[1]Department of Genetics, Cell Biology and Development, University Minnesota, Minneapolis, MN, United States

[2]Center for Genome Engineering, University of Minnesota, Minneapolis, MN, United States

[3]Department of Pediatrics, University of Minnesota, Minneapolis, MN, United States

[4]Mouse Genetics Laboratory, University of Minnesota, Minneapolis, MN, United States

[5]Comparative Pathology Shared Resource, University of Minnesota, St. Paul, MN, United States

[6]Stem Cell Institute, University of Minnesota, Minneapolis, MN, United States

[7]Masonic Cancer Center, University of Minnesota, Minneapolis, MN, United States

* Corresponding Author:

R. Scott McIvor

mcivo001@umn.edu

Summary

Mucopolysaccharidosis type II (Hunter syndrome, MPS II) is an inherited X-linked recessive disease caused by deficiency of iduronate-2-sulfatase (IDS), resulting in the accumulation of the glycosaminoglycans (GAG) heparan and dermatan sulfates. Mouse models of MPS II have been used in several reports to study both disease pathology and preclinical studies for current and next generation therapies. Here, we report the generation and characterization of an immunodeficient mouse model of MPS II, where CRISPR/Cas9 was employed to knock out a portion of the murine *IDS* gene on the NOD/SCID/Il2rγ (NSG) immunodeficient background. *IDS*$^{-/-}$ NSG mice lacked detectable IDS activity in plasma and all analyzed tissues, as well as elevated levels of GAGs in those same tissues and in the urine. Histopathology revealed vacuolized cells in both the periphery and CNS of NSG-MPS II mice. This model also recapitulates skeletal and neurocognitive manifestations associated with MPS II in humans and in immunocompetent MPS II mice. We anticipate that this new immunodeficient model will be appropriate for preclinical studies involving xenotransplantation of human cell products intended for the treatment of MPS II.

Introduction

Mucopolysaccharidosis type II (Hunter syndrome, MPS II) is an X-linked recessive lysosomal storage disease (LSD) caused by deficiency of iduronate-2-sulfatase (IDS). IDS functions along with other lysosomal hydrolases to catabolize the glycosaminoglycans (GAGs) heparan sulfate and dermatan sulfate[57]. Insufficient IDS

leads to the accumulation of fully or partially undegraded GAGs within the cell and the emergence of progressive and multisystemic disease[57]. This includes, but is not limited to, joint stiffness, hearing loss, organomegaly, cardiopulmonary dysfunction, skeletal dysplasias (dysostosis multiplex), cognitive impairment, and death[87]. Globally, MPS II affects ~1:160,000 live male births[86].

Currently, the only FDA approved treatment for MPS II is enzyme replacement therapy (ERT) with recombinant IDS (idursulfase)[76]. However, ERT requires frequent enzyme infusions and does not remedy neurological manifestations of the disease. Next generation treatment options, such as cell and gene therapies, have thus been under investigation to overcome the limitations of ERT. Much of the preclinical work on ERT as well as cell and gene therapies for MPS II has relied on C57BL/6J MPS II mouse models[293,295,300]. These mouse models have been invaluable for understanding disease pathology and for the development of novel therapies because of their relatively short lifespans and ability to recapitulate disease manifestations[294]. Here we report details of a new addition to the *IDS* knockout mouse repertoire with the generation and characterization of an *IDS* knockout on the NOD/SCID/Il2rγ (NSG) background. On this background, engraftment of human cells, such as CD34+ hematopoietic stem and progenitor cells, will be possible in future cell and gene therapy studies, as has been previously reported for MPS I[433].

As described herein, the NSG-MPS II mouse model is IDS deficient and shows widespread accumulation of GAGs in all tissues analyzed. Histopathology reveals vacuolization and GAG storage in both the periphery and in the CNS. Functional deficits include both skeletal and neurological manifestations of disease. Overall, this model

recapitulates many of the disease manifestations seen in C57BL/6J MPS II mice and in human MPS II, while maintaining an immunodeficient background suitable for xenotransplantation studies.

Materials and Methods

Animal care and husbandry

All animal care and procedures performed in this study were approved by the University of Minnesota Institutional Animal Care and Use Committee (IACUC). Animal housing and care was provided by the University of Minnesota Research Animal Resources facilities under specific pathogen free conditions. Animals were provided food and water *ad libitum*. NSG (NOD.Cg-*Prkdc*^{scid} *Il2rg*^{tm1Wjl}/SzJ) mice were purchased from The Jackson Laboratory[434].

Generation of *IDS* knockout mice (NSG-MPS II)

Two sgRNAs were synthesized using the HiScribe Quick T7 High Yield RNA Synthesis Kit (NEB #E2050) following the manufacturer's instructions. Template DNA used in the reaction were two gBlocks Gene Fragments of 125bp in length obtained from Integrated DNA Technologies. These sgRNAs were designed to target Cas9 to the 5' UTR and intron 5 of the murine *IDS* gene (Figure 19). Cas9 encoding mRNA was purchased from TriLink Biotechnologies. sgRNAs and Cas9 mRNA were mixed in RNase-free water. Ten NSG female mice aged between 8 - 9 weeks were super-ovulated by first injection of 5 IU of Pregnant Mare Serum Gonadotropin (PMSG, C1063, Sigma),

intraperitoneal (*i. p.*), per female, and 48 hours later, followed by injection of 5 IU of human Chorionic Gonadotropin (hCG, HOR-250, PROSPEC Protein Specialists), *i. p.*, per female, and these mice were immediately crossed to male NSG mice. The next morning, zygotes were collected and washed using standard methods[11]. The sgRNA+Cas9 mRNA mixture was injected into the pronuclei of zygotes using standard procedures. The injected embryos were then transferred into pseudo-pregnant CD-1 (Charles River Laboratory) females as previously described[435]. Blood or tissues of offspring generated from this process were subsequently genotyped for *IDS* gene knockout as described below.

Genotypic analysis

The distal toe was taken from all offspring within the first week of birth for DNA extraction using ArchivePure DNA Cell/Tissue Kit from 5Prime, Cat# 2900269. DNA was extracted from blood using Whatman FTA Elute Micro Cards from GE Life Sciences. Six primers were designed to evaluate potential *IDS* gene knockout mice. These included primers upstream and downstream of the sgRNA target sites and primers for exon 4. PCR reactions were run in several combinations to identify the expected presence or absence of bands based on the location of the primers. A seventh primer (primer G) was added to correctly identify the deletions in strains 1849 and 1850. PCR reactions contained Taq polymerase, 350ng gDNA, 10μM primers (Table 1), Blue Master Mix, 25mM $MgCl_2$, and dH_2O. The reactions were run on an Applied Biosystems 2720 Thermal Cycler with the following conditions: 94°C for 5 minutes and then 35 cycles of 94°C for 45 seconds, 56°C for 45 seconds, and 68°C for 45 seconds. The presence and

size of PCR products was then evaluated by electrophoresis on 1% agarose gels. *IDS* gene knockout alleles were then characterized by Sanger sequencing of PCR product generated from reactions containing primers A and F, including the recombination site (Figure 19).

Tissue processing

Animals between the ages of 7-12 months were euthanized by CO_2 asphyxiation. Prior to necropsy, whole blood was collected by cardiac puncture into heparin-coated tubes. Tissues (brain, spinal cord, liver, kidney, spleen, lung, and heart) were harvested, placed on dry ice, and stored at -20 °C until processing for biochemical analysis. Tissues were also fixed in 10% neutral buffered formalin (VWR) at a ratio of 1:10-20 tissue to formalin overnight and then transferred to 70% ethanol until processing for histology. Tissues were processed for biochemical analysis by homogenizing in 0.9% saline using a Bullet Blender bead mill (Storm 24 Homogenizer, NEXT ADVANCE) as previously described and clarified in a 5424R Eppendorf centrifuge[318]. Supernatants were collected and stored at -20 °C until analyzed.

Iduronate-2-sulfatase enzyme assay

IDS activity was determined in plasma and tissue samples by a fluorometric assay using 4-methylumbelliferyl α-l-iduronide 2-sulfate disodium salt (4-MU2S) as substrate (Cat #: EM03201, Carbosynth) as previously described[436]. 4-MU2S (10 mg) substrate was dissolved in 16.66 mL substrate buffer (0.1M Na-Acetate buffer, pH 5.0 + 10 mM Pb-Acetate + 0.02% (w/v) Na-azide) to yield a 1.25 mM working substrate. 10 μL

aliquots of plasma or tissue lysates were mixed with 20 μL aliquots of working substrate and incubated at 37 °C for 90 minutes. The IDS reaction was then stopped with 20 μL of PiCi Buffer (0.2M Na2HPO4 + 0.1M Citric Acid, 0.02% Na-Azide, pH 4.5). 10 μL of 5 μg/mL alpha-L-iduronidase (IDUA) (Cat #: 4119-GH, Bio-Techne) was added and the sample was incubated at 37 °C overnight. 200 μL stop buffer (0.5 M Na2CO3 + 0.5 M NaHCO3, pH 10.7) was added to terminate the reaction. Tubes were then centrifuged at ~13,000 rpm for 1 minute to pellet the precipitate. Supernatant was transferred into a black 96-well round bottom plate and the resulting fluorescence was measured using a Bio-Tek Synergy Mx plate reader with excitation at 355 nm and emission at 460 nm. A standard curve was used for the calculation of 4-MU generated in the reaction using 4-MU from Sigma (Cat# M1381). Pierce protein assay reagent (Cat #: 22660, ThermoFisher) was used to measure protein content. Enzyme activity is expressed as nmol 4-MU released per mg protein per hour (nmol/h/mg protein) for tissues extracts, and as nmol/h/ml for plasma. All samples were assayed in duplicate.

Glycosaminoglycan assay

Tissue lysates were digested in proteinase K (20 mg/mL) at a ratio of 1:10 (ProK:tissue lysate) at 55 °C overnight. Proteinase K was inactivated by boiling for 10 minutes the next day. Samples were then incubated with 200 units of DNase and 2 mg of RNase per 50 μL tissue lysate at room temperature overnight and heat inactivated the next day by boiling for 10 minutes. GAG levels were then assayed using the Blyscan Sulfated Glycosaminoglycan Assay kit (Biocolor Life Science Assays, Accurate

Chemical, NY Inc. Cat # CLRB1000) according to the manufacturer's instructions. For tissues, GAG levels were normalized to protein as determined using the Pierce protein assay (Cat #: 22660, ThermoFisher). The results are expressed as μg GAG/mg protein. For urine, GAG levels were normalized to creatinine as determined using a creatinine assay kit from Sigma (MAK080). The results are expressed as μg GAG/mg creatinine.

Skeletal analysis

Test animals were sedated with 5% isoflurane and whole-body micro-computed tomography (CT) images captured using a Siemens Inveon PET/CT machine. The acquired DICOM files were exported and converted to Imaris image files using Imaris File Converter software. Imaris 3D Analysis software was then utilized to obtain body measurements of the micro-CT scans, including zygomatic arch diameter (midpoint), snout length, femur length and midpoint femur diameter.

Histology

Formalin-fixed tissues were processed through a series of graded alcohols, embedded in paraffin, and individual 4 μm sections were cut and stained with hematoxylin and eosin (H&E). For Alcian Blue staining, individual 4 μm sections were cut, deparaffinized, and hydrated to distilled water. Slides were immersed in 3% acetic acid for 3 minutes followed by Alcian Blue stain for 30 minutes. Slides were then rinsed with running tap water for 2 minutes, rinsed with distilled water and counterstained with nuclear fast red. For LAMP1 preparations, 4 μm formalin-fixed, paraffin-embedded sections of tissue were deparaffinized and rehydrated, followed by heat induced antigen

retrieval in EDTA. Slides were incubated overnight at 4 degrees C with a rabbit monoclonal anti-LAMP antibody (ab208943, Abcam) diluted at 1:500. Slides were incubated with Rabbit Envision (Dako) for 30 minutes followed by the chromogen 3,3'-diaminobenzidine (DAB) before counterstaining with hematoxylin.

Barnes Maze

The Barnes maze is a measure of spatial navigation and memory[437]. It consists of a circular platform with twenty holes positioned around the periphery, all of which are blocked except for one hole which has an escape box positioned underneath that the mouse can access using an inclined ramp. Visual cues are placed on the walls around the maze for spatial navigation. The animal is released into the center of the maze with the lights dimmed, bright overhead lights are then turned on, and the mouse is given 3 minutes to explore the maze. If the mouse does not enter the escape box within 3 minutes, it is guided to the escape hole and left there for 30 seconds before returning to its home cage. The mice were trained on the Barnes maze for 4 days at 4 trials a day, with an interval of 12-15 minutes between any two consecutive trials for each animal. The time taken by the animal to escape was recorded as latency to escape.

Y-Maze spontaneous alternation

The Y-maze assesses spatial learning and working memory[438]. Animals are placed in a testing room and allowed to habituate for 15-30 minutes in low light. The Y-maze apparatus consists of three identical arms (zones) each with a distinct visual cue. The

mouse was placed in one of the arms and allowed to explore the maze freely for a single 5-minute trial. Zone choices were recorded sequentially. Spontaneous alternation was determined when the animal explored an overlapping triplet of three distinct zones. Percent spontaneous alternation was scored as *(# of alternations/(total zone entries-2))*100*.

Statistics

GraphPad Prism was used for all graphing and statistics. Error bars on graphs represent group mean ± standard deviation (SD) or standard error of the mean (SEM). Multiple group comparisons were evaluated by 2-way ANOVA for Barnes maze. Y-maze spontaneous alternation data were analyzed by nonparametric comparisons using the Mann-Whitney U test. P values of < 0.05 were considered statistically significant for all tests. Biochemical data and radiographic data were grouped into mouse treatment types and evaluated using unpaired t-tests.

Results

Generation of NSG iduronate-2-sulfatase knockout mouse model

We set out to establish an immunodeficient mouse model of MPS II by introducing a deletion into the mouse *IDS* gene using CRISPR Cas9 in NSG mouse embryos. Guide RNA's targeting a sequence upstream of exon 1 (in the 5'UTR) and downstream of exon 5 (intron 5) of the *IDS* gene were designed and expression plasmids encoding either of these two gRNA's as well as Cas9 were generated by Genscript (see

Materials and Methods) (Figure 19). The effectiveness of these guides plus Cas9 was first tested by PEI-mediated co-transfection of both plasmids into mouse NIH 3T3 cells, demonstrating reduced IDS activity in extracts two days post-transfection (data not shown). Guide RNAs were then generated by *in vitro* transcription, and a mixture of both gRNA's along with Cas9-encoding mRNA was microinjected into fertilized NSG mouse embryos as described in Materials and Methods Out of 181 injected zygotes, 101 embryos survived. They were all transferred into 3 pseudo-pregnant CD-1 female mice and 35 pups were born 19 days later.

Toe snips were collected for DNA extraction and used for genotyping by PCR. Presence of the wild type *IDS* sequence was evaluated by PCR between exon 4 flanking primers C and D or intron 5 primers E and F, while deletion-bearing alleles were assayed by PCR between primers A and F, which flank the breakpoint of the intended deletion (Figure 19). Eight candidates of the 34 offspring (#s 428, 429, 432, 447, 448, 449, 459, and 460) exhibited one or two appropriately sized PCR products between primers A and F, indicative of *IDS* knockout. Several of these animals also exhibited absence of the wildtype PCR product between primers C and D (#s 428, 429, 447, 448, and 459) or between primers E and F (#s 428, 429, 451, and 459), also consistent with knockout of the *IDS* gene. Candidates not exhibiting absence of the wildtype allele (#s 432, 449, and 460) are likely either female monoallelic knockouts or mosaic of either gender for IDS knockout. All candidates except #449 were deficient in IDS activity in extracts from peripheral blood mononuclear cells.

Mice generating PCR products flanking the intended *IDS* deletion (i.e., between primers A and F) using DNA from either blood and/or toe tissue were suspected as *IDS*

knockouts and the PCR products were sequenced (Table 2.) Candidate *IDS* knockout alleles exhibited the intended deletion between positions 172 and 5686 plus an additional 2 to 1100 bp, consistent with erroneous non-homologous end joining[439-441]. Several animals (429, 447) were shown to be mosaic by the presence of different knockout alleles in blood vs toe DNA extracts. To isolate the *IDS* KO allele, mouse f449 was mated with male wild type mice, producing two separate lineages (1849 and 1850), male offspring of which exhibited absence of plasma IDS activity but also absence of any test PCR product (Table 3). Far downstream primers were required to recover PCR product from each of these *IDS* alleles, sequencing of which demonstrated different deletions both of which are distinct from the f449 founder and extend several hundred bp downstream of the intron 5 gRNA. After several generations of backcrossing to NSG mice, the 1850 lineage was chosen for characterization.

Peripheral blood IDS activity and urine GAG excretion

A group of 5-10 lineage 1850 NSG *IDS* knockouts were studied to determine metabolic and physiologic manifestations of disease in comparison to 6-11 NSG IDS+ male littermates at 7-12 months of age. Evaluation of IDS enzyme in NSG-MPS II mice revealed no detectable IDS activity in either plasma or PBMCs (Figure 20A, B). Conversely, NSG IDS+ male littermates showed an average of 25.9 nmol/hr/ml in plasma and 13.5 nmol/hr/mg protein in PBMC. Urinary GAGs were increased in NSG-MPS II mice to an average of 4493 µg GAG/mg creatinine when compared to NSG mice with a mean of 2331 µg GAG/mg creatinine (Figure 20C). NSG-MPS II mice are thus deficient

for IDS activity in the peripheral blood and show elevated levels of urinary GAG excretion.

Tissue IDS enzyme and GAG storage

IDS activity in the tissues of NSG-MPS II mice was undetectable i.e., below our limit of detection. Background fluorescence was detected in some samples, notably in the spleen, kidney, and liver, but nearly all data points were < 1 nmol/hr/mg protein and do not reflect quantifiable levels IDS enzyme activity. In contrast, NSG mice exhibited consistent levels of IDS in all tissues analyzed. These levels varied widely by tissue, from a mean of 6.6 nmol/hr/mg protein in the heart to 244 nmol/hr/mg protein in the brain (Figure 21A). Consistent with the absence of IDS enzyme activity, tissue GAG levels in NSG-MPS II mice were predictably elevated in all tissues analyzed. GAG levels in NSG-MPS II mice were increased over NSG mice from 2.25-fold in the brain to 75.96-fold in the lung from NSG GAG levels (Figure 21B). NSG-MPS II mice thus show a deficiency in IDS enzyme activity as well as accumulation of GAGs in major systemic and CNS organs.

Histopathology of NSG-MPS II

Histological analysis by H&E staining revealed intraneuronal vacuolization throughout the cerebellar cortex of the brain, especially in resident Purkinje cells, of NSG-MPS II mice when compared to NSG mice. (Figure 22A, D). These same Purkinje cells in NSG-MPS II mice were positive for storage material when stained with Alcian Blue (Figure 22G, J). An increase in LAMP-1, a membrane associated lysosomal protein,

is seen in both LSD patients and models of those disease[181,442]. Elevated LAMP-1 is thus associated with lysosomal enlargement and cellular dysfunction. LAMP-1 IHC showed sparse staining in the cerebellar cortex of NSG mice, but NSG-MPS II mice had noticeable increase in intracellular LAMP-1 (Figure 22M, P). Liver staining revealed numerous vacuolated macrophages (foam cells) in the perivascular regions of NSG-MPS II, but not NSG mice (Figure 22B, E). Alcian blue staining of these same foam cells showed distinctly stained storage material (Figure 22H, K). Both the foam cells and hepatocytes in NSG-MPS II mice had increased and widespread LAMP-1 staining compared to livers from NSG mice (Figure 22N, Q). Aortas of NSG-MPS II mice exhibited rarefaction of the smooth muscle, compared to NSG mice. Additionally, vacuolated macrophages were present in multiple layers of the blood vessel walls, including the tunica media and adventitia. (Figure 22C, F). No differences were noted between groups for Alcian blue staining in the aorta (Figure 22I, L). Compared to the minimal LAMP-1 staining noted in aortas of NSG mice, NSG-MPS II mice had extensive staining in both smooth muscle and macrophages (Figure 22O, R).

NSG-MPS II skeletal analysis

To evaluate the emergence of skeletal manifestations, NSG-MPS II mice full body micro-CT images were collected from NSG-MPS II mice. Zygomatic arch thickening has been observed as a skeletal manifestation in C57BL/6 $IDS^{Y/-}$ mice[294,311,313]. Zygomatic arch thickening was observed in the NSG-MPS II mice when compared to IDS+ NSG controls (Figure 23A). Analysis of NSG MPS II femurs showed a significant decrease in overall length compared to NSG controls (Figure 23C).

Differences in snout length and femur midshaft diameter between NSG and NSG-MPS II were not statistically significant by the Mann-Whitney U test (Figures 23B, D). These data reveal the skeletal manifestations associated with IDS deficiency the NSG-MPS II model.

Neurobehavioral analysis of NSG-MPS II mice.

Neurocognitive deficits are associated with MPS II both in patients and in mouse models of the disease[105,300,304]. To evaluate NSG-MPS II mice for neurocognitive deficits, test animals underwent several neurobehavioral analyses at six months of age. Mice were first tested on the 20-hole Barnes maze, which evaluates spatial memory and learning[437]. The Barnes maze consisted of four 180s trials a day for four days (see Materials and Methods). After the first day, NSG and NSG-MPS II mice showed similar latency to escape the maze with means of 175.4s and 176.8s, respectively. On day 2 of testing, a trend emerged whereby NSG mice learned to escape the maze faster, on average, than NSG-MPS II mice. This trend culminated on day 4, when the mean latency to escape of 54.9s for NSG mice was significantly different compared to 94.5s for NSG-MPS II mice (Figure 24A). The Y-maze spontaneous alternation test relies on a mouse's predisposition to explore new arms during testing (see Materials and Methods)[438]. The mean percent alternation for NSG mice was 62.2%, while the mean for NSG-MPS II was 51.8%, a significant difference of 10.4% between the two groups (Figure 24B). NSG MPS II mice were also evaluated using rotarod (motor function) and fear conditioning (neurocognitive) tests, but their performance was not significantly different from that of

IDS+ NSG mice. We conclude that NSG-MPS II mice have significant neurocognitive deficits in NSG-MPS II mice in comparison with IDS+ NSG control littermates.

Discussion

We generated a novel NSG-MPS II mouse model using CRISPR/Cas9 which included dual sgRNAs in fertilized NSG mouse embryos to create a structural deletion from the 5'UTR to the 5th intron of the mouse *IDS* gene. Male mice with a deletion in this region had no detectable IDS activity in blood plasma, in PBMCs, and in any tissues analyzed. Concomitantly, these mice showed elevated GAG excretion in the urine as well as GAG storage in analyzed tissues. Histologically, vacuolized cells were seen in all tissues analyzed, including throughout the CNS. These mice also showed functional deficits in the form of skeletal and neurological manifestations. NSG-MPS II mice were observed to have an increased zygomatic arch diameter and decreased femur length. Lastly, NSG-MPS II mice exhibited neurocognitive deficits in spatial learning and memory in the Barnes maze and working memory in the Y-maze.

The phenotypes we observed in NSG-MPS II mice are similar to those previously reported for C57BL/6J *IDS* knockout mice[294,295]. In addition to deficiency in IDS activity and elevated storage material, NSG-MPS II mice show skeletal and neurological manifestations that are similar to the immunocompetent C57BL/6J model[294,304,311,316,318]. This model also recapitulates some of the biochemical and clinical manifestations that are seen in human MPS II[86]. Although we did not conduct a detailed natural history of disease in these animals (i.e., assessment of disease manifestations over time), it is likely that the phenotypes seen here are progressive in nature, given that disease progression is

observed in both C57BL/6J-MPS II mice and in the human disease[95,304]. Recently, Shimada et al published a NOG-MPS II mouse model which was used to evaluate an *ex vivo* lentiviral vector gene therapy[301]. However, this NOG-MPS II mouse model has not been physiologically characterized for manifestations of MPS disease.

The first clinical trial (NCT00004454) of a gene therapy for Hunter syndrome was conducted in 1996, testing *IDS* gene transfer into T lymphocytes using a retroviral vector[346,443]. This study never published any results of the trial. Developments in vector safety and technology have recently brought MPS II gene therapy back to the clinic[323,389]. Although a gene editing approach using zinc finger nucleases (NCT03041324) was terminated due to lack of detectable IDS enzyme in patient plasma, several other AAV-based trials have been initiated. REGENXBIO launched the first of these trials (NCT03566043) in 2018 evaluating a dose escalation of their AAV9 vector administered intracisternally. An additional clinical trial (NCT04571970) evaluating the same route of administration at a single dose in older (5-17 years of age) neuronopathic patients launched in 2020. In 2022, Homology Medicines began recruiting for their clinical trial (NCT05238324), which uses a novel AAV-HSC vector to deliver h*IDS* by IV infusion. New and more effective therapies for neuronopathic MPS II constitute a substantial unmet need, so it is likely that other cell and gene therapies will soon make their way into the clinic. The NSG-MPS II mouse strain described in this paper provides an immunodeficient animal model that recapitulates many of the metabolic, skeletal, and neurologic manifestations of the human disease and in this regard will be useful for preclinical testing.

Based on the NSG background, this model will be particularly useful for studies involving xenotransplantation, such as *ex vivo* transduction of autologous hematopoietic stem cells using an integrating viral vector[43]. Investigations into *ex vivo* gene therapy for MPS II have generally involved transplantation of engineered mouse cells into syngeneic or congenic hosts[310-313]. In contrast, the NSG MPS II mouse model presents the opportunity to test the *ex vivo* approach by xenotransplantation of genetically modified human cells, as demonstrated for other LSDs[433,444]. Other possible candidates for xenotransplantation include the engraftment of human neural stem cells, other human induced pluripotent stem cell (iPSC)-derived cell lines, human T cells, and human B cells[445-448]. A gene therapy using patient iPSC-derived NSCs has been tested in a NOD/SCID/MPS VII mouse model[449]. Engraftment of lentiviral-modified human T cells to deliver therapeutic enzymes in models of Fabry, Farber, Gaucher, and Pompe diseases was recently evaluated in a xenograft model[450]. Engraftment of genetically modified human B cells has also been tested in an immunodeficient NSG model of MPS I[451]. There is thus a wide range of cell and gene therapy technologies for which the NSG-MPS II mouse model described in this paper will be highly useful for both basic and translational research activities into the biology of and the development of new treatments for MPS II.

5'UTR sgRNA Sequence	5' CTTCTTGCAAGACTGCGCCG
Intron 5 sgRNA Sequence	5' GATTACACAATGACGTACAG
Primer A	5' CTCAGAGACTTTGGTGGTGACAGC
Primer B	5' GATGCAGAAGGAGCCTAGCAACA
Primer C	5' GGGGAGGAGCTACTTGCATAGTTG
Primer D	5' AGGTGGAAAAGACCAGCTATATGG
Primer E	5' ATAGAGGGTTCCAACACAACCAAGC
Primer F	5' CAACATCAAAGGGCATACTTCCCAG
Primer G	5' AGGCTTGGACATCTTCCCTCTC

Table 1. sgRNA and primer sequences. Primers were designed to evaluate potential m*IDS* gene knockout mice.

MOUSE #	SEQUENCE	DELETION COMPARED TO REFERENCE
INTENDED DELETION	CACGCCACCTTCTTGCAAGACTGCG CAGAGGTGACATAAAGCCACCAGGA	g.172_5686del
428 T	CACGCCACCTTCTTGCAAGACTGCG GACATAAAGCCACCAGGAGCCATAC	g.172_5693del
428 B	CACGCCACCTTCTTGCAAGACTGCG GACATAAAGCCACCAGGAGCCATAC	g.172_5693del
429 T	(142) GCCACCAGGAGCCATACTCTTTGGA	g.142_5700del
429 BU	(157) GCCACCAGGAGCCATACTCTTTGGA	g.157_5700del
429 BL	(?) CCACCAGGAGCCATACTCTTTGGA	g.? _5703del
432 T	(128) (5730)	g.128_5730del
447 T	CACGCCACCTTCTTGCAAGA AAGCCACCAGGAGCCATACTCTTTG	g.166_5698del
447 BU	CACGCCACCTTCTTGCAAGACTGCG GAGGTGACATAAAGCCACCAGGAGC	g.172_5688del
447 BL	CACGCCACCTTCTTGCAAGA GGTGACATAAAGCCACCAGGAGCCA	g.167_5690del
448 T	(144) AAGCCACCAGGAGCCATACTCTTTG	g.144_5694del
449 T	CACGCCACCTTCTTGCAAGACTGC AGAGGTGACATAAAGCCACCAGGAG	g.171_5687del
1849B	CACGCCACCTTCTTGCAAGACTGC (6021)	g.171_6021del
1850B	CACGCCACCTTCTTGCAAGACTG (6784)	g.170_6784del
451 B	CACGCCACCTT GACATAAAGCCACCAGGAGCCATAC	g.158_5693del
459 T	CACGCCACCTTCTTGCA GAGGTGACATAAAGCCACCAGGAGC	g.164_5688del
460 T	CACGCCACCTTCTTGCAAGACT GCCACCAGGAGCCATACTCTTTGGA	g.169_5701del

Table 2. Sequence alignment of the genotyped blood (B) or toe (T) sample. T, B; toe or blood as source of DNA template for PCR genotyping; U, L; upper or lower band present after PCR. PCR for sequencing carried out with primers A and F, with the exception of 1849 and 1850 where F was replaced with a 7th primer (Primer G, not shown in Figure 1).

MOUSE #, SEX	PBMC IDS ACTIVITY (nmol/hr/mg protein)	PCR PRIMERS A, F	PCR PRIMERS C, D	PCR PRIMERS E, F
Wildtype	NA	No band	152bp	460bp
Intended Deletion	NA	411bp	No band	No band
428, f	0	411bp	No band	No band
429, F	0	2 bands, ~300-400bp	No band	No band
432, F	0	~300bp	152bp	Faint Band
447, F	0	411bp	No band	Faint Band
448, F	0	2 bands, 150 and 400bp	No band	Faint Band
449, F	0.34	411bp	152bp	460bp
1849, M	0	No band	No band	No band
1850, M	0	No band	No band	No band
451, F	0	411bp	Unclear	No band
459, M	0	411bp	No band	No band
460, M	0	411bp	152bp	460bp
C57Bl/6(Y/+)	1.07	NA	152bp	460bp

Table 3. Genotyping information generated from potential IDS knockout mice. Primer pair letter correlates to those shown in Figure 1 and the expected fragment size from the PCR reaction.

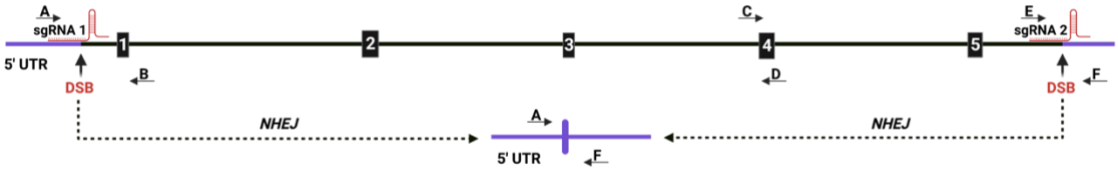

Figure 19. mIDS gene knockout and genotyping strategies. Partial depiction of IDS gene showing exons 1 through 5 (labeled) with locations of sgRNA 1 and sgRNA 2 (in red) for double sgRNA knockout strategy. Sites for Cas9 mediated double-strand break (DSB), NHEJ generated deletion product (thick purple line) and positions of primers A through F for PCR genotyping and sequencing (see Table 2) are shown.

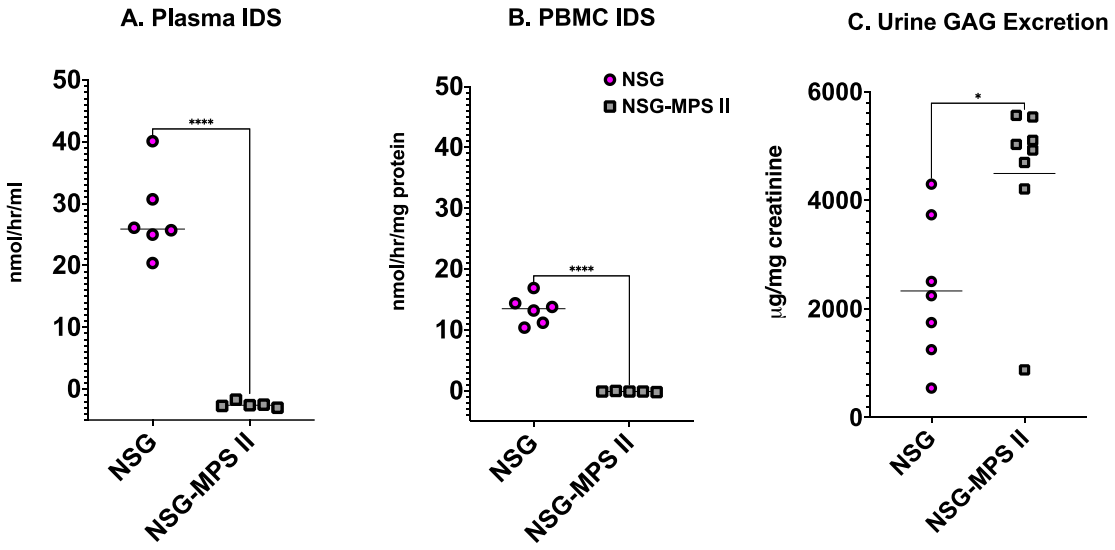

Figure 20. Plasma and PBMC IDS enzyme activities and urine GAG excretion in NSG and NSG-MPS II mice. (A, B) Plasma and PBMC IDS activity at time of euthanasia. (C) Excreted urine GAGs at the time of euthanasia. Ages at sample collection range from 7 months to 12 months. Cross bar shows mean activity. For plasma and PBMC, N=6 for NSG and N=5 for NSG-MPS II. For urine, N=7 for NSG and N=8 for NSG-MPS II. Statistical analysis was by t-test. *: P <.05, ****: P<.0001.

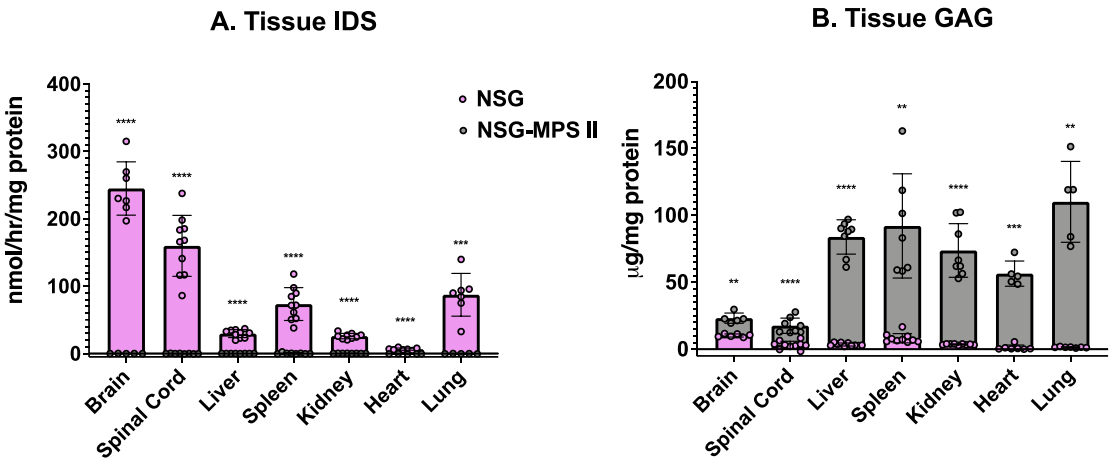

Figure 21. Tissue IDS activity and GAG storage levels in NSG and NSG-MPS II Mice. (A) IDS activity levels by tissue. (B) GAG storage levels by tissue. Data for both NSG and NSG-MPS II are shown on superimposed columns for both graphs. Sample sizes are N=6-10 for NSG and N=5-8 for NSG-MPS II. N values vary depending on tissue type as some tissues were instead taken for histological analysis. Error bars show mean +/- S.D. Statistical analysis by multiple t-tests. **: P<0.01, ***: P<0.001, and ****: P<0.0001.

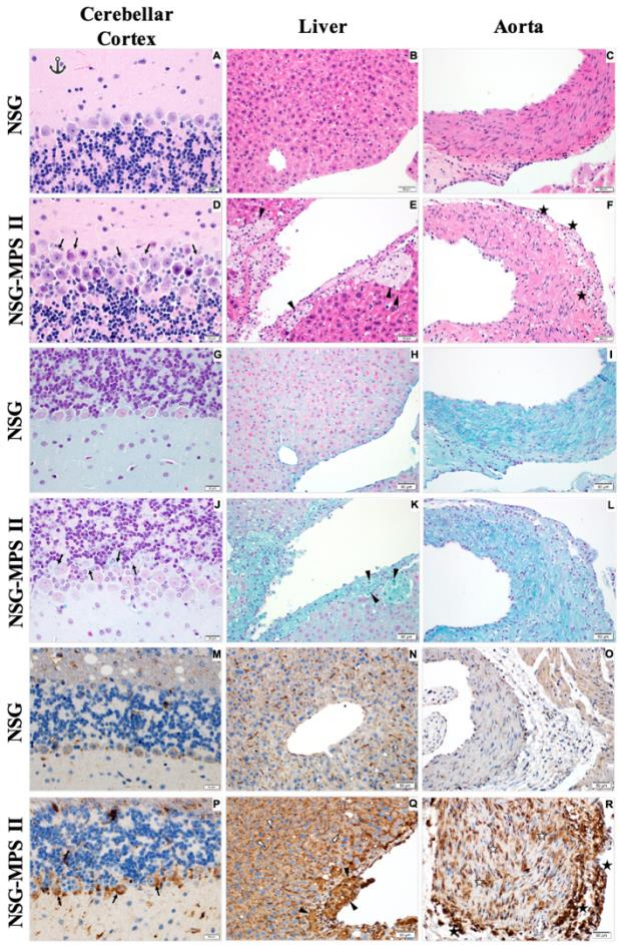

Figure 22. Hematoxylin and Eosin (H&E), Alcian blue (AB), and LAMP-1 IHC stained sections from NSG and NSG-MPS II mice. (A, D) Cerebellar cortex: In contrast to the NSG mice (A), intracytoplasmic vacuolization (black arrows) was noted in the Purkinje cells from all NSG-MPS II mice (D). (B, E) Liver: In contrast to the NSG mice (B), numerous fine-vacuolated perivascular macrophages ("foam cells", black arrowheads) were seen in all NSG-MPS II mice (E). (C, F) Aorta: In contrast to the NSG mice (C), there was extensive rarefaction of the smooth muscle and moderate numbers of finely-vacuolated macrophages (black stars) within the tunica media and adventitia from the NSG-MPS II mice (F). (G, J) Cerebellar cortex: In contrast to the NSG mice (G), intracytoplasmic AB-positive blue material (black arrows) was noted in the Purkinje cells from all NSG-MPS II mice (J). (H, K) Liver: In contrast to the NSG mice (H), moderate amounts of AB-positive blue material (black arrowheads) were seen all NSG-MPS II mice (K). (I, L) Aorta: No significant differences were noted in the AB-stained aortic tissues from the NSG (I) and NSG-MPS II mice (L). (M, P) Cerebellar cortex: In contrast to the sparse intracytoplasmic LAMP1 staining in the Purkinje cells from the NSG mice (M), there was marked intracytoplasmic LAMP1 staining (black arrows) in the Purkinje cells from all NSG-MPS II mice (P). (N, Q) Liver: In contrast to the minimal LAMP1 staining in the liver from the NSG mice (N), there was marked LAMP1 staining in the perivascular macrophages (black arrowheads) and hepatocytes (white arrowheads) in all NSG-MPS II mice (Q). (O, R) Aorta: In contrast to the minimal LAMP1 staining in the NSG mice (O), there was marked LAMP1 staining within the smooth muscle (white stars) and macrophages (black stars) (R). Scale bars show 50μm.

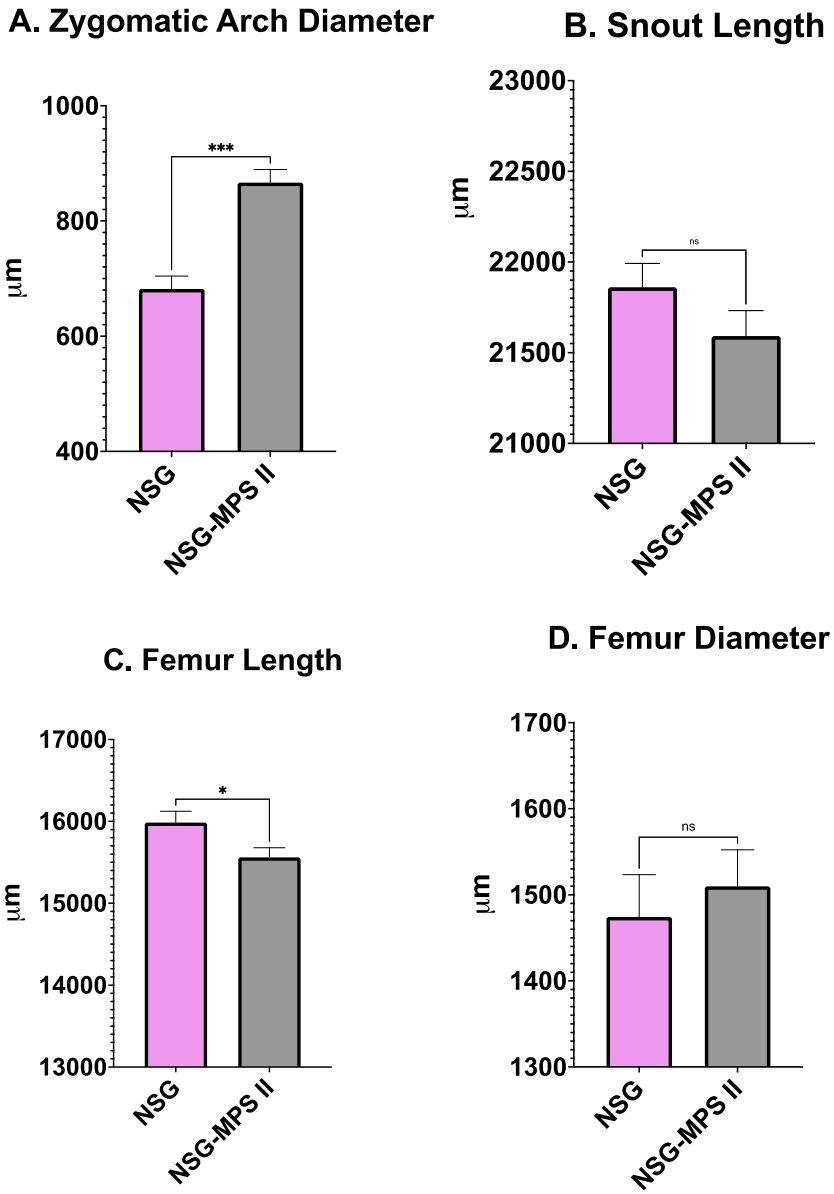

Figure 23. Skeletal manifestations in NSG-MPS II mice. Radiographic analysis at 6-7 months of age. (A) Zygomatic arch diameter. (B) Snout length. (C) Femur length. (D) Femur diameter. Significance was determined by Mann-Whitney U test. Sample sizes: NSG N=10, NSG-MPS II N=9. Error bars show SEM. ns: not significance, *: P <.05, ***: P<.001.

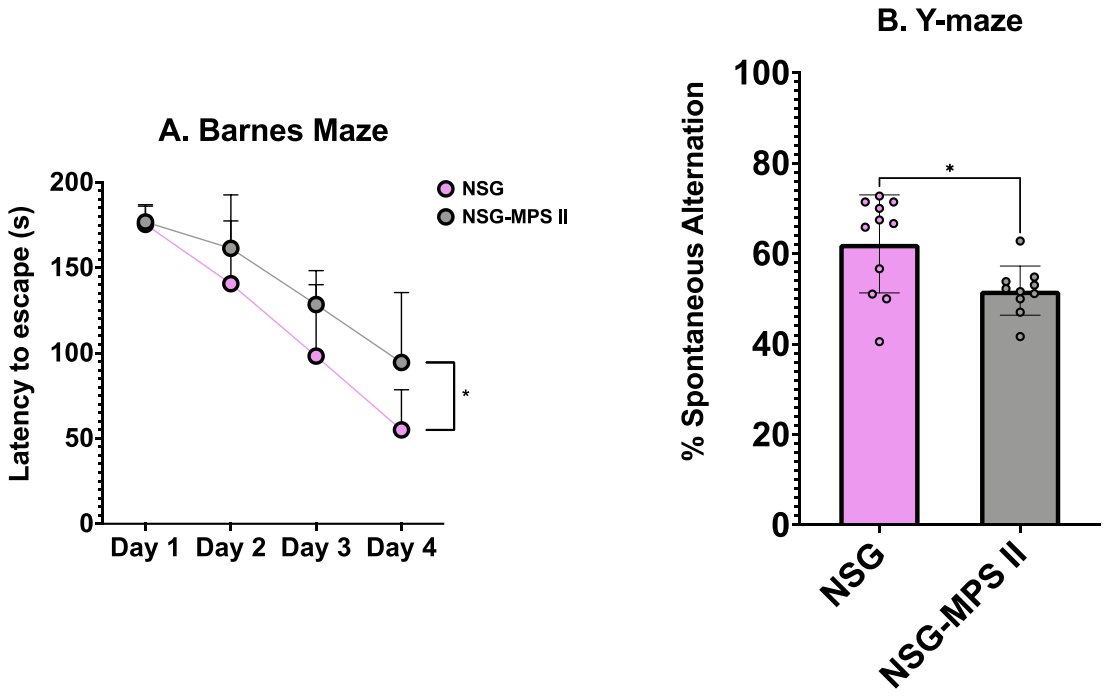

Figure 24. Neurocognitive analysis in NSG and NSG-MPS II Mice. Both groups were evaluated neurobehaviorally at 4 months of age. (A) Barnes maze evaluation for spatial navigation and memory. Results are shown as the mean latency to escape for 4 trials a day over 4 days. Significance was evaluated by two-way ANOVA. (B) Y-maze spontaneous alternation for evaluation of short-term spatial memory and reported as percent alternation. Results are shown as average of a 5-minute trial. Significance was evaluated by Mann-Whitney test. Sample sizes are N=11 for NSG and N=10 for NSG-MPS II. Error bars shown mean +/- S.D.

Chapter V: Conclusions and Future Directions

Iduronate-2-sulfatase is an essential enzyme required for the catabolism the GAGs heparan sulfate and dermatan sulfate. Mutations in the *IDS* gene lead to a deficiency in IDS activity, the subsequent accumulations of GAGs, and the emergence of the lysosomal disease MPS II[57]. Current treatment for MPS II is ERT with Elaprase®. However, ERT is limited by the fact that it cannot fully address disease manifestations, especially those of the CNS[76]. Thus, there is a need for a more effective therapy to be developed. The work detailed in Chapter II and Chapter III took two different gene transfer approaches towards developing a gene therapy for MPS II. Additionally, Chapter IV generated and characterized a novel immunodeficient model of MPS II for future preclinical work.

HSCT vs HSCGT

Chapter II discusses the development of an HSCGT for MPS II. Understanding the reasons HSCT is not a current treatment option for MPS II gives insight into why HSCGT is worth pursuing for MPS II. The relatively limited and varied data on HSCT for MPS II make it difficult to assess its therapeutic benefit[348]. In particular, it is challenging to say how HSCT would impact the neurological manifestations. Some studies suggest early HSCT could ameliorate neurodegeneration[398,399]. However, many of these reports examine HSCT patient cohorts of undetermined neurocognitive status and long-term data on patients with severe phenotypes when treated <2 years of age is sparse[254,348]. Thus, poor and inconsistent data on HSCT situate its therapeutic potential as uncertain for MPS II. There simply is not enough evidence that HSCT can be a durable and potent therapy to address the CNS pathology of Hunter syndrome.

Contrast this with MPS I where the data are clear: HSCT shows great benefit and is the standard of care for treating neuronopathic Hurler syndrome[62,249]. Why is HSCT more efficacious for this closely related disorder than for MPS II? Certainly, the earlier time to diagnosis in MPS I vs. MPS II plays a role[170]. This effect of diagnosis can be seen in the neurological benefit some MPS II patients show when treated by HSCT early in life. A possibility is that engrafted cells do not generate enough IDS to achieve therapeutic effectiveness. The basis of HSCT affecting the CNS in patients is donor-derived microglia that cross correct neurons in the brain[38]. These microglia may express a higher level of IDUA compared to IDS, and thus less enzyme is being made available. However, mouse HSCT data show IDUA and IDS activity levels are similar, with IDS actually showing higher activity levels than IDUA in plasma, PBMC, and tissues (Chapter II Figures 11A&B, 12A; L.R. Belur, unpublished). An alternate explanation is that the required level of enzyme for a therapeutic benefit in the brain may be higher for MPS II than MPS I. For MPS diseases, a fraction of wild type activity is needed to see a therapeutic benefit[329]. In mouse studies, supplying as little as 1.5-5% of the deficient enzyme is needed for brain GAG reduction and neurocognitive benefit[295,316,318]. However, that percentage reflects a much higher absolute level of IDS enzyme compared to IDUA enzyme. Endogenous levels of IDS in the brain of mice are 250-300 nmol/hr/mg protein, while for IDUA they are ~1-3 nmol/hr/mg protein[383,397] (Chapter II Figure 12A). Thus, reaching an impactful level of IDS is more difficult than it is for IDUA using the same treatment method, i.e., HSCT.

Although HSCT is the standard therapy for MPS I, HSCGT is being pursued as better alternative treatment option. HLA-donor matching, myeloablative preconditioning,

GvHD, and low enzyme expression are complications that may arise with HSCT for MPS I and MPS II[348,400]. While myeloablative precondition is still required, the other three problems are addressed by HSCGT. The autologous nature of the therapy removes the need to find a matched donor. Additionally, risks related to GvHD are eliminated by using the patient's own cells. Supraphysiological levels of enzyme can be achieved by transducing patient cells with a LVV encoding functional *IDS* or *IDUA* cDNA regulated by a strong, constitutively active promoter. A HSCGT clinical trial for MPS I from November 2021 reported impressive and encouraging results in patients[401]. A commentary on the work suggested it was "the beginning of the end of allogeneic transplantation for Hurler syndrome"[400]. The advantages HSCGT has over HSCT for MPS I translate to MPS II. The preclinical work detailed in Chapter II, along with work done by others, shows that a higher level of IDS expression compared to HSCT is achievable and that it can ameliorate both peripheral and CNS manifestations in the mouse model[311,313]. With the strong preclinical data generated and its impact in the MPS I clinical trial, it is time to consider HSCGT as a treatment option for MPS II.

Routes of Administration for AAV9 encoding *IDS*

Chapter III details a comparison of IT vs IV dosing of an AAV9 vector encoding *IDS* cDNA regulated by a strong promoter. This study showed IT administration was best able to prevent the emergence of neurocognitive disease in MPS II mice (Chapter III Figure 18). Additionally, a large portion of the vector was released into the periphery to mainly transduce liver cells that serve as a source of bioavailable IDS (Chapter III Figure 13B). The level of IDS produced was sufficient to normalize GAG content and zygomatic

arch diameter in the mice (Chapter III Figure 12B, 14B). Overall, IT administration was sufficient to address both peripheral and CNS disease manifestations in MPS II mice. This agrees with previous studies that administered AAV9 by a CSF-directed (ICV, ICM) route[300,315,316]. The doses in those studies were $3x10^{10}$gc-$5x10^{10}$gc, similar to the most effective dose at 10^{11}gc described in Chapter III. The work in Chapter III also shows equivalent doses delivered IV were less efficacious in addressing the CNS compared to IT. Additionally, studies administering systemically had to use much higher doses (10^{12}gc-$2x10^{13}$gc) to achieve effective results in the CNS, with lower IDS activities recorded overall[317,464]. These comparisons suggest that the dose required to address both peripheral and CNS manifestations is lower overall by CSF-directed administration compared to IV administration.

Based on the preclinical data discussed in the above paragraph, and in Chapters I and III, a CSF-directed ROA should be favored over systemic administration for neuronopathic MPS II. Because of the targeted nature of CSF-directed administration, a lower dose can be used than by systemic administration to address neurological disease in mice. In addition to the CNS manifestations, patients also suffer from severe peripheral disease, such as skeletal dysplasias and cardiopulmonary dysfunction[86,87]. In Chapter III, targeted administration into the CNS simultaneously addressed both peripheral and CNS disease manifestations in the mouse model. Thus, no supplemental systemic administration was required. There are efficacy and safety benefits to administering a lower dose of AAV9. The immunogenic characteristics of AAV mean higher doses can cause loss of efficacy through AAV capsid activation of CD8+ T cells that destroy transduced cells[375]. High dose AAV administration can lead to toxicity, particularly in the

liver, leading to severe adverse events such as sepsis or even death[402,403]. Overall, CSF-directed administration of AAV9 is likely to be more efficacious and safe compared to similar IV administration for neuronopathic MPS II.

Data from Chapter III suggest systemic administration as a possible treatment for non-neuronopathic MPS II. ERT leaves some peripheral manifestations unaddressed for non-neuronopathic patients, such as cardiopulmonary manifestations, skeletal abnormalities and joint stiffness[87,94]. AAV9 administered IV normalized GAG content and zygomatic arch diameter in mice. This was accomplished by a dose lower (10^{10}gc) than what was needed to address CNS manifestations (10^{11}gc) by IT administration. In contrast to ERT, IV administration of AAV9 benefits from reduced invasiveness and long-term expression.

Comparison of HSCGT and AAV-vector approach to Gene Therapy for MPS II

While the need of a more effective therapy for MPS II is clear, the work detailed in Chapter II and Chapter III raises the question: how do these two different gene therapy approaches compare? Both CSF-directed administration of AAV9 and HSCGT can address peripheral disease manifestations, provide appreciable levels of IDS in the brain, and prevent neurocognitive deficits in the MPS II mouse model. Widespread IDS activity and GAG normalization was seen in peripheral tissues for both strategies. Treatment of a skeletal abnormality, a thickened zygomatic arch, was normalized by both approaches as well. In the brain, higher enzyme activity levels were achieved by HSCGT (13% of wild type) than by 10^{11}gc IT administration (1.65% of wild type). This is reflected in measured

brain GAG content, which was normalized in HSCGT and 65% corrected in 10^{11}gc IT administration. Regardless, functional improvements in spatial learning and memory were observed in treated mice from both studies, in accordance with past publications[300,311,314,318]. Overall, the AAV-vector strategy conferred lower IDS enzyme levels and GAG reduction in the CNS in the 10 ^{11}gc IT group compared to HSCGT.

HSCGT poses risks related to the preconditioning regimens required to allow for engraftment of genetically modified cells. Immunosuppression to prevent rejection of transplanted HSPCs is accomplished through chemotherapy and is toxic to the transplant recipient[62,400]. However, alternative preconditioning regimens may reduce issues regarding myeloablation related toxicity in the future[308]. As discussed in Chapter I, insertional mutagenesis is a potential risk with HSCGT and can lead to myelodysplastic syndrome, and leukemia[389]. Nonetheless, if engrafted cells produce high and consistent levels of IDS enzyme (including in the brain), this approach will be a substantial step towards a more successful therapy for MPS II. Host immune response is a still a barrier for AAV-vector approaches[375]. Capsid related immunogenicity can decrease therapeutic efficacy and lead to severe adverse events such as sepsis or even death[374,402,403]. Investigations into minimal effective dose, as done in Chapter III, can help overcome this barrier. By using a minimal effective dose, it is possible to maintain efficacy by overcoming neutralizing antibodies and avoiding capsid specific T-cell activation[375]. While the MPS II mouse model does not develop an immune response to the transgene product, MPS II patients can mount a response to hIDS, as seen with ERT[214,316,375]. Thus, transgene immune response may need to be considered when evaluating an AAV-vector therapy in other preclinical models or clinically. Both of these strategies share a major

challenge in terms of cost. While ERT with idursulfase is expensive, companies can be expected to charge millions of dollars for gene therapies[404]. An HSCGT for beta thalassemia is expected to cost $2.1 million USD and the list price for an AAV gene therapy for spinal muscular dystrophy is $2.125 million USD[452,453]. Thus, financial burden and equitable access are problems for gene therapy in general[400].

From a preclinical perspective, both *ex vivo* and *in vivo* gene therapy approaches are viable options to consider as potential treatments for MPS II. They confer high and durable levels of IDS activity and address both peripheral and CNS disease manifestations. In this way, HSCGT and CSF-directed administration of AAV show distinct improvements in efficacy over ERT and HSCT. However, safety and cost are challenges for both strategies. Thus, both are worth pursuing clinically as future treatment options for MPS II.

Future Preclinical Work Using the NSG-MPS II Mouse Model

Preclinical work, such as those described in Chapters II and III, paves the way for future therapies, to reach the clinic[318,464]. Thus, additional tools to accomplish this work more effectively can lead to better understanding of a therapy before moving into the clinic. For MPS II, a new addition to the preclinical toolbox is detailed in Chapter IV with the development of the NSG-MPS II mouse model. Cell based therapies, such as HSCGT, can be evaluated in human cells before translating to a clinical setting. To see the possible future uses of the model, it is helpful to look at how immunodeficient mouse strains has been used for other MPS diseases. Gene editing of human CD34+ cells to produce IDUA enzyme was evaluated in an immunodeficient MPS I mouse model[405]. A

recent publication used an NSG-MPS I mouse strain to investigate the role that innate and adaptive immunity plays in aortic dilation[184]. NSG mice have also been used to study the safety and efficacy of an *ex vivo* LVV HSCGT for MPS IIIA[406]. Lastly, a NOG model of MPS II was developed to test an *ex vivo* LVV based gene therapy [301]. These examples show that there is considerable interest in developing cell and gene therapies, as well as investigating disease pathology using immunodeficient models. Thus, future studies can utilize the immunodeficient model described in Chapter IV to accomplish such work for MPS II.

The Prospect of Gene Editing for MPS II

Future gene editing for MPS II has two major goals. First, the therapy must engineer the production of high and consistent levels of IDS. Second, the enzyme needs to be supplied to the brain to address CNS manifestations. Current *ex vivo* LVV work, such as that described in Chapter II, shows that genetically modified HSPCs can achieve both these goals. Thus, an *ex vivo* gene editing approach may be ideal. In addition, gene editing can generate targeted modifications in the genome rather than the randomly integrating nature of an *ex vivo* LVV approach. Targeted integration would avoid the insertional mutagenesis safety problems associated with LVVs that are described above. The central question is how to engineer a highly expressing *IDS* cDNA in HSPCs using gene editing. One strategy would be to employ double strand breaks (DSB) and an AAV-vector supplied donor molecule encoding both *IDS* cDNA and a strong promoter[407]. Here, a gene editing tool, such as CRISPR/Cas9, creates a DSB at a specific locus and DNA repair machinery installs the AAV donor template at the site by homologous

recombination. In MPS I mice, this approach generated low levels of IDUA and did not reduce brain GAG content but showed correction of some skeletal manifestations[405]. However, DSBs can lead to unintended insertions or deletions, and in the case of CRISPR/Cas9 off target edits are possible[408]. One approach to circumvent this problem is to use an engineering tool that does not create DSBs. One such tool is a base editor. Base editors use the customizable targeting of CRISPR/Cas9 combined with a deaminase to institute a deamination reaction at a specific DNA base. Using either adenine or cytosine base editors, it is possible to chemically modify a base from A to G or C to T, respectively[409,410]. An MPS I mouse model generated by an IDUA point mutation, W392X, was treated *in utero* by intravenous administration of an AAV9-vector encoding an adenine base editor targeting the mutation. The study showed some biochemical improvements, with modest IDUA expression and GAG reduction in the liver and heart[411]. However, it failed to show biochemical correction in most tissues, including the CNS. This study highlights the problems base editors face for MPS II. First, base editing to correct a mutation in the *IDS* locus will not confer high and consistent levels of IDS activity. Second, there are over 660 different recorded *IDS* mutations for MPS II, and base editing will not be able to address them all, as many are not transition mutations[144]. Prime editing combines CRISPR/Cas9 targeting with a reverse transcriptase and an RNA template (pegRNA) to insert or delete short DNA sequences at a specific locus without generating DSBs[412]. A major disadvantage is that insertions can only be up to 40 bp long, too short to install a promoter and *IDS* cDNA[412]. However, recent advances combining prime editing with site specific recombinases has allowed the targeted insertion of DNA sequences up to 5kb in length[413]. This strategy is called twin-prime editing and functions

by prime editor inserting recombinase recognition sites at a specific locus and subsequent introduction of a recombinase to integrate a DNA sequence of choice. An *ex vivo* strategy could employ twin-prime editing to insert a highly active promoter and *IDS* cDNA at a targeted location in the genome. Overall, treatment of genetic disease like MPS II may be possible with new gene editing capabilities that allow for targeted integration.

Conclusion

Collectively, the work carried out and detailed in this thesis progresses novel therapies from the bench to the clinic for Hunter syndrome. Chapters II and III describe two different gene therapy strategies for MPS II. HSCGT is being pursued clinically in related diseases, such as MPS I, and the data generated in Chapter II gives hope that HSCGT for MPS II will also be translated to the clinic. The AAV-vector approach is already in clinical trials, and Chapter III defines what ROA and dose would be minimally effective for RGX-121. Lastly, it is anticipated that the immunodeficient mouse model generated and characterized in Chapter IV will be employed to develop new treatments for MPS II. Overall, the development of gene therapy technologies promises that a new and better treatment will be available for Hunter syndrome.

Bibliography

1. Bainton, D. F. The discovery of lysosomes. *Journal of Cell Biology* **91**, 66s–76s (1981).
2. Mehta, A., Beck, M., Linhart, A., Sunder-Plassmann, G. & Widmer, U. History of lysosomal storage diseases: an overview. in *Fabry Disease: Perspectives from 5 Years of FOS* (eds. Mehta, A., Beck, M. & Sunder-Plassmann, G.) (Oxford PharmaGenesis, 2006).
3. de Duve, C., Pressman, B. C., Gianetto, R., Wattiaux, R. & Appelmans, F. Tissue fractionation studies. 6. Intracellular distribution patterns of enzymes in rat-liver tissue. *Biochem J* **60**, 604–617 (1955).
4. Novikoff, A. B., Beaufay, H. & de Duve, C. ELECTRON MICROSCOPY OF LYSOSOME-RICH FRACTIONS FROM RAT LIVER. *J Biophys Biochem Cytol* **2**, 179–184 (1956).
5. Saftig, P. & Klumperman, J. Lysosome biogenesis and lysosomal membrane proteins: trafficking meets function. *Nat Rev Mol Cell Biol* **10**, 623–635 (2009).
6. Schwake, M., Schröder, B. & Saftig, P. Lysosomal Membrane Proteins and Their Central Role in Physiology. *Traffic* **14**, 739–748 (2013).
7. Trivedi, P. C., Bartlett, J. J. & Pulinilkunnil, T. Lysosomal Biology and Function: Modern View of Cellular Debris Bin. *Cells* **9**, 1131 (2020).
8. Li, P., Gu, M. & Xu, H. Lysosomal Ion Channels as Decoders of Cellular Signals. *Trends Biochem Sci* **44**, 110–124 (2019).
9. Perera, R. M. & Zoncu, R. The Lysosome as a Regulatory Hub. *Annu Rev Cell Dev Biol* **32**, 223–253 (2016).
10. Bouhamdani, N., Comeau, D. & Turcotte, S. A Compendium of Information on the Lysosome. *Frontiers in Cell and Developmental Biology* **9**, (2021).
11. Lüllmann-Rauch, R. History and Morphology of the Lysosome. in *Lysosomes* (ed. Saftig, P.) 1–16 (Springer US, 2005). doi:10.1007/0-387-28957-7_1.
12. Bohnert, K. A. & Johnson, A. E. Branching Off: New Insight Into Lysosomes as Tubular Organelles. *Front Cell Dev Biol* **10**, 863922 (2022).
13. Poteryaev, D., Datta, S., Ackema, K., Zerial, M. & Spang, A. Identification of the Switch in Early-to-Late Endosome Transition. *Cell* **141**, 497–508 (2010).
14. Ho, C. Y., Alghamdi, T. A. & Botelho, R. J. Phosphatidylinositol-3,5-Bisphosphate: No Longer the Poor PIP2. *Traffic* **13**, 1–8 (2012).
15.Phan, T. K. *et al.* Phosphoinositides: multipurpose cellular lipids with emerging roles in cell death. *Cell Death Differ* **26**, 781–793 (2019).
16. Palmieri, M. *et al.* Characterization of the CLEAR network reveals an integrated control of cellular clearance pathways. *Hum Mol Genet* **20**, 3852–3866 (2011).
17. Settembre, C. *et al.* TFEB links autophagy to lysosomal biogenesis. *Science* **332**, 1429–1433 (2011).
18. Sardiello, M. *et al.* A Gene Network Regulating Lysosomal Biogenesis and Function. *Science* **325**, 473–477 (2009).
19. Luzio, J. P., Pryor, P. R. & Bright, N. A. Lysosomes: fusion and function. *Nat Rev Mol Cell Biol* **8**, 622–632 (2007).
20. Luzio, J. P. *et al.* Membrane dynamics and the biogenesis of lysosomes (Review). *Molecular Membrane Biology* **20**, 141–154 (2003).
21. Mullins, C. & Bonifacino, J. S. The molecular machinery for lysosome biogenesis*. *BioEssays* **23**, 333–343 (2001).
22. Luzio, J. P. *et al.* Lysosome-endosome fusion and lysosome biogenesis. *Journal of Cell Science* **113**, 1515–1524 (2000).
23. Storrie, B. & Desjardins, M. The biogenesis of lysosomes: is it a kiss and run, continuous fusion and fission process? *Bioessays* **18**, 895–903 (1996).
24. Luzio, J. P. *et al.* Membrane traffic to and from lysosomes. *Biochemical Society Symposia* **72**, 77–86 (2005).
25. Luzio, J. P., Hackmann, Y., Dieckmann, N. M. G. & Griffiths, G. M. The Biogenesis of Lysosomes and Lysosome-Related Organelles. *Cold Spring Harb Perspect Biol* **6**, a016840 (2014).
26. Christensen, K. A., Myers, J. T. & Swanson, J. A. pH-dependent regulation of lysosomal calcium in macrophages. *Journal of Cell Science* **115**, 599–607 (2002).
27. Lloyd-Evans, E. *et al.* Niemann-Pick disease type C1 is a sphingosine storage disease that causes deregulation of lysosomal calcium. *Nat Med* **14**, 1247–1255 (2008).
28. Medina, D. L. Lysosomal calcium and autophagy. *Int Rev Cell Mol Biol* **362**, 141–170 (2021).

29. Appelqvist, H., Wäster, P., Kågedal, K. & Öllinger, K. The lysosome: from waste bag to potential therapeutic target. *Journal of Molecular Cell Biology* **5**, 214–226 (2013).
30. Coffey, J. W. & de Duve, C. Digestive Activity of Lysosomes: I. THE DIGESTION OF PROTEINS BY EXTRACTS OF RAT LIVER LYSOSOMES. *Journal of Biological Chemistry* **243**, 3255–3263 (1968).
31. Ohkuma, S. & Poole, B. Fluorescence probe measurement of the intralysosomal pH in living cells and the perturbation of pH by various agents. *Proceedings of the National Academy of Sciences* **75**, 3327–3331 (1978).
32. Ohkuma, S., Moriyama, Y. & Takano, T. Identification and characterization of a proton pump on lysosomes by fluorescein-isothiocyanate-dextran fluorescence. *Proceedings of the National Academy of Sciences* **79**, 2758–2762 (1982).
33. Mindell, J. A. Lysosomal acidification mechanisms. *Annu Rev Physiol* **74**, 69–86 (2012).
34. Braulke, T. & Bonifacino, J. S. Sorting of lysosomal proteins. *Biochimica et Biophysica Acta (BBA) - Molecular Cell Research* **1793**, 605–614 (2009).
35. Helenius, A. & Aebi, and M. Intracellular Functions of N-Linked Glycans. *Science* **291**, 2364–2369 (2001).
36. Ghosh, D. Human sulfatases: A structural perspective to catalysis. *Cell. Mol. Life Sci.* **64**, 2013–2022 (2007).
37. Dierks, T. *et al.* Multiple Sulfatase Deficiency Is Caused by Mutations in the Gene Encoding the Human Cα-Formylglycine Generating Enzyme. *Cell* **113**, 435–444 (2003).
38. Capotondo, A. *et al.* Brain conditioning is instrumental for successful microglia reconstitution following hematopoietic stem cell transplantation. *PNAS* **109**, 15018–15023 (2012).
39. Duden, R. ER-to-Golgi transport: COP I and COP II function (Review). *Molecular Membrane Biology* **20**, 197–207 (2003).
40. Lazzarino, D. A. & Gabel, C. A. Mannose processing is an important determinant in the assembly of phosphorylated high mannose-type oligosaccharides. *J Biol Chem* **264**, 5015–5023 (1989).
41. Rohrer, J. & Kornfeld, R. Lysosomal hydrolase mannose 6-phosphate uncovering enzyme resides in the trans-Golgi network. *Mol Biol Cell* **12**, 1623–1631 (2001).
42. Borgne, R. L. & Hoflack, B. Mannose 6-Phosphate Receptors Regulate the Formation of Clathrin-coated Vesicles in the TGN. *J Cell Biol* **137**, 335–345 (1997).
43. Biffi, A. Hematopoietic Stem Cell Gene Therapy for Storage Disease: Current and New Indications. *Molecular Therapy* **25**, 1155–1162 (2017).
44. Barton, N. W., Furbish, F. S., Murray, G. J., Garfield, M. & Brady, R. O. Therapeutic response to intravenous infusions of glucocerebrosidase in a patient with Gaucher disease. *Proc Natl Acad Sci U S A* **87**, 1913–1916 (1990).
45. Barton, N. W. *et al.* Replacement therapy for inherited enzyme deficiency--macrophage-targeted glucocerebrosidase for Gaucher's disease. *N Engl J Med* **324**, 1464–1470 (1991).
46. Reczek, D. *et al.* LIMP-2 is a receptor for lysosomal mannose-6-phosphate-independent targeting of beta-glucocerebrosidase. *Cell* **131**, 770–783 (2007).
47. Lefrancois, S., Zeng, J., Hassan, A. J., Canuel, M. & Morales, C. R. The lysosomal trafficking of sphingolipid activator proteins (SAPs) is mediated by sortilin. *EMBO J* **22**, 6430–6437 (2003).
48. Mehta, A. Epidemiology and natural history of Gaucher's disease. *European Journal of Internal Medicine* **17**, S2–S5 (2006).
49. Gaggl, M., El-Hadi, S., Aigner, C. & Sunder-Plassmann, G. The Renal History of Fabry Disease. *G Ital Nefrol* **33 Suppl 66**, 33.S66.14 (2016).
50. Hers, H. G. α-Glucosidase deficiency in generalized glycogen-storage disease (Pompe's disease). *Biochem J* **86**, 11–16 (1963).
51. Platt, F. M., d'Azzo, A., Davidson, B. L., Neufeld, E. F. & Tifft, C. J. Lysosomal storage diseases. *Nat Rev Dis Primers* **4**, 1–25 (2018).
52. Meikle, P. J., Hopwood, J. J., Clague, A. E. & Carey, W. F. Prevalence of lysosomal storage disorders. *JAMA* **281**, 249–254 (1999).
53. Parenti, G., Medina, D. L. & Ballabio, A. The rapidly evolving view of lysosomal storage diseases. *EMBO Mol Med* **13**, e12836 (2021).
54. Beck, M. Variable clinical presentation in lysosomal storage disorders. *J Inherit Metab Dis* **24 Suppl 2**, 47–51; discussion 45-46 (2001).

55. Wolf, D. A. *et al.* Gene Therapy for Neurologic Manifestations of Mucopolysaccharidoses. *Expert Opin Drug Deliv* **12**, 283–296 (2015).
56. Khan, S. A. *et al.* Epidemiology of mucopolysaccharidoses. *Molecular Genetics and Metabolism* **121**, 227–240 (2017).
57. Neufeld, E. F. & Muenzer, J. The Mucopolysaccharidoses. in *The Online Metabolic and Molecular Bases of Inherited Disease* (eds. Valle, D. L., Antonarakis, S., Ballabio, A., Beaudet, A. L. & Mitchell, G. A.) (McGraw-Hill Education, 2019).
58. Muenzer, J. Overview of the mucopolysaccharidoses. *Rheumatology* **50**, v4–v12 (2011).
59. Donati, M. A., Pasquini, E., Spada, M., Polo, G. & Burlina, A. Newborn screening in mucopolysaccharidoses. *Ital J Pediatr* **44**, 126 (2018).
60. Bosfield, K. *et al.* Mucopolysaccharidosis type I newborn screening: Importance of second tier testing for ethnically diverse populations. *American Journal of Medical Genetics Part A* **185**, 134–140 (2021).
61. Concolino, D., Deodato, F. & Parini, R. Enzyme replacement therapy: efficacy and limitations. *Ital J Pediatr* **44**, 120 (2018).
62. Taylor, M. *et al.* Hematopoietic stem cell transplantation for mucopolysaccharidoses; past, present, and future. *Biol Blood Marrow Transplant* **25**, e226–e246 (2019).
63. Hunter, C. A Rare Disease in Two Brothers. *Proc R Soc Med* **10**, 104–116 (1917).
64. Brante, G. Gargoylism – A mucopolysaccharidosis. *Scandinavian Journal of Clinical and Laboratory Investigation* **4**, 43–46 (1952).
65. Dorfman, A. & Lorincz, A. E. OCCURRENCE OF URINARY ACID MUCOPOLYSACCHARIDES IN THE HURLER SYNDROME. *Proc Natl Acad Sci U S A* **43**, 443–446 (1957).
66. Fratantoni, J. C., Hall, C. W. & Neufeld, E. F. The defect in Hurler's and Hunter's syndromes: faulty degradation of mucopolysaccharide. *Proc Natl Acad Sci U S A* **60**, 699–706 (1968).
67. Fratantoni, J. C., Hall, C. W. & Neufeld, E. F. Hurler and Hunter Syndromes: Mutual Correction of the Defect in Cultured Fibroblasts. *Science* **162**, 570–572 (1968).
68. Fratantoni, J. C., Hall, C. W. & Neufeld, E. F. THE DEFECT IN HURLER AND HUNTER SYNDROMES, II. DEFICIENCY OF SPECIFIC FACTORS INVOLVED IN MUCOPOLYSACCHARIDE DEGRADATION. *Proc Natl Acad Sci U S A* **64**, 360–366 (1969).
69. Cantz, M., Chrambach, A., Bach, G. & Neufeld, E. F. The Hunter Corrective Factor. *Journal of Biological Chemistry* **247**, 5456–5462 (1972).
70. Cantz, M., Chrambach, A. & Neufeld, E. F. Characterization of the factor deficient in the Hunter syndrome by polyacrylamide gel electrophoresis. *Biochemical and Biophysical Research Communications* **39**, 936–942 (1970).
71. van Hoof, F. & Hers, H. G. The Abnormalities of Lysosomal Enzymes in Mucopolysaccharidoses. *European Journal of Biochemistry* **7**, 34–44 (1968).
72. Bach, G., Eisenberg, F., Cantz, M. & Neufeld, E. F. The Defect in the Hunter Syndrome: Deficiency of Sulfoiduronate Sulfatase. *Proc Natl Acad Sci U S A* **70**, 2134–2138 (1973).
73. Wilson, P. J. *et al.* Hunter syndrome: isolation of an iduronate-2-sulfatase cDNA clone and analysis of patient DNA. *Proc Natl Acad Sci U S A* **87**, 8531–8535 (1990).
74. Flomen, R. H., Green, E. P., Green, P. M., Bentley, D. R. & Giannelli, F. Determination of the organisation of coding sequences within the iduronate sulphate sulphatase (IDS) gene. *Human Molecular Genetics* **2**, 5–10 (1993).
75. Wilson, P. J., Meaney, C. A., Hopwood, J. J. & Morris, C. P. Sequence of the Human Iduronate 2-Sulfatase (IDS) Gene. *Genomics* **17**, 773–775 (1993).
76. Muenzer, J. *et al.* A phase II/III clinical study of enzyme replacement therapy with idursulfase in mucopolysaccharidosis II (Hunter syndrome). *Genetics in Medicine* **8**, 465–473 (2006).
77. Muenzer, J., Gucsavas-Calikoglu, M., McCandless, S. E., Schuetz, T. J. & Kimura, A. A phase I/II clinical trial of enzyme replacement therapy in mucopolysaccharidosis II (Hunter syndrome). *Molecular Genetics and Metabolism* **90**, 329–337 (2007).
78. Guillén-Navarro, E. *et al.* Clinical manifestations in female carriers of mucopolysaccharidosis type II: a spanish cross-sectional study. *Orphanet J Rare Dis* **8**, 92 (2013).
79. Cudry, S. *et al.* MPS II in females: molecular basis of two different cases. *Journal of Medical Genetics* **37**, e29–e29 (2000).

80. Piña-Aguilar, R. E. *et al.* Mucopolysaccharidosis type II in a female carrying a heterozygous stop mutation of the iduronate-2-sulfatase gene and showing a skewed X chromosome inactivation. *European Journal of Medical Genetics* **56**, 159–162 (2013).
81. Malm, G., Lund, A. M., Månsson, J.-E. & Heiberg, A. Mucopolysaccharidoses in the Scandinavian countries: incidence and prevalence. *Acta Paediatrica* **97**, 1577–1581 (2008).
82. Pinto, R. *et al.* Prevalence of lysosomal storage diseases in Portugal. *Eur J Hum Genet* **12**, 87–92 (2004).
83. Krabbi, K. *et al.* The Live-Birth Prevalence of Mucopolysaccharidoses in Estonia. *Genetic Testing and Molecular Biomarkers* **16**, 846–849 (2012).
84. Hashimoto, A., Kumagai, T. & Mineta, H. Hunter Syndrome Diagnosed by Otorhinolaryngologist. *Case Rep Otolaryngol* **2018**, 4252696 (2018).
85. Jones, S. A. *et al.* The effect of idursulfase on growth in patients with Hunter syndrome: Data from the Hunter Outcome Survey (HOS). *Molecular Genetics and Metabolism* **109**, 41–48 (2013).
86. Hampe, C. S. *et al.* Differences in MPS I and MPS II Disease Manifestations. *Int J Mol Sci* **22**, 7888 (2021).
87. Wraith, J. E. *et al.* Mucopolysaccharidosis type II (Hunter syndrome): a clinical review and recommendations for treatment in the era of enzyme replacement therapy. *Eur J Pediatr* **167**, 267–277 (2008).
88. Al Sawaf, S., Mayatepek, E. & Hoffmann, B. Neurological findings in Hunter disease: pathology and possible therapeutic effects reviewed. *J Inherit Metab Dis* **31**, 473–480 (2008).
89. Schwartz, I. V. *et al.* A clinical study of 77 patients with mucopolysaccharidosis type II. *Acta Paediatrica* **96**, 63–70 (2007).
90. Scarpa, M. Mucopolysaccharidosis Type II. in *GeneReviews*® (eds. Adam, M. P. et al.) (University of Washington, Seattle, 1993).
91. Sapadin, A. N. & Friedman, I. S. Extensive Mongolian spots associated with Hunter syndrome. *Journal of the American Academy of Dermatology* **39**, 1013–1015 (1998).
92. Seo, J.-H., Okuyama, T., Shapiro, E., Fukuhara, Y. & Kosuga, M. Natural history of cognitive development in neuronopathic mucopolysaccharidosis type II (Hunter syndrome): Contribution of genotype to cognitive developmental course. *Molecular Genetics and Metabolism Reports* **24**, 100630 (2020).
93. Young, I. D. & Harper, P. S. The Natural History of the Severe Form of Hunter's Syndrome: A Study Based on 52 Cases. *Developmental Medicine & Child Neurology* **25**, 481–489 (1983).
94. Martin, R. *et al.* Recognition and Diagnosis of Mucopolysaccharidosis II (Hunter Syndrome). *Pediatrics* **121**, e377–e386 (2008).
95. Holt, J. B., Poe, M. D. & Escolar, M. L. Natural Progression of Neurological Disease in Mucopolysaccharidosis Type II. *Pediatrics* **127**, e1258–e1265 (2011).
96. Thappa, D. M., Singh, A., Jaisankar, T. J., Rao, R. & Ratnakar, C. Pebbling of the Skin: A Marker of Hunter's Syndrome. *Pediatric Dermatology* **15**, 370–373 (1998).
97. Topping, T. M., Kenyon, K. R., Goldberg, M. F. & Maumenee, A. E. Ultrastructural Ocular Pathology of Hunter's Syndrome: Systemic Mucopolysaccharidosis Type II. *Archives of Ophthalmology* **86**, 164–177 (1971).
98. Muenzer, J. *et al.* Ten years of the Hunter Outcome Survey (HOS): insights, achievements, and lessons learned from a global patient registry. *Orphanet Journal of Rare Diseases* **12**, 82 (2017).
99. Warner, T. F. *et al.* Heparan sulphate proteoglycan in scleromyxedema promotes FGF-2 activity. *Pathol Res Pract* **198**, 701–707 (2002).
100. Link, B. *et al.* Orthopedic manifestations in patients with mucopolysaccharidosis type II (Hunter syndrome) enrolled in the Hunter Outcome Survey. *Orthop Rev (Pavia)* **2**, e16 (2010).
101. Parker, H. & Bigger, B. W. The role of innate immunity in mucopolysaccharide diseases. *J Neurochem* **148**, 639–651 (2019).
102. Braunlin, E. A. *et al.* Cardiac disease in patients with mucopolysaccharidosis: presentation, diagnosis and management. *Journal of Inherited Metabolic Disease* **34**, 1183–1197 (2011).
103. Shapiro, J., Strome, M. & Crocker, A. C. Airway Obstruction and Sleep Apnea in Hurler and Hunter Syndromes. *Ann Otol Rhinol Laryngol* **94**, 458–461 (1985).
104. Orliaguet, O. *et al.* Hunter's syndrome and associated sleep apnoea cured by CPAP and surgery. *European Respiratory Journal* **13**, 1195–1197 (1999).

105. Shapiro, E. G. & Eisengart, J. B. The natural history of neurocognition in MPS disorders: A review. *Molecular Genetics and Metabolism* **133**, 8–34 (2021).
106. Shinomiya, N., Nagayama, T., Fujioka, Y. & Aoki, T. MRI in the mild type of mucopolysaccharidosis II (Hunter's syndrome). *Neuroradiology* **38**, 483–485 (1996).
107. Yund, B. *et al.* Cognitive, medical, and neuroimaging characteristics of attenuated mucopolysaccharidosis type II. *Molecular Genetics and Metabolism* **114**, 170–177 (2015).
108. Bigger, B. W., Begley, D. J., Virgintino, D. & Pshezhetsky, A. V. Anatomical changes and pathophysiology of the brain in mucopolysaccharidosis disorders. *Molecular Genetics and Metabolism* **125**, 322–331 (2018).
109. Yatziv, S. & Epstein, C. J. Hunter syndrome presenting as macrocephaly and hydrocephalus. *J Med Genet* **14**, 445–447 (1977).
110. Parsons, V. J., Hughes, D. G. & Wraith, J. E. Magnetic resonance imaging of the brain, neck and cervical spine in mild Hunter's syndrome (mucopolysaccharidoses type II). *Clin Radiol* **51**, 719–723 (1996).
111. Shapiro, E. G., Escolar, M. L., Delaney, K. A. & Mitchell, J. J. Assessments of neurocognitive and behavioral function in the mucopolysaccharidoses. *Mol Genet Metab* **122S**, 8–16 (2017).
112. Keilmann, A. *et al.* Hearing loss in patients with mucopolysaccharidosis II: Data from HOS – the Hunter Outcome Survey. *Journal of Inherited Metabolic Disease* **35**, 343–353 (2012).
113. Ashworth, J. L., Biswas, S., Wraith, E. & Lloyd, I. C. Mucopolysaccharidoses and the eye. *Surv Ophthalmol* **51**, 1–17 (2006).
114. Tomatsu, S., Pitz, S. & Hampel, U. Ophthalmological Findings in Mucopolysaccharidoses. *J Clin Med* **8**, 1467 (2019).
115. Young, I. D. & Harper, P. S. Mild form of Hunter's syndrome: clinical delineation based on 31 cases. *Arch Dis Child* **57**, 828–836 (1982).
116. Archer, I. M., Kingston, H. M. & Harper, P. S. Prenatal diagnosis of hunter syndrome. *Prenatal Diagnosis* **4**, 195–200 (1984).
117. Keulemans, J. L. M. *et al.* Prenatal diagnosis of the Hunter syndrome and the introduction of a new fluorimetric enzyme assay. *Prenatal Diagnosis* **22**, 1016–1021 (2002).
118. Cooper, A., Thornley, M. & Wraith, J. E. First-trimester diagnosis of hunter syndrome: Very low iduronate sulphatase activity in chorionic villi from a heterozygous female fetus. *Prenatal Diagnosis* **11**, 731–735 (1991).
119. Colville, G. A. & Bax, M. A. Early presentation in the mucopolysaccharide disorders. *Child: Care, Health and Development* **22**, 31–36 (1996).
120. Parini, R., Jones, S. A., Harmatz, P. R., Giugliani, R. & Mendelsohn, N. J. The natural history of growth in patients with Hunter syndrome: Data from the Hunter Outcome Survey (HOS). *Molecular Genetics and Metabolism* **117**, 438–446 (2016).
121. Joseph, R., DiCesare, E. B. & Miller, A. Hunter Syndrome: Is It Time to Make It Part of Newborn Screening? *Advances in Neonatal Care* **18**, 480–487 (2018).
122. Gelb, M. H., Scott, C. R. & Turecek, F. Newborn Screening for Lysosomal Storage Diseases. *Clin Chem* **61**, 335–346 (2015).
123. Bilyeu, H., Washburn, J., Vermette, L. & Klug, T. Validation and Implementation of a Highly Sensitive and Efficient Newborn Screening Assay for Mucopolysaccharidosis Type II. *Int J Neonatal Screen* **6**, 79 (2020).
124. Chan, M.-J. *et al.* Taiwan National Newborn Screening Program by Tandem Mass Spectrometry for Mucopolysaccharidoses Types I, II, and VI. *J Pediatr* **205**, 176–182 (2019).
125. Menkovic, I., Marchand, A.-S., Boutin, M. & Auray-Blais, C. Neonatal Mass Urine Screening Approach for Early Detection of Mucopolysaccharidoses by UPLC-MS/MS. *Diagnostics (Basel)* **9**, 195 (2019).
126. Stapleton, M. *et al.* Newborn screening for mucopolysaccharidoses: Measurement of glycosaminoglycans by LC-MS/MS. *Mol Genet Metab Rep* **22**, 100563 (2020).
127. Millington, D. S. S. & Ficicioglu, C. Addition of MPS-II to the Recommended Uniform Screening Panel in the United States. *International Journal of Neonatal Screening* **8**, 55 (2022).
128. Dean, C. J., Bockmann, M. R., Hopwood, J. J., Brooks, D. A. & Meikle, P. J. Detection of mucopolysaccharidosis type II by measurement of iduronate-2-sulfatase in dried blood spots and plasma samples. *Clin Chem* **52**, 643–649 (2006).

129. Sukegawa-Hayasaka, K. *et al.* Effect of Hunter disease (mucopolysaccharidosis type II) mutations on molecular phenotypes of iduronate-2-sulfatase: Enzymatic activity, protein processing and structural analysis. *Journal of Inherited Metabolic Disease* **29**, 755–761 (2006).
130. Tolun, A. A. *et al.* A novel fluorometric enzyme analysis method for Hunter syndrome using dried blood spots. *Molecular Genetics and Metabolism* **105**, 519–521 (2012).
131. Spacil, Z. *et al.* High-Throughput Assay of 9 Lysosomal Enzymes for Newborn Screening. *Clinical Chemistry* **59**, 502–511 (2013).
132. Whitley, C. B., Ridnour, M. D., Draper, K. A., Dutton, C. M. & Neglia, J. P. Diagnostic test for mucopolysaccharidosis. I. Direct method for quantifying excessive urinary glycosaminoglycan excretion. *Clin Chem* **35**, 374–379 (1989).
133. Whitley, C. B. *et al.* Diagnostic test for mucopolysaccharidosis. II. Rapid quantification of glycosaminoglycan in urine samples collected on a paper matrix. *Clin Chem* **35**, 2074–2081 (1989).
134. Lawrence, R. *et al.* Glycan-based biomarkers for mucopolysaccharidoses. *Mol Genet Metab* **111**, 73–83 (2014).
135. Kubaski, F. *et al.* Glycosaminoglycans detection methods: Applications of mass spectrometry. *Mol Genet Metab* **120**, 67–77 (2017).
136. Zhang, H., Wood, T., Young, S. P. & Millington, D. S. A straightforward, quantitative ultra-performance liquid chromatography-tandem mass spectrometric method for heparan sulfate, dermatan sulfate and chondroitin sulfate in urine: An improved clinical screening test for the mucopolysaccharidoses. *Molecular Genetics and Metabolism* **114**, 123–128 (2015).
137. Filocamo, M., Tomanin, R., Bertola, F. & Morrone, A. Biochemical and molecular analysis in mucopolysaccharidoses: what a paediatrician must know. *Italian Journal of Pediatrics* **44**, 129 (2018).
138. Hendriksz, C. J. *et al.* A Cerebrospinal Fluid Collection Study in Pediatric and Adult Patients With Hunter Syndrome. *Journal of Inborn Errors of Metabolism and Screening* **3**, 2326409815595821 (2015).
139. Jonsson, J. J., Aronovich, E. L., Braun, S. E. & Whitley, C. B. Molecular diagnosis of mucopolysaccharidosis type II (Hunter syndrome) by automated sequencing and computer-assisted interpretation: toward mutation mapping of the iduronate-2-sulfatase gene. *Am J Hum Genet* **56**, 597–607 (1995).
140. Lualdi, S. *et al.* Multiple cryptic splice sites can be activated by IDS point mutations generating misspliced transcripts. *J Mol Med* **84**, 692–700 (2006).
141. Zanetti, A. *et al.* Setup and Validation of a Targeted Next-Generation Sequencing Approach for the Diagnosis of Lysosomal Storage Disorders. *J Mol Diagn* **22**, 488–502 (2020).
142. Fernández-Marmiesse, A. *et al.* Assessment of a targeted resequencing assay as a support tool in the diagnosis of lysosomal storage disorders. *Orphanet Journal of Rare Diseases* **9**, 59 (2014).
143. Lualdi, S. *et al.* Characterization of iduronate-2-sulfatase gene–pseudogene recombinations in eight patients with Mucopolysaccharidosis type II revealed by a rapid PCR-based method. *Human Mutation* **25**, 491–497 (2005).
144. Verma, S. *et al.* A molecular genetics view on Mucopolysaccharidosis Type II. *Mutation Research/Reviews in Mutation Research* **788**, 108392 (2021).
145. Tomatsu, S. *et al.* General implications for CpG hot spot mutations: Methylation patterns of the human iduronate-2-sulfatase gene locus. *Human Mutation* **23**, 590–598 (2004).
146. Timms, K. M. *et al.* 130 kb of DNA sequence reveals two new genes and a regional duplication distal to the human iduronate-2-sulfate sulfatase locus. *Genome Res.* **5**, 71–78 (1995).
147. Holmes, R. S. Comparative studies of vertebrate iduronate 2-sulfatase (IDS) genes and proteins: evolution of A mammalian X-linked gene. *3 Biotech* **7**, 22 (2017).
148. Li, P., Bellows, A. & Thompson, J. Molecular basis of iduronate-2-sulphatase gene mutations in patients with mucopolysaccharidosis type II (Hunter syndrome). *J Med Genet* **36**, 21–27 (1999).
149. Dvorakova, L. *et al.* Genotype-phenotype correlation in 44 Czech, Slovak, Croatian and Serbian patients with mucopolysaccharidosis type II. *Clin Genet* **91**, 787–796 (2017).
150. Froissart, R., Da Silva, I. M. & Maire, I. Mucopolysaccharidosis type II: an update on mutation spectrum. *Acta Paediatr* **96**, 71–77 (2007).
151. Brusius-Facchin, A. C. *et al.* Mucopolysaccharidosis type II: Identification of 30 novel mutations among Latin American patients. *Molecular Genetics and Metabolism* **111**, 133–138 (2014).

152. M, K. *et al.* Molecular diagnosis of 65 families with mucopolysaccharidosis type II (Hunter syndrome) characterized by 16 novel mutations in the IDS gene: Genetic, pathological, and structural studies on iduronate-2-sulfatase. *Molecular genetics and metabolism* **118**, (2016).
153. Semyachkina, A. N., Voskoboeva, E. Y., Nikolaeva, E. A. & Zakharova, E. Y. Analysis of long-term observations of the large group of Russian patients with Hunter syndrome (mucopolysaccharidosis type II). *BMC Medical Genomics* **14**, 71 (2021).
154. Vollebregt, A. A. M. *et al.* Genotype–phenotype relationship in mucopolysaccharidosis II: predictive power of IDS variants for the neuronopathic phenotype. *Developmental Medicine & Child Neurology* **59**, 1063–1070 (2017).
155. Demydchuk, M. *et al.* Insights into Hunter syndrome from the structure of iduronate-2-sulfatase. *Nat Commun* **8**, 15786 (2017).
156. Kang, J.-Y. *et al.* Lysosomal Targeting Enhancement by Conjugation of Glycopeptides Containing Mannose-6-phosphate Glycans Derived from Glyco-engineered Yeast. *Sci Rep* **8**, 8730 (2018).
157. PARKINSON-LAWRENCE, E., TURNER, C., HOPWOOD, J. & BROOKS, D. Analysis of normal and mutant iduronate-2-sulphatase conformation. *Biochemical Journal* **386**, 395–400 (2005).
158. Pomin, V. H. & Mulloy, B. Glycosaminoglycans and Proteoglycans. *Pharmaceuticals (Basel)* **11**, 27 (2018).
159. Sugahara, K. *et al.* Recent advances in the structural biology of chondroitin sulfate and dermatan sulfate. *Current Opinion in Structural Biology* **13**, 612–620 (2003).
160. Rabenstein, D. L. Heparin and heparan sulfate: structure and function. *Nat. Prod. Rep.* **19**, 312–331 (2002).
161. Wei, G. *et al.* Location of the Glucuronosyltransferase Domain in the Heparan Sulfate Copolymerase EXT1 by Analysis of Chinese Hamster Ovary Cell Mutants*. *Journal of Biological Chemistry* **275**, 27733–27740 (2000).
162. McCormick, C., Duncan, G., Goutsos, K. T. & Tufaro, F. The putative tumor suppressors EXT1 and EXT2 form a stable complex that accumulates in the Golgi apparatus and catalyzes the synthesis of heparan sulfate. *Proceedings of the National Academy of Sciences* **97**, 668–673 (2000).
163. Rosenberg, R. D., Shworak, N. W., Liu, J., Schwartz, J. J. & Zhang, L. Heparan sulfate proteoglycans of the cardiovascular system. Specific structures emerge but how is synthesis regulated? *J. Clin. Invest.* **99**, 2062–2070 (1997).
164. Sasisekharan, R. & Venkataraman, G. Heparin and heparan sulfate: biosynthesis, structure and function. *Current Opinion in Chemical Biology* **4**, 626–631 (2000).
165. Rowlands, D., Sugahara, K. & Kwok, J. C. F. Glycosaminoglycans and Glycomimetics in the Central Nervous System. *Molecules* **20**, 3527–3548 (2015).
166. Billings, P. C. & Pacifici, M. Interactions of signaling proteins, growth factors and other proteins with heparan sulfate: Mechanisms and mysteries. *Connect Tissue Res* **56**, 272–280 (2015).
167. Celie, J. W. A. M., Beelen, R. H. J. & van den Born, J. Heparan sulfate proteoglycans in extravasation: assisting leukocyte guidance. *Front Biosci (Landmark Ed)* **14**, 4932–4949 (2009).
168. Tanaka, Y., Adams, D. H. & Shaw, S. Proteoglycans on endothelial cells present adhesion-inducing cytokines to leukocytes. *Immunology Today* **14**, 111–115 (1993).
169. Chen, Y. *et al.* Dengue virus infectivity depends on envelope protein binding to target cell heparan sulfate. *Nat Med* **3**, 866–871 (1997).
170. Nan, H., Park, C. & Maeng, S. Mucopolysaccharidoses I and II: Brief Review of Therapeutic Options and Supportive/Palliative Therapies. *BioMed Research International* **2020**, e2408402 (2020).
171. Trowbridge, J. M. & Gallo, R. L. Dermatan sulfate: new functions from an old glycosaminoglycan. *Glycobiology* **12**, 117R-125R (2002).
172. Ernst, S., Langer, R., Cooney, C. L. & Sasisekharan, R. Enzymatic Degradation of GlycosaminogIycans. *Critical Reviews in Biochemistry and Molecular Biology* **30**, 387–444 (1995).
173. Langereis, E. J. *et al.* Biomarker responses correlate with antibody status in mucopolysaccharidosis type I patients on long-term enzyme replacement therapy. *Molecular Genetics and Metabolism* **114**, 129–137 (2015).
174. Tanaka, N. *et al.* Evaluation of cerebrospinal fluid heparan sulfate as a biomarker of neuropathology in a murine model of mucopolysaccharidosis type II using high-sensitivity LC/MS/MS. *Molecular Genetics and Metabolism* **125**, 53–58 (2018).

175.Węgrzyn, G. *et al.* Why are behaviors of children suffering from various neuronopathic types of mucopolysaccharidoses different? *Medical Hypotheses* **75**, 605–609 (2010).
176. Gallagher, J. T. Multiprotein signalling complexes: regional assembly on heparan sulphate. *Biochemical Society Transactions* **34**, 438–441 (2006).
177. Azambuja, A. S. *et al.* Evidence for inflammasome activation in the brain of mucopolysaccharidosis type II mice. *Metab Brain Dis* (2020) doi:10.1007/s11011-020-00592-5.
178. Lloyd-Evans, E. & Haslett, L. J. The lysosomal storage disease continuum with ageing-related neurodegenerative disease. *Ageing Res Rev* **32**, 104–121 (2016).
179. Maïza, A. *et al.* The role of heparan sulfates in protein aggregation and their potential impact on neurodegeneration. *FEBS Letters* **592**, 3806–3818 (2018).
180. Mah, D. *et al.* The Sulfation Code of Tauopathies: Heparan Sulfate Proteoglycans in the Prion Like Spread of Tau Pathology. *Frontiers in Molecular Biosciences* **8**, (2021).
181. Morimoto, H. *et al.* Clearance of heparan sulfate in the brain prevents neurodegeneration and neurocognitive impairment in MPS II mice. *Molecular Therapy* **29**, 1853–1861 (2021).
182. Resnick, J. M. *et al.* Pathology of the liver in mucopolysaccharidosis: light and electron microscopic assessment before and after bone marrow transplantation. *Bone Marrow Transplant* **10**, 273–280 (1992).
183. Aldenhoven, M., Sakkers, R. J. B., Boelens, J., de Koning, T. J. & Wulffraat, N. M. Musculoskeletal manifestations of lysosomal storage disorders. *Annals of the Rheumatic Diseases* **68**, 1659–1665 (2009).
184. Braunlin, E. *et al.* Contribution of the innate and adaptive immune systems to aortic dilation in murine mucopolysaccharidosis type I. *Molecular Genetics and Metabolism* S1096719222001329 (2022) doi:10.1016/j.ymgme.2022.01.104.
185. Simonaro, C. M. *et al.* Mechanism of Glycosaminoglycan-Mediated Bone and Joint Disease. *Am J Pathol* **172**, 112–122 (2008).
186. MacFarlane, E. G., Haupt, J., Dietz, H. C. & Shore, E. M. TGF-β Family Signaling in Connective Tissue and Skeletal Diseases. *Cold Spring Harb Perspect Biol* **9**, a022269 (2017).
187. Polgreen, L. E. *et al.* Elevated TNF-α is associated with pain and physical disability in mucopolysaccharidosis types I, II, and VI. *Mol Genet Metab* **117**, 427–430 (2016).
188. Constantopoulos, G., Iqbal, K. & Dekaban, A. S. Mucopolysaccharidosis types IH, IS, II, and IIIA: glycosaminoglycans and lipids of isolated brain cells and other fractions from autopsied tissues. *J Neurochem* **34**, 1399–1411 (1980).
189. D'Avanzo, F., Rigon, L., Zanetti, A. & Tomanin, R. Mucopolysaccharidosis Type II: One Hundred Years of Research, Diagnosis, and Treatment. *Int J Mol Sci* **21**, (2020).
190. Muenzer, J. *et al.* Multidisciplinary Management of Hunter Syndrome. *Pediatrics* **124**, e1228–e1239 (2009).
191. Mendelsohn, N. J. *et al.* Importance of surgical history in diagnosing mucopolysaccharidosis type II (Hunter syndrome): Data from the Hunter Outcome Survey. *Genetics in Medicine* **12**, 816–822 (2010).
192. Stapleton, M. *et al.* Presentation and Treatments for Mucopolysaccharidosis Type II (MPS II; Hunter Syndrome). *Expert Opin Orphan Drugs* **5**, 295–307 (2017).
193. Bhattacharya, K., Gibson, S. C. & Pathi, V. L. Mitral Valve Replacement for Mitral Stenosis Secondary to Hunter's Syndrome. *The Annals of Thoracic Surgery* **80**, 1911–1912 (2005).
194. Amartino, H. & Head of Child Neurology Department, Hospital Universitario Austral, Buenos Aires, Argentina. Hunter Syndrome (Mucopolysaccharidosis II) – The Signs and Symptoms a Neurologist Needs to Know. *European Neurological Review* **10**, 90 (2015).
195. Scarpa, M., Lourenço, C. M. & Amartino, H. Epilepsy in mucopolysaccharidosis disorders. *Molecular Genetics and Metabolism* **122**, 55–61 (2017).
196. Peck, S. H., Casal, M. L., Malhotra, N. R., Ficicioglu, C. & Smith, L. J. Pathogenesis and Treatment of Spine Disease in the Mucopolysaccharidoses. *Mol Genet Metab* **118**, 232–243 (2016).
197. Kwon, J.-Y. *et al.* High prevalence of carpal tunnel syndrome in children with mucopolysaccharidosis type II (Hunter syndrome). *American Journal of Medical Genetics Part A* **155**, 1329–1335 (2011).
198. Argenta, A. E. & Davit, A. Carpal Tunnel Syndrome in the Setting of Mucopolysaccharidosis II (Hunter Syndrome). *Plast Reconstr Surg Glob Open* **5**, e1477 (2017).
199. Broomfield, A. *et al.* Ten years of enzyme replacement therapy in paediatric onset mucopolysaccharidosis II in England. *Molecular Genetics and Metabolism* **129**, 98–105 (2020).
200. Brady, R. O. The Sphingolipidoses. *New England Journal of Medicine* **275**, 312–318 (1966).

201. Brady, R. O. *et al.* Replacement Therapy for Inherited Enzyme Deficiency. *New England Journal of Medicine* **289**, 9–14 (1973).
202. Yatziv, S., Statter, M., Abeliuk, P., Meshulam, M. & Russel, A. A therapeutic trial of fresh plasma infusions over a period of 22 months in two siblings with Hunter's syndrome. *Isr J Med Sci* **11**, 802–808 (1975).
203. Knudson, A. G., Ferrante, N. D. & Curtis, J. E. Effect of Leukocyte Transfusion in a Child with Type II Mucopolysaccharidosis. *Proc Natl Acad Sci U S A* **68**, 1738–1741 (1971).
204. Wikman-Jorgensen, P. E. *et al.* Enzyme replacement therapy for the treatment of Hunter disease: A systematic review with narrative synthesis and meta-analysis. *Molecular Genetics and Metabolism* **131**, 206–210 (2020).
205. Chung, Y. K. *et al.* A biochemical and physicochemical comparison of two recombinant enzymes used for enzyme replacement therapies of hunter syndrome. *Glycoconj J* **31**, 309–315 (2014).
206. Muenzer, J. *et al.* Long-term, open-labeled extension study of idursulfase in the treatment of Hunter syndrome. *Genetics in Medicine* **13**, 95–101 (2011).
207. Muenzer, J. *et al.* The role of enzyme replacement therapy in severe Hunter syndrome-an expert panel consensus. *Eur J Pediatr* **171**, 181–188 (2012).
208. Muhlebach, M. S., Wooten, W. & Muenzer, J. Respiratory Manifestations in Mucopolysaccharidoses. *Paediatric Respiratory Reviews* **12**, 133–138 (2011).
209. Tajima, G., Sakura, N., Kosuga, M., Okuyama, T. & Kobayashi, M. Effects of idursulfase enzyme replacement therapy for Mucopolysaccharidosis type II when started in early infancy: Comparison in two siblings. *Molecular Genetics and Metabolism* **108**, 172–177 (2013).
210. Lampe, C. *et al.* Long-term experience with enzyme replacement therapy (ERT) in MPS II patients with a severe phenotype: an international case series. *Journal of Inherited Metabolic Disease* **37**, 823–829 (2014).
211. Parini, R. *et al.* Enzymatic replacement therapy for Hunter disease: Up to 9 years experience with 17 patients. *Molecular Genetics and Metabolism Reports* **3**, 65–74 (2015).
212. Whiteman, D. A. & Kimura, A. Development of idursulfase therapy for mucopolysaccharidosis type II (Hunter syndrome): the past, the present and the future. *DDDT* **11**, 2467–2480 (2017).
213. Sawamoto, K. *et al.* Therapeutic Options for Mucopolysaccharidoses: Current and Emerging Treatments. *Drugs* **79**, 1103–1134 (2019).
214. Afroze, B. & Brown, N. Ethical issues in managing Lysosomal storage disorders in children in low and middle income countries. *Pakistan Journal of Medical Sciences* **33**, 1036 (2017).
215. Bagewadi, S. *et al.* Home treatment with Elaprase® and Naglazyme® is safe in patients with mucopolysaccharidoses types II and VI, respectively. *Journal of Inherited Metabolic Disease* **31**, 733–737 (2008).
216. Bigger, B. W., Saif, M. & Linthorst, G. E. The role of antibodies in enzyme treatments and therapeutic strategies. *Best Practice & Research Clinical Endocrinology & Metabolism* **29**, 183–194 (2015).
217. Giugliani, R. *et al.* Evaluation of impact of anti-idursulfase antibodies during long-term idursulfase enzyme replacement therapy in mucopolysaccharidosis II patients. *Mol Genet Metab Rep* **12**, 2–7 (2017).
218. Muenzer, J. Early initiation of enzyme replacement therapy for the mucopolysaccharidoses. *Molecular Genetics and Metabolism* **111**, 63–72 (2014).
219. Eisengart, J. B. *et al.* Intrathecal enzyme replacement for Hurler syndrome: biomarker association with neurocognitive outcomes. *Genet Med* **21**, 2552–2560 (2019).
220. Bhalla, A. *et al.* Characterization of Fluid Biomarkers Reveals Lysosome Dysfunction and Neurodegeneration in Neuronopathic MPS II Patients. *Int J Mol Sci* **21**, 5188 (2020).
221. Parini, R. & Deodato, F. Intravenous Enzyme Replacement Therapy in Mucopolysaccharidoses: Clinical Effectiveness and Limitations. *Int J Mol Sci* **21**, 2975 (2020).
222. Calias, P. *et al.* CNS Penetration of Intrathecal-Lumbar Idursulfase in the Monkey, Dog and Mouse: Implications for Neurological Outcomes of Lysosomal Storage Disorder. *PLOS ONE* **7**, e30341 (2012).
223. Giugliani, R. *et al.* Intrathecal/Intracerebroventricular enzyme replacement therapy for the mucopolysaccharidoses: efficacy, safety, and prospects. *Expert Opinion on Orphan Drugs* **6**, 403–411 (2018).
224. Muenzer, J. *et al.* Long-term open-label phase I/II extension study of intrathecal idursulfase-IT in the treatment of neuronopathic mucopolysaccharidosis II. *Genet Med* S1098-3600(22)00719–5 (2022) doi:10.1016/j.gim.2022.04.002.

225. Seo, J.-H., Kosuga, M., Hamazaki, T., Shintaku, H. & Okuyama, T. Impact of intracerebroventricular enzyme replacement therapy in patients with neuronopathic mucopolysaccharidosis type II. *Mol Ther Methods Clin Dev* **21**, 67–75 (2021).
226. Muenzer, J. *et al.* A phase I/II study of intrathecal idursulfase-IT in children with severe mucopolysaccharidosis II. *Genetics in Medicine* **18**, 73–81 (2016).
227.Sato, Y. *et al.* Drug delivery for neuronopathic lysosomal storage diseases: evolving roles of the blood brain barrier and cerebrospinal fluid. *Metab Brain Dis* **37**, 1745–1756 (2022).
228. Sonoda, H. *et al.* A Blood-Brain-Barrier-Penetrating Anti-human Transferrin Receptor Antibody Fusion Protein for Neuronopathic Mucopolysaccharidosis II. *Mol Ther* **26**, 1366–1374 (2018).
229. Okuyama, T. *et al.* Iduronate-2-Sulfatase with Anti-human Transferrin Receptor Antibody for Neuropathic Mucopolysaccharidosis II: A Phase 1/2 Trial. *Mol Ther* **27**, 456–464 (2019).
230. Okuyama, T. *et al.* A Phase 2/3 Trial of Pabinafusp Alfa, IDS Fused with Anti-Human Transferrin Receptor Antibody, Targeting Neurodegeneration in MPS-II. *Mol Ther* **29**, 671–679 (2021).
231. Giugliani, R. *et al.* Enzyme Replacement Therapy with Pabinafusp Alfa for Neuronopathic Mucopolysaccharidosis II: An Integrated Analysis of Preclinical and Clinical Data. *Int J Mol Sci* **22**, 10938 (2021).
232. Boado, R. J., Hui, E. K.-W., Lu, J. Z., Sumbria, R. K. & Pardridge, W. M. Blood-Brain Barrier Molecular Trojan Horse Enables Imaging of Brain Uptake of Radioiodinated Recombinant Protein in the Rhesus Monkey. *Bioconjugate Chem.* **24**, 1741–1749 (2013).
233. Boado, R. J., Ka-Wai Hui, E., Zhiqiang Lu, J. & Pardridge, W. M. Insulin receptor antibody-iduronate 2-sulfatase fusion protein: Pharmacokinetics, anti-drug antibody, and safety pharmacology in Rhesus monkeys. *Biotechnology and Bioengineering* **111**, 2317–2325 (2014).
234. Rigon, L. *et al.* Targeting Brain Disease in MPSII: Preclinical Evaluation of IDS-Loaded PLGA Nanoparticles. *Int J Mol Sci* **20**, (2019).
235. Dean, M. F. *et al.* Enzyme replacement therapy by fibroblast transplantation: long-term biochemical study in three cases of Hunter's syndrome. *J Clin Invest* **63**, 138–146 (1979).
236. Friso, A. *et al.* Reduction of GAG storage in MPS II mouse model following implantation of encapsulated recombinant myoblasts. *The Journal of Gene Medicine* **7**, 1482–1491 (2005).
237. Muenzer, J. *et al.* Attempted enzyme replacement using human amnion membane implantations in mucopolysaccharidoses. *Journal of Inherited Metabolic Disease* **15**, 25–37 (1992).
238. Barth, A. L. & Horovitz, D. D. G. Hematopoietic Stem Cell Transplantation in Mucopolysaccharidosis Type II: A Literature Review and Critical Analysis. *Journal of Inborn Errors of Metabolism and Screening* **6**, 2326409818779097 (2018).
239. Araya, K. *et al.* Localized donor cells in brain of a Hunter disease patient after cord blood stem cell transplantation. *Molecular Genetics and Metabolism* **98**, 255–263 (2009).
240. Bhatia, S. Long-term health impacts of hematopoietic stem cell transplantation inform recommendations for follow-up. *Expert Rev Hematol* **4**, 437–454 (2011).
241. Kurtzberg, J. Early HSCT corrects the skeleton in MPS. *Blood* **125**, 1518–1519 (2015).
242. Wang, J. *et al.* Allogeneic Hematopoietic Stem Cell Transplantation in Thirty-Four Pediatric Cases of Mucopolysaccharidosis—A Ten-Year Report from the China Children Transplant Group. *Biology of Blood and Marrow Transplantation* **22**, 2104–2108 (2016).
243. Warkentin, P. I., Dixon, M. S., Schafer, I., Strandjord, S. E. & Coccia, P. F. Bone marrow transplantation in Hunter syndrome: a preliminary report. *Birth Defects Orig Artic Ser* **22**, 31–39 (1986).
244. Vellodi, A. *et al.* Long-term follow-up following bone marrow transplantation for Hunter disease. *Journal of Inherited Metabolic Disease* **22**, 638–648 (1999).
245. Guffon, N., Bertrand, Y., Forest, I., Fouilhoux, A. & Froissart, R. Bone Marrow Transplantation in Children with Hunter Syndrome: Outcome after 7 to 17 Years. *The Journal of Pediatrics* **154**, 733–737 (2009).
246. Barth, A. L. *et al.* Early hematopoietic stem cell transplantation in a patient with severe mucopolysaccharidosis II: A 7years follow-up. *Molecular Genetics and Metabolism Reports* **12**, 62–68 (2017).
247. Suzuki, Y. *et al.* Assessment of Activity of Daily Life in Mucopolysaccharidosis Type II Patients with Hematopoietic Stem Cell Transplantation. *Diagnostics (Basel)* **10**, 46 (2020).
248. Patel, P. *et al.* Impact of enzyme replacement therapy and hematopoietic stem cell therapy on growth in patients with Hunter syndrome. *Molecular Genetics and Metabolism Reports* **1**, 184–196 (2014).

249. Prasad, V. K. & Kurtzberg, J. Transplant Outcomes in Mucopolysaccharidoses. *Seminars in Hematology* **47**, 59–69 (2010).
250. Tanaka, A. *et al.* Long-term efficacy of hematopoietic stem cell transplantation on brain involvement in patients with mucopolysaccharidosis type II: A nationwide survey in Japan. *Molecular Genetics and Metabolism* **107**, 513–520 (2012).
251. Selvanathan, A. *et al.* Effectiveness of Early Hematopoietic Stem Cell Transplantation in Preventing Neurocognitive Decline in Mucopolysaccharidosis Type II: A Case Series. *JIMD Rep* **41**, 81–89 (2018).
252. Imaizumi, M. *et al.* Long-term effects of bone marrow transplantation for inborn errors of metabolism: a study of four patients with lysosomal storage diseases. *Acta Paediatr Jpn* **36**, 30–36 (1994).
253. McKinnis, E. J. R., Sulzbacher, S., Rutledge, J. C., Sanders, J. & Scott, C. R. Bone marrow transplantation in Hunter syndrome. *The Journal of Pediatrics* **129**, 145–148 (1996).
254. Kubaski, F. *et al.* Hematopoietic Stem Cell Transplantation for Patients with Mucopolysaccharidosis II. *Biology of Blood and Marrow Transplantation* **23**, 1795–1803 (2017).
255. Tolar, J. *et al.* Combination of enzyme replacement and hematopoietic stem cell transplantation as therapy for Hurler syndrome. *Bone Marrow Transplant* **41**, 531–535 (2008).
256. Coutinho, M. F., Santos, J. I. & Alves, S. Less Is More: Substrate Reduction Therapy for Lysosomal Storage Disorders. *International Journal of Molecular Sciences* **17**, 1065 (2016).
257. Piotrowska, E. *et al.* Genistein-mediated inhibition of glycosaminoglycan synthesis as a basis for gene expression-targeted isoflavone therapy for mucopolysaccharidoses. *Eur J Hum Genet* **14**, 846–852 (2006).
258. Jakóbkiewicz-Banecka, J., Piotrowska, E., Narajczyk, M., Barańska, S. & Węgrzyn, G. Genistein-mediated inhibition of glycosaminoglycan synthesis, which corrects storage in cells of patients suffering from mucopolysaccharidoses, acts by influencing an epidermal growth factor-dependent pathway. *Journal of Biomedical Science* **16**, 26 (2009).
259. Moskot, M. *et al.* Cell cycle is disturbed in mucopolysaccharidosis type II fibroblasts, and can be improved by genistein. *Gene* **585**, 100–103 (2016).
260. Friso, A., Tomanin, R., Salvalaio, M. & Scarpa, M. Genistein reduces glycosaminoglycan levels in a mouse model of mucopolysaccharidosis type II. *British Journal of Pharmacology* **159**, 1082–1091 (2010).
261. Marucha, J. *et al.* Improvement in the range of joint motion in seven patients with mucopolysaccharidosis type II during experimental gene expression-targeted isoflavone therapy (GET IT). *American Journal of Medical Genetics Part A* **155**, 2257–2262 (2011).
262. de Ruijter, J. *et al.* Genistein in Sanfilippo disease: A randomized controlled crossover trial. *Annals of Neurology* **71**, 110–120 (2012).
263. Entchev, E. *et al.* Odiparcil, a potential glycosaminoglycans clearance therapy in mucopolysaccharidosis VI—Evidence from in vitro and in vivo models. *PLoS One* **15**, e0233032 (2020).
264. Osaki, Y. *et al.* Shutdown of ER-associated degradation pathway rescues functions of mutant iduronate 2-sulfatase linked to mucopolysaccharidosis type II. *Cell Death Dis* **9**, 1–14 (2018).
265. Losada Díaz, J. C., Cepeda del Castillo, J., Rodriguez-López, E. A. & Alméciga-Díaz, C. J. Advances in the Development of Pharmacological Chaperones for the Mucopolysaccharidoses. *International Journal of Molecular Sciences* **21**, 232 (2020).
266. Hoshina, H. *et al.* Chaperone effect of sulfated disaccharide from heparin on mutant iduronate-2-sulfatase in mucopolysaccharidosis type II. *Molecular Genetics and Metabolism* **123**, 118–122 (2018).
267. Clarke, L. A. Pathogenesis of skeletal and connective tissue involvement in the mucopolysaccharidoses: glycosaminoglycan storage is merely the instigator. *Rheumatology* **50**, v13–v18 (2011).
268. Simonaro, C. M. *et al.* Pentosan Polysulfate: Oral Versus Subcutaneous Injection in Mucopolysaccharidosis Type I Dogs. *PLoS One* **11**, e0153136 (2016).
269. Kennedy, D. W. & Abkowitz, J. L. Kinetics of Central Nervous System Microglial and Macrophage Engraftment: Analysis Using a Transgenic Bone Marrow Transplantation Model. *Blood* **90**, 986–993 (1997).
270. Kurtzberg, J. *et al.* Preclinical characterization of DUOC-01, a cell therapy product derived from banked umbilical cord blood for use as an adjuvant to umbilical cord blood transplantation for treatment of inherited metabolic diseases. *Cytotherapy* **17**, 803–815 (2015).
271. Saha, A. *et al.* A cord blood monocyte–derived cell therapy product accelerates brain remyelination. *JCI Insight* **1**, e86667.

272. Giugliani, R. *et al.* Emerging drugs for the treatment of mucopolysaccharidoses. *Expert Opinion on Emerging Drugs* **21**, 9–26 (2016).
273. Tietz, D. *et al.* SIG-018: Novel encapsulated non-viral cell-based therapy for MPS II. *Molecular Genetics and Metabolism* **132**, S106 (2021).
274. Danes, B. S. & Bearn, A. G. Hurler's Syndrome: Demonstration of an Inherited Disorder of Connective Tissue in Cell Culture. *Science* **149**, 987–989 (1965).
275. Danes, B. S. & Bearn, A. G. HURLER'S SYNDROME : A GENETIC STUDY IN CELL CULTURE. *Journal of Experimental Medicine* **123**, 1–16 (1966).
276. Mazzoccoli, G. *et al.* Circadian transcriptome analysis in human fibroblasts from Hunter syndrome and impact of iduronate-2-sulfatase treatment. *BMC Med Genomics* **6**, 37 (2013).
277. Fusar Poli, E. *et al.* Murine neural stem cells model Hunter disease in vitro: glial cell-mediated neurodegeneration as a possible mechanism involved. *Cell Death Dis* **4**, e906 (2013).
278. Zalfa, C. *et al.* Glial degeneration with oxidative damage drives neuronal demise in MPSII disease. *Cell Death Dis* **7**, e2331 (2016).
279. Takahashi, K. & Yamanaka, S. Induction of Pluripotent Stem Cells from Mouse Embryonic and Adult Fibroblast Cultures by Defined Factors. *Cell* **126**, 663–676 (2006).
280. Varga, E. *et al.* Generation of human induced pluripotent stem cell (iPSC) line from an unaffected female carrier of Mucopolysaccharidosis type II (MPS II) disorder. *Stem Cell Research* **17**, 514–516 (2016).
281. Varga, E. *et al.* Generation of Mucopolysaccharidosis type II (MPS II) human induced pluripotent stem cell (iPSC) line from a 1-year-old male with pathogenic IDS mutation. *Stem Cell Research* **17**, 482–484 (2016).
282. Varga, E. *et al.* Generation of Mucopolysaccharidosis type II (MPS II) human induced pluripotent stem cell (iPSC) line from a 3-year-old male with pathogenic IDS mutation. *Stem Cell Research* **17**, 479–481 (2016).
283. Varga, E. *et al.* Generation of Mucopolysaccharidosis type II (MPS II) human induced pluripotent stem cell (iPSC) line from a 7-year-old male with pathogenic IDS mutation. *Stem Cell Research* **17**, 463–465 (2016).
284. Kobolák, J. *et al.* Modelling the neuropathology of lysosomal storage disorders through disease-specific human induced pluripotent stem cells. *Experimental Cell Research* **380**, 216–233 (2019).
285. Rybová, J., Ledvinová, J., Sikora, J., Kuchař, L. & Dobrovolný, R. Neural cells generated from human induced pluripotent stem cells as a model of CNS involvement in mucopolysaccharidosis type II. *Journal of Inherited Metabolic Disease* **41**, 221–229 (2018).
286. Hong, J. *et al.* iPS-derived neural stem cells for disease modeling and evaluation of therapeutics for mucopolysaccharidosis type II. *Experimental Cell Research* **412**, 113007 (2022).
287. Wilkerson, M. J., Lewis, D. C., Marks, S. L. & Prieur, D. J. Clinical and Morphologic Features of Mucopolysaccharidosis Type II in a Dog: Naturally Occurring Model of Hunter Syndrome. *Vet Pathol* **35**, 230–233 (1998).
288. Moro, E. *et al.* A novel functional role of iduronate-2-sulfatase in zebrafish early development. *Matrix Biology* **29**, 43–50 (2010).
289. Costa, R. *et al.* Perturbations in cell signaling elicit early cardiac defects in mucopolysaccharidosis type II. *Human Molecular Genetics* **26**, 1643–1655 (2017).
290. Bellesso, S. *et al.* FGF signaling deregulation is associated with early developmental skeletal defects in animal models for mucopolysaccharidosis type II (MPSII). *Human Molecular Genetics* **27**, 2262–2275 (2018).
291. Lin, C.-Y. *et al.* Effect of Mutated ids Overexpression on IDS Enzyme Activity and Developmental Phenotypes in Zebrafish Embryos: A Valuable Index for Assessing Critical Point-Mutations Associated with Mucopolysaccharidosis Type II Occurrence in Humans. *Diagnostics (Basel)* **10**, (2020).
292. Rigon, L., Kucharowski, N., Eckardt, F. & Bauer, R. Modeling Mucopolysaccharidosis Type II in the Fruit Fly by Using the RNA Interference Approach. *Life (Basel)* **10**, (2020).
293. Muenzer, J. *et al.* Enzyme replacement therapy in mucopolysaccharidosis type II (Hunter syndrome): a preliminary report. *Acta Paediatr Suppl* **91**, 98–99 (2002).
294. Garcia, A. R., Pan, J., Lamsa, J. C. & Muenzer, J. The characterization of a murine model of mucopolysaccharidosis II (Hunter syndrome). *Journal of Inherited Metabolic Disease* **30**, 924–934 (2007).

295. Cardone, M. *et al.* Correction of Hunter syndrome in the MPSII mouse model by AAV2/8-mediated gene delivery. *Hum Mol Genet* **15**, 1225–1236 (2006).
296. Jung, S.-C. *et al.* Characterization of a novel mucopolysaccharidosis type II mouse model and recombinant AAV2/8 vector-mediated gene therapy. *Mol Cells* **30**, 13–18 (2010).
297. Hong, S. H. *et al.* Auditory characteristics and therapeutic effects of enzyme replacement in mouse model of the mucopolysaccharidosis (MPS) II. *American Journal of Medical Genetics Part A* **158A**, 2131–2138 (2012).
298. Maeda, M. *et al.* Autophagy in the Central Nervous System and Effects of Chloroquine in Mucopolysaccharidosis Type II Mice. *International Journal of Molecular Sciences* **20**, 5829 (2019).
299. Higuchi, T. *et al.* Enzyme replacement therapy (ERT) procedure for mucopolysaccharidosis type II (MPS II) by intraventricular administration (IVA) in murine MPS II. *Molecular Genetics and Metabolism* **107**, 122–128 (2012).
300. Motas, S. *et al.* CNS-directed gene therapy for the treatment of neurologic and somatic mucopolysaccharidosis type II (Hunter syndrome). *JCI Insight* **1**, e86696 (2016).
301. Shimada, Y. *et al.* A novel preclinical model of mucopolysaccharidosis type II for developing human hematopoietic stem cell gene therapy. *Gene Ther* 1–9 (2022) doi:10.1038/s41434-022-00357-y.
302. Thierry-Mieg, D. & Thierry-Mieg, J. AceView: a comprehensive cDNA-supported gene and transcripts annotation. *Genome Biol* **7**, S12 (2006).
303. Salvalaio, M. *et al.* Brain RNA-Seq Profiling of the Mucopolysaccharidosis Type II Mouse Model. *Int J Mol Sci* **18**, (2017).
304. Gleitz, H. F. E., O'Leary, C., Holley, R. J. & Bigger, B. W. Identification of age-dependent motor and neuropsychological behavioural abnormalities in a mouse model of Mucopolysaccharidosis Type II. *PLoS One* **12**, (2017).
305. Garcia, A. R., DaCosta, J. M., Pan, J., Muenzer, J. & Lamsa, J. C. Preclinical dose ranging studies for enzyme replacement therapy with idursulfase in a knock-out mouse model of MPS II. *Molecular Genetics and Metabolism* **91**, 183–190 (2007).
306. Akiyama, K. *et al.* Enzyme augmentation therapy enhances the therapeutic efficacy of bone marrow transplantation in mucopolysaccharidosis type II mice. *Molecular Genetics and Metabolism* **111**, 139–146 (2014).
307. Yokoi, K. *et al.* Effect of donor chimerism to reduce the level of glycosaminoglycans following bone marrow transplantation in a murine model of mucopolysaccharidosis type II. *Journal of Inherited Metabolic Disease* **38**, 333–340 (2015).
308. Yokoi, T. *et al.* Non-myeloablative preconditioning with ACK2 (anti-c-kit antibody) is efficient in bone marrow transplantation for murine models of mucopolysaccharidosis type II. *Molecular Genetics and Metabolism* **119**, 232–238 (2016).
309. Capotondo, A. *et al.* Intracerebroventricular delivery of hematopoietic progenitors results in rapid and robust engraftment of microglia-like cells. *Sci Adv* **3**, (2017).
310. Wakabayashi, T. *et al.* Hematopoietic Stem Cell Gene Therapy Corrects Neuropathic Phenotype in Murine Model of Mucopolysaccharidosis Type II. *Human Gene Therapy* **26**, 357–366 (2015).
311. Gleitz, H. F. *et al.* Brain-targeted stem cell gene therapy corrects mucopolysaccharidosis type II via multiple mechanisms. *EMBO Molecular Medicine* **10**, e8730 (2018).
312. Miwa, S. *et al.* Efficient engraftment of genetically modified cells is necessary to ameliorate central nervous system involvement of murine model of mucopolysaccharidosis type II by hematopoietic stem cell targeted gene therapy. *Molecular Genetics and Metabolism* **130**, 262–273 (2020).
313. Wada, M. *et al.* Ex Vivo Gene Therapy Treats Bone Complications of Mucopolysaccharidosis Type II Mouse Models through Bone Remodeling Reactivation. *Molecular Therapy - Methods & Clinical Development* **19**, 261–274 (2020).
314. Polito, V. A. & Cosma, M. P. IDS Crossing of the Blood-Brain Barrier Corrects CNS Defects in MPSII Mice. *Am J Hum Genet* **85**, 296–301 (2009).
315. Hinderer, C. *et al.* Delivery of an Adeno-Associated Virus Vector into Cerebrospinal Fluid Attenuates Central Nervous System Disease in Mucopolysaccharidosis Type II Mice. *Human Gene Therapy* **27**, 906–915 (2016).
316. Laoharawee, K. *et al.* Prevention of Neurocognitive Deficiency in Mucopolysaccharidosis Type II Mice by Central Nervous System–Directed, AAV9-Mediated Iduronate Sulfatase Gene Transfer. *Human Gene Therapy* **28**, 626–638 (2017).

317. Fu, H. *et al.* Targeting Root Cause by Systemic scAAV9-hIDS Gene Delivery: Functional Correction and Reversal of Severe MPS II in Mice. *Molecular Therapy - Methods & Clinical Development* **10**, 327–340 (2018).
318. Laoharawee, K. *et al.* Dose-Dependent Prevention of Metabolic and Neurologic Disease in Murine MPS II by ZFN-Mediated In Vivo Genome Editing. *Molecular Therapy* **26**, 1127–1136 (2018).
319. Casamassa, A. *et al.* Generation of an induced pluripotent stem cells line, CSSi014-A 9407, carrying the variant c.479C>T in the human iduronate 2-sulfatase (hIDS) gene. *Stem Cell Res* **63**, 102846 (2022).
320. Dunbar, C. E. *et al.* Gene therapy comes of age. *Science* **359**, eaan4672 (2018).
321. Bulcha, J. T., Wang, Y., Ma, H., Tai, P. W. L. & Gao, G. Viral vector platforms within the gene therapy landscape. *Sig Transduct Target Ther* **6**, 1–24 (2021).
322. Foldvari, M. *et al.* Non-viral gene therapy: Gains and challenges of non-invasive administration methods. *Journal of Controlled Release* **240**, 165–190 (2016).
323. Zapolnik, P. & Pyrkosz, A. Gene Therapy for Mucopolysaccharidosis Type II—A Review of the Current Possibilities. *International Journal of Molecular Sciences* **22**, 5490 (2021).
324. Taha, E. A., Lee, J. & Hotta, A. Delivery of CRISPR-Cas tools for in vivo genome editing therapy: Trends and challenges. *Journal of Controlled Release* **342**, 345–361 (2022).
325. Glass, Z., Lee, M., Li, Y. & Xu, Q. Engineering the Delivery System for CRISPR-Based Genome Editing. *Trends Biotechnol* **36**, 173–185 (2018).
326. Banskota, S. *et al.* Engineered virus-like particles for efficient in vivo delivery of therapeutic proteins. *Cell* **185**, 250-265.e16 (2022).
327. Ramamoorth, M. & Narvekar, A. Non Viral Vectors in Gene Therapy- An Overview. *J Clin Diagn Res* **9**, GE01–GE06 (2015).
328. Ghosh, S., Brown, A. M., Jenkins, C. & Campbell, K. Viral Vector Systems for Gene Therapy: A Comprehensive Literature Review of Progress and Biosafety Challenges. *Applied Biosafety* **25**, 7–18 (2020).
329. Sands, M. S. & Davidson, B. L. Gene therapy for lysosomal storage diseases. *Molecular Therapy* **13**, 839–849 (2006).
330. Sawamoto, K., Chen, H.-H., Alméciga-Díaz, C. J., Mason, R. W. & Tomatsu, S. Gene therapy for Mucopolysaccharidoses. *Mol Genet Metab* **123**, 59–68 (2018).
331. Fraldi, A. *et al.* Gene therapy for mucopolysaccharidoses: in vivo and ex vivo approaches. *Italian Journal of Pediatrics* **44**, 130 (2018).
332. Milone, M. C. & O'Doherty, U. Clinical use of lentiviral vectors. *Leukemia* **32**, 1529–1541 (2018).
333. Retroviridae. in *Virus Taxonomy* 477–495 (Elsevier, 2012). doi:10.1016/B978-0-12-384684-6.00044-6.
334. Petropoulos, C. *Retroviral Taxonomy, Protein Structures, Sequences, and Genetic Maps*. *Retroviruses* (Cold Spring Harbor Laboratory Press, 1997).
335. *Retroviruses*. Coffin JM, Hughes SH, Varmus HE, editors. Retroviruses. Cold Spring Harbor (NY): Cold Spring Harbor Laboratory Press; 1997. Available from: https://www.ncbi.nlm.nih.gov/books/NBK19376/
336. Anson, D. S. The use of retroviral vectors for gene therapy-what are the risks? A review of retroviral pathogenesis and its relevance to retroviral vector-mediated gene delivery. *Genet Vaccines Ther* **2**, 9 (2004).
337. Vargas, J. E. *et al.* Retroviral vectors and transposons for stable gene therapy: advances, current challenges and perspectives. *Journal of Translational Medicine* **14**, 288 (2016).
338. Elis, E., Ehrlich, M. & Bacharach, E. Dynamics and restriction of murine leukemia virus cores in mitotic and interphase cells. *Retrovirology* **12**, 95 (2015).
339. Dull, T. *et al.* A Third-Generation Lentivirus Vector with a Conditional Packaging System. *J Virol* **72**, 8463–8471 (1998).
340. Naldini, L. *et al.* In Vivo Gene Delivery and Stable Transduction of Nondividing Cells by a Lentiviral Vector. *Science* **272**, 263–267 (1996).
341. Zufferey, R., Nagy, D., Mandel, R. J., Naldini, L. & Trono, D. Multiply attenuated lentiviral vector achieves efficient gene delivery in vivo. *Nat Biotechnol* **15**, 871–875 (1997).
342. Zufferey, R. *et al.* Self-Inactivating Lentivirus Vector for Safe and Efficient In Vivo Gene Delivery. *J Virol* **72**, 9873–9880 (1998).

343. Merten, O.-W., Hebben, M. & Bovolenta, C. Production of lentiviral vectors. *Mol Ther Methods Clin Dev* **3**, 16017 (2016).
344. Nikolic, J. *et al.* Structural basis for the recognition of LDL-receptor family members by VSV glycoprotein. *Nat Commun* **9**, 1029 (2018).
345. Braun, S. E. *et al.* Metabolic correction and cross-correction of mucopolysaccharidosis type II (Hunter syndrome) by retroviral-mediated gene transfer and expression of human iduronate-2-sulfatase. *Proc Natl Acad Sci U S A* **90**, 11830–11834 (1993).
346. Braun, S. E. *et al.* Preclinical Studies of Lymphocyte Gene Therapy for Mild Hunter Syndrome (Mucopolysaccharidosis Type II). *Human Gene Therapy* **7**, 283–290 (1996).
347. Hong, Y. *et al.* Construction of a high efficiency retroviral vector for gene therapy of Hunter's syndrome. *The Journal of Gene Medicine* **5**, 18–29 (2003).
348. Horgan, C., Jones, S. A., Bigger, B. W. & Wynn, R. Current and Future Treatment of Mucopolysaccharidosis (MPS) Type II: Is Brain-Targeted Stem Cell Gene Therapy the Solution for This Devastating Disorder? *International Journal of Molecular Sciences* **23**, 4854 (2022).
349. Aiuti, A. *et al.* The Committee for Advanced Therapies' of the European Medicines Agency Reflection Paper on Management of Clinical Risks Deriving from Insertional Mutagenesis. *Human Gene Therapy Clinical Development* **24**, 47–54 (2013).
350. McCormack, M. P., Forster, A., Drynan, L., Pannell, R. & Rabbitts, T. H. The LMO2 T-Cell Oncogene Is Activated via Chromosomal Translocations or Retroviral Insertion during Gene Therapy but Has No Mandatory Role in Normal T-Cell Development. *Mol Cell Biol* **23**, 9003–9013 (2003).
351. McCormack, M. P. & Rabbitts, T. H. Activation of the T-Cell Oncogene LMO2 after Gene Therapy for X-Linked Severe Combined Immunodeficiency. *New England Journal of Medicine* **350**, 913–922 (2004).
352. Cavazzana-Calvo, M. *et al.* Transfusion independence and HMGA2 activation after gene therapy of human β-thalassaemia. *Nature* **467**, 318–322 (2010).
353. Stein, S. *et al.* Genomic instability and myelodysplasia with monosomy 7 consequent to EVI1 activation after gene therapy for chronic granulomatous disease. *Nat Med* **16**, 198–204 (2010).
354. Aiuti, A. *et al.* Lentivirus-based Gene Therapy of Hematopoietic Stem Cells in Wiskott-Aldrich Syndrome. *Science* **341**, 1233151 (2013).
355. Hsieh, M. M. *et al.* Myelodysplastic syndrome unrelated to lentiviral vector in a patient treated with gene therapy for sickle cell disease. *Blood Adv* **4**, 2058–2063 (2020).
356. Tomanin, R. *et al.* Non-viral transfer approaches for the gene therapy of mucopolysaccharidosis type II (Hunter syndrome). *Acta Paediatrica* **91**, 100–104 (2002).
357. Friso, A. *et al.* Gene therapy of Hunter syndrome: Evaluation of the efficiency of muscle electro gene transfer for the production and release of recombinant iduronate-2-sulfatase (IDS). *Biochimica et Biophysica Acta (BBA) - Molecular Basis of Disease* **1782**, 574–580 (2008).
358. Parvoviridae. in *Virus Taxonomy* 405–425 (Elsevier, 2012). doi:10.1016/B978-0-12-384684-6.00039-2.
359. Weitzman, M. D. & Linden, R. M. Adeno-Associated Virus Biology. in *Adeno-Associated Virus: Methods and Protocols* (eds. Snyder, R. O. & Moullier, P.) 1–23 (Humana Press, 2011). doi:10.1007/978-1-61779-370-7_1.
360. Naso, M. F., Tomkowicz, B., Perry, W. L. & Strohl, W. R. Adeno-Associated Virus (AAV) as a Vector for Gene Therapy. *BioDrugs* **31**, 317–334 (2017).
361. Li, C. & Samulski, R. J. Engineering adeno-associated virus vectors for gene therapy. *Nature Reviews Genetics* 1–18 (2020) doi:10.1038/s41576-019-0205-4.
362. Hastie, E. & Samulski, R. J. Adeno-Associated Virus at 50: A Golden Anniversary of Discovery, Research, and Gene Therapy Success—A Personal Perspective. *Hum Gene Ther* **26**, 257–265 (2015).
363. Gao, G.-P. *et al.* Novel adeno-associated viruses from rhesus monkeys as vectors for human gene therapy. *Proc Natl Acad Sci U S A* **99**, 11854–11859 (2002).
364. Gao, G. *et al.* Purification of Recombinant Adeno-Associated Virus Vectors by Column Chromatography and Its Performance in Vivo. *Human Gene Therapy* **11**, 2079–2091 (2000).
365. Schuster, D. J. *et al.* Biodistribution of adeno-associated virus serotype 9 (AAV9) vector after intrathecal and intravenous delivery in mouse. *Front Neuroanat* **8**, (2014).
366. Gray, S. J. *et al.* Preclinical Differences of Intravascular AAV9 Delivery to Neurons and Glia: A Comparative Study of Adult Mice and Nonhuman Primates. *Mol Ther* **19**, 1058–1069 (2011).

367. Duque, S. *et al.* Intravenous Administration of Self-complementary AAV9 Enables Transgene Delivery to Adult Motor Neurons. *Molecular Therapy* **17**, 1187–1196 (2009).
368. Weismann, C. M. *et al.* Systemic AAV9 gene transfer in adult GM1 gangliosidosis mice reduces lysosomal storage in CNS and extends lifespan. *Hum. Mol. Genet.* **24**, 4353–4364 (2015).
369. Hinderer, C. *et al.* Evaluation of Intrathecal Routes of Administration for Adeno-Associated Viral Vectors in Large Animals. *Hum Gene Ther* **29**, 15–24 (2018).
370. Bey, K. *et al.* Intra-CSF AAV9 and AAVrh10 Administration in Nonhuman Primates: Promising Routes and Vectors for Which Neurological Diseases? *Molecular Therapy - Methods & Clinical Development* **17**, 771–784 (2020).
371. Vassalli, G., Büeler, H., Dudler, J., von Segesser, L. K. & Kappenberger, L. Adeno-associated virus (AAV) vectors achieve prolonged transgene expression in mouse myocardium and arteries in vivo: a comparative study with adenovirus vectors. *Int J Cardiol* **90**, 229–238 (2003).
372. Nguyen, G. N. *et al.* A long-term study of AAV gene therapy in dogs with hemophilia A identifies clonal expansions of transduced liver cells. *Nat Biotechnol* **39**, 47–55 (2021).
373. George, L. A. *et al.* Multiyear Factor VIII Expression after AAV Gene Transfer for Hemophilia A. *New England Journal of Medicine* **385**, 1961–1973 (2021).
374. Berns, K. I. & Muzyczka, N. AAV: An Overview of Unanswered Questions. *Hum Gene Ther* **28**, 308–313 (2017).
375. Mingozzi, F. & High, K. A. Immune responses to AAV vectors: overcoming barriers to successful gene therapy. *Blood* **122**, 23–36 (2013).
376. Au, H. K. E., Isalan, M. & Mielcarek, M. Gene Therapy Advances: A Meta-Analysis of AAV Usage in Clinical Settings. *Front Med (Lausanne)* **8**, 809118 (2022).
377. Suzuki, M. *et al.* Differential Type I Interferon-dependent Transgene Silencing of Helper-dependent Adenoviral vs. Adeno-associated Viral Vectors In Vivo. *Mol Ther* **21**, 796–805 (2013).
378. Murphy, S. L., Li, H., Zhou, S., Schlachterman, A. & High, K. Prolonged Susceptibility to Antibody-mediated Neutralization for Adeno-associated Vectors Targeted to the Liver. *Molecular Therapy* **16**, 138–145 (2008).
379. Jiang, H. *et al.* Effects of transient immunosuppression on adenoassociated, virus-mediated, liver-directed gene transfer in rhesus macaques and implications for human gene therapy. *Blood* **108**, 3321–3328 (2006).
380. Manno, C. S. *et al.* Successful transduction of liver in hemophilia by AAV-Factor IX and limitations imposed by the host immune response. *Nat Med* **12**, 342–347 (2006).
381. Fraldi, A. *et al.* SUMF1 enhances sulfatase activities in vivo in five sulfatase deficiencies. *Biochem J* **403**, 305–312 (2007).
382. Fraldi, A. *et al.* Functional correction of CNS lesions in an MPS-IIIA mouse model by intracerebral AAV-mediated delivery of sulfamidase and SUMF1 genes. *Human Molecular Genetics* **16**, 2693–2702 (2007).
383. Belur, L. R. *et al.* Intravenous delivery for treatment of mucopolysaccharidosis type I: A comparison of AAV serotypes 9 and rh10. *Mol Genet Metab Rep* **24**, (2020).
384. Sheridan, C. Sangamo's landmark genome editing trial gets mixed reception. *Nature Biotechnology* **36**, 907–908 (2018).
385. Smith, L. J. *et al.* Gene Transfer Properties and Structural Modeling of Human Stem Cell-derived AAV. *Molecular Therapy* **22**, 1625–1634 (2014).
386. Smith, L. J. *et al.* Stem cell-derived clade F AAVs mediate high-efficiency homologous recombination-based genome editing. *PNAS* **115**, E7379–E7388 (2018).
387. Pechincha, C. *et al.* Lysosomal enzyme trafficking factor LYSET enables nutritional usage of extracellular proteins. *Science* **0**, eabn5637 (2022).
388. Richards, C. M. *et al.* The human disease gene LYSET is essential for lysosomal enzyme transport and viral infection. *Science* **378**, eabn5648 (2022).
389. Bueren, J. A. *et al.* Advances in the gene therapy of monogenic blood cell diseases. *Clinical Genetics* **97**, 89–102 (2020).
390. Pu, J. *et al.* BORC, a multisubunit complex that regulates lysosome positioning. *Dev Cell* **33**, 176–188 (2015).
391. Watson, G. L. *et al.* Treatment of lysosomal storage disease in MPS VII mice using a recombinant adeno-associated virus. *Gene Ther* **5**, 1642–1649 (1998).

392. Bosch, A., Perret, E., Desmaris, N. & Heard, J. M. Long-Term and Significant Correction of Brain Lesions in Adult Mucopolysaccharidosis Type VII Mice Using Recombinant AAV Vectors. *Molecular Therapy* **1**, 63–70 (2000).
393. Fraites, T. J. *et al.* Correction of the Enzymatic and Functional Deficits in a Model of Pompe Disease Using Adeno-associated Virus Vectors. *Molecular Therapy* **5**, 571–578 (2002).
394. Savas, P. S., Hemsley, K. M. & Hopwood, J. J. Intracerebral injection of sulfamidase delays neuropathology in murine MPS-IIIA. *Molecular Genetics and Metabolism* **82**, 273–285 (2004).
395. Belur, L. R. *et al.* Comparative Effectiveness of Intracerebroventricular, Intrathecal, and Intranasal Routes of AAV9 Vector Administration for Genetic Therapy of Neurologic Disease in Murine Mucopolysaccharidosis Type I. *Frontiers in Molecular Neuroscience* **14**, (2021).
396. Hinderer, C. *et al.* Intrathecal Gene Therapy Corrects CNS Pathology in a Feline Model of Mucopolysaccharidosis I. *Molecular Therapy* **22**, 2018–2027 (2014).
397. Belur, L. R. *et al.* Intranasal Adeno-Associated Virus Mediated Gene Delivery and Expression of Human Iduronidase in the Central Nervous System: A Noninvasive and Effective Approach for Prevention of Neurologic Disease in Mucopolysaccharidosis Type I. *Hum Gene Ther* **28**, 576–587 (2017).
398. Escolar, M., Poe, M., Rajan, D. & Szabolcs, P. Longterm outcomes of patients receiving umbilical blood stem cell transplantation for MPS II. *Molecular Genetics and Metabolism* **108**, S37–S38 (2013).
399. Poe, M. *et al.* MPS II: developmental outcomes after hematopoietic stem cell transplantation. *Molecular Genetics and Metabolism* **102**, S35–S36 (2011).
400. Kharbanda, S. & Dvorak, C. C. The Beginning of the End of Allogeneic Transplantation for Hurler Syndrome? *New England Journal of Medicine* **385**, 2003–2004 (2021).
401. Gentner, B. *et al.* Hematopoietic Stem- and Progenitor-Cell Gene Therapy for Hurler Syndrome. *New England Journal of Medicine* **385**, 1929–1940 (2021).
402. Paulk, N. Gene Therapy: It Is Time to Talk about High-Dose AAV. *Genetic Engineering & Biotechnology News* **40**, 14–16 (2020).
403. Wilson, J. M. & Flotte, T. R. Moving Forward After Two Deaths in a Gene Therapy Trial of Myotubular Myopathy. *Human Gene Therapy* **31**, 695–696 (2020).
404. Wong, C. H. *et al.* Estimating the Financial Impact of Gene Therapy in the U.S. Working Paper at https://doi.org/10.3386/w28628 (2021).
405. Gomez-Ospina, N. *et al.* Human genome-edited hematopoietic stem cells phenotypically correct Mucopolysaccharidosis type I. *Nat Commun* **10**, 4045 (2019).
406. Ellison, S. M. *et al.* Pre-clinical Safety and Efficacy of Lentiviral Vector-Mediated Ex Vivo Stem Cell Gene Therapy for the Treatment of Mucopolysaccharidosis IIIA. *Mol Ther Methods Clin Dev* **13**, 399–413 (2019).
407. Poletto, E., Baldo, G. & Gomez-Ospina, N. Genome Editing for Mucopolysaccharidoses. *Int J Mol Sci* **21**, 500 (2020).
408. Zhang, X.-H., Tee, L. Y., Wang, X.-G., Huang, Q.-S. & Yang, S.-H. Off-target Effects in CRISPR/Cas9-mediated Genome Engineering. *Molecular Therapy - Nucleic Acids* **4**, e264 (2015).
409. Gaudelli, N. M. *et al.* Programmable base editing of A•T to G•C in genomic DNA without DNA cleavage. *Nature* **551**, 464–471 (2017).
410. Komor, A. C., Kim, Y. B., Packer, M. S., Zuris, J. A. & Liu, D. R. Programmable editing of a target base in genomic DNA without double-stranded DNA cleavage. *Nature* **533**, 420–424 (2016).
411. Bose, S. K. *et al.* In utero adenine base editing corrects multi-organ pathology in a lethal lysosomal storage disease. *Nat Commun* **12**, 4291 (2021).
412. Anzalone, A. V. *et al.* Search-and-replace genome editing without double-strand breaks or donor DNA. *Nature* **576**, 149–157 (2019).
413. Anzalone, A. V. *et al.* Programmable deletion, replacement, integration, and inversion of large DNA sequences with twin prime editing. *Nat Biotechnol* **40**, 731–740 (2022).
414. Muenzer, J. *et al.* Intrathecal idursulfase-IT in patients with neuronopathic mucopolysaccharidosis II: Results from a phase 2/3 randomized study. *Molecular Genetics and Metabolism* **137**, 127–139 (2022).
415. Xiao, X., Li, J. & Samulski, R. J. Production of High-Titer Recombinant Adeno-Associated Virus Vectors in the Absence of Helper Adenovirus. *J Virol* **72**, 2224–2232 (1998).
416. Kim, C. *et al.* Comparative study of idursulfase beta and idursulfase in vitro and in vivo. *J Hum Genet* **62**, 167–174 (2017).

417. Sohn, Y. B. *et al.* Phase I/II clinical trial of enzyme replacement therapy with idursulfase beta in patients with mucopolysaccharidosis II (Hunter syndrome). *Orphanet J Rare Dis* **8**, 42 (2013).
418. Lagler, F. B. Current and Emerging Therapies for Mucopolysaccharidoses. in *Pediatric Pharmacotherapy* (eds. Kiess, W., Schwab, M. & van den Anker, J.) 39–56 (Springer International Publishing, 2020). doi:10.1007/164_2019_263.
419. Biffi, A. Gene therapy for lysosomal storage disorders: a good start. *Human Molecular Genetics* **25**, R65–R75 (2016).
420. Friedman, K. M. *et al.* Effective Targeting of Multiple B-Cell Maturation Antigen–Expressing Hematological Malignances by Anti-B-Cell Maturation Antigen Chimeric Antigen Receptor T Cells. *Hum Gene Ther* **29**, 585–601 (2018).
421. Forte, G. *et al.* Hepatocyte Growth Factor Effects on Mesenchymal Stem Cells: Proliferation, Migration, and Differentiation. *STEM CELLS* **24**, 23–33 (2006).
422. Heffner, G. C. *et al.* Prostaglandin E2 Increases Lentiviral Vector Transduction Efficiency of Adult Human Hematopoietic Stem and Progenitor Cells. *Mol Ther* **26**, 320–328 (2018).
423. Xu, L. *et al.* Evaluation of Pathological Manifestations of Disease in Mucopolysaccharidosis VII Mice after Neonatal Hepatic Gene Therapy. *Molecular Therapy* **6**, 745–758 (2002).
424. Pitts, M. W. Barnes Maze Procedure for Spatial Learning and Memory in Mice. *Bio Protoc* **8**, (2018).
425. Shoji, H., Takao, K., Hattori, S. & Miyakawa, T. Contextual and Cued Fear Conditioning Test Using a Video Analyzing System in Mice. *J Vis Exp* (2014) doi:10.3791/50871.
426. Anson, D. S., Bielicki, J. & Hopwood, J. J. Correction of Mucopolysaccharidosis Type I Fibroblasts by Retroviral-Mediated Transfer of the Human α-l-Iduronidase Gene. *Human Gene Therapy* **3**, 371–379 (1992).
427. Wolf, D. A. *et al.* Direct gene transfer to the CNS prevents emergence of neurologic disease in a murine model of mucopolysaccharidosis type I. *Neurobiology of Disease* **43**, 123–133 (2011).
428. Visigalli, I. *et al.* Gene therapy augments the efficacy of hematopoietic cell transplantation and fully corrects mucopolysaccharidosis type I phenotype in the mouse model. *Blood* **116**, 5130–5139 (2010).
429. Bobo, T. A., Samowitz, P. N., Robinson, M. I. & Fu, H. Targeting the Root Cause of Mucopolysaccharidosis IIIA with a New scAAV9 Gene Replacement Vector. *Mol Ther Methods Clin Dev* **19**, 474–485 (2020).
430. Sergijenko, A. *et al.* Myeloid/Microglial Driven Autologous Hematopoietic Stem Cell Gene Therapy Corrects a Neuronopathic Lysosomal Disease. *Molecular Therapy* **21**, 1938–1949 (2013).
431. Ou, L. *et al.* ZFN-Mediated In Vivo Genome Editing Corrects Murine Hurler Syndrome. *Molecular Therapy* **27**, 178–187 (2019).
432. Challita, P. M. *et al.* Multiple modifications in cis elements of the long terminal repeat of retroviral vectors lead to increased expression and decreased DNA methylation in embryonic carcinoma cells. *J Virol* **69**, 748–755 (1995).
433. Mendez, D. C. *et al.* A novel, long-lived, and highly engraftable immunodeficient mouse model of mucopolysaccharidosis type I. *Mol Ther Methods Clin Dev* **2**, 14068 (2015).
434. Shultz, L. D. *et al.* Human lymphoid and myeloid cell development in NOD/LtSz-scid IL2R gamma null mice engrafted with mobilized human hemopoietic stem cells. *J Immunol* **174**, 6477–6489 (2005).
435. Behringer, R. *Manipulating the mouse embryo: a laboratory manual*. (Cold Spring Harbor Laboratory Press, 2014).
436. Voznyi, Y. V., Keulemans, J. L. M. & Diggelen, O. P. van. A fluorimetric enzyme assay for the diagnosis of MPS II (Hunter disease). *Journal of Inherited Metabolic Disease* **24**, 675–680 (2001).
437. Barnes, C. A. Memory deficits associated with senescence: a neurophysiological and behavioral study in the rat. *J Comp Physiol Psychol* **93**, 74–104 (1979).
438. Kraeuter, A.-K., Guest, P. C. & Sarnyai, Z. The Y-Maze for Assessment of Spatial Working and Reference Memory in Mice. in *Pre-Clinical Models: Techniques and Protocols* (ed. Guest, P. C.) 105–111 (Springer, 2019). doi:10.1007/978-1-4939-8994-2_10.
439. Lieber, M. R. The Mechanism of Double-Strand DNA Break Repair by the Nonhomologous DNA End Joining Pathway. *Annu Rev Biochem* **79**, 181–211 (2010).
440. Shin, H. Y. *et al.* CRISPR/Cas9 targeting events cause complex deletions and insertions at 17 sites in the mouse genome. *Nat Commun* **8**, 15464 (2017).
441. Kosicki, M., Tomberg, K. & Bradley, A. Repair of double-strand breaks induced by CRISPR–Cas9 leads to large deletions and complex rearrangements. *Nat Biotechnol* **36**, 765–771 (2018).

442. Meikle, P. J. *et al.* Diagnosis of lysosomal storage disorders: evaluation of lysosome-associated membrane protein LAMP-1 as a diagnostic marker. *Clinical Chemistry* **43**, 1325–1335 (1997).
443. Whitley, C. B. *et al.* Retroviral-Mediated Transfer of the Iduronate-2-Sulfatase Gene into Lymphocytes for Treatment of Mild Hunter Syndrome (Mucopolysaccharidosis Type II). University of Minnesota Medical School, Minneapolis, Minnesota. *Human Gene Therapy* **7**, 537–549 (1996).
444. Hofling, A. A., Devine, S., Vogler, C. & Sands, M. S. Human CD34+ hematopoietic progenitor cell-directed lentiviral-mediated gene therapy in a xenotransplantation model of lysosomal storage disease. *Molecular Therapy* **9**, 856–865 (2004).
445. Lee, J. Y., Han, A.-R. & Lee, D. R. T Lymphocyte Development and Activation in Humanized Mouse Model. *Development & Reproduction* **23**, 79–92 (2019).
446. Jangalwe, S., Shultz, L. D., Mathew, A. & Brehm, M. A. Improved B cell development in humanized NOD-scid IL2Rγnull mice transgenically expressing human stem cell factor, granulocyte-macrophage colony-stimulating factor and interleukin-3. *Immunity, Inflammation and Disease* **4**, 427–440 (2016).
447. Fortin, J. M. *et al.* Transplantation of Defined Populations of Differentiated Human Neural Stem Cell Progeny. *Sci Rep* **6**, 23579 (2016).
448. Kenney, L. L., Shultz, L. D., Greiner, D. L. & Brehm, M. A. Humanized Mouse Models for Transplant Immunology. *American Journal of Transplantation* **16**, 389–397 (2016).
449. Griffin, T. A., Anderson, H. C. & Wolfe, J. H. Ex Vivo Gene Therapy Using Patient iPSC-Derived NSCs Reverses Pathology in the Brain of a Homologous Mouse Model. *Stem Cell Reports* **4**, 835–846 (2015).
450. Nagree, M. S. *et al.* Autologous, lentivirus-modified, T-rapa cell "micropharmacies" for lysosomal storage disorders. *EMBO Molecular Medicine* **14**, e14297 (2022).
451. Herbig, E. J. *et al.* 373. Expression of Human Iduronidase from Sleeping Beauty Engineered Human B Lymphocytes as a Cellular Therapy for Mucopolysaccharidosis Type I. *Molecular Therapy* **23**, S148 (2015).
452. Dean, R. *et al.* An updated cost-utility model for onasemnogene abeparvovec (Zolgensma®) in spinal muscular atrophy type 1 patients and comparison with evaluation by the Institute for Clinical and Effectiveness Review (ICER). *J Mark Access Health Policy* **9**, 1889841.
453. Lancaster, V. *et al.* The effectiveness and value of betibeglogene autotemcel for the management of transfusion-dependent beta-thalassemia. *JMCP* **28**, 1316–1320 (2022).
454. Zincarelli, C., Soltys, S., Rengo, G. & Rabinowitz, J. E. Analysis of AAV Serotypes 1–9 Mediated Gene Expression and Tropism in Mice After Systemic Injection. *Molecular Therapy* **16**, 1073–1080 (2008).
455. Shirley, J. L., Jong, Y. P. de, Terhorst, C. & Herzog, R. W. Immune Responses to Viral Gene Therapy Vectors. *Molecular Therapy* **28**, 709–722 (2020).
456. Foust, K. D. *et al.* Intravascular AAV9 preferentially targets neonatal neurons and adult astrocytes. *Nat Biotechnol* **27**, 59–65 (2009).
457. Piechnik, M. *et al.* Sex Difference Leads to Differential Gene Expression Patterns and Therapeutic Efficacy in Mucopolysaccharidosis IVA Murine Model Receiving AAV8 Gene Therapy. *International Journal of Molecular Sciences* **23**, 12693 (2022).
458. Han, S.-O., Gheorghiu, D., Li, S., Kang, H. R. & Koeberl, D. Minimum Effective Dose to Achieve Biochemical Correction with Adeno-Associated Virus Vector-Mediated Gene Therapy in Mice with Pompe Disease. *Human Gene Therapy* **33**, 492–498 (2022).
459. Malato, Y. *et al.* Fate tracing of mature hepatocytes in mouse liver homeostasis and regeneration. *J Clin Invest* **121**, 4850–4860 (2011).
460. Scallan, C. D. *et al.* Human immunoglobulin inhibits liver transduction by AAV vectors at low AAV2 neutralizing titers in SCID mice. *Blood* **107**, 1810–1817 (2006).
461. Fu, H., DiRosario, J., Killedar, S., Zaraspe, K. & McCarty, D. M. Correction of Neurological Disease of Mucopolysaccharidosis IIIB in Adult Mice by rAAV9 Trans-Blood–Brain Barrier Gene Delivery. *Molecular Therapy* **19**, 1025–1033 (2011).
462. Ertl, H. C. J. T Cell-Mediated Immune Responses to AAV and AAV Vectors. *Frontiers in Immunology* **12**, (2021).
463. Nathwani, A. C. *et al.* Adenovirus-Associated Virus Vector–Mediated Gene Transfer in Hemophilia B. *New England Journal of Medicine* **365**, 2357–2365 (2011).

464. Harmatz, P. *et al.* First-in-human in vivo genome editing via AAV-zinc-finger nucleases for mucopolysaccharidosis I/II and hemophilia B. *Molecular Therapy* **0**, (2022).
465. Laoharawee, K. *et al.* Non-invasive Intravenous Administration of AAV9 Transducing Iduronate-2-Sulfatase Leads to Global Metabolic Correction and Prevention of Neurologic Deficits in a Mouse Model of Hunter Syndrome. Submitted, *Molecular Genetics and Metabolism* (2022).

Appendix

Copyright Clearance

Chapters II contains portions of text, full figures, and tables from a manuscript that was published by *Human Gene Therapy.* The manuscript is available under the terms of the Creative Commons Attribution License and is Open Access and permission to publish the material in this thesis was obtained from the publisher. A full reference to this publication is listed below. Sections from this manuscript were adapted for publication in this dissertation. These changes were made at the sole discretion of the author of this dissertation and are not endorsed by Mary Ann Liebert, Inc Publishers.

Smith MC, Belur LR, Karlen AD, et al. Phenotypic correction of murine mucopolysaccharidosis type II by engraftment of ex vivo lentiviral vector transduced hematopoietic stem and progenitor cells. Human Gene Therapy 2022; doi: 10.1089/hum.2022.141.